GEORG-AUGUST-UNIVERSITÄT
GÖTTINGEN

Master's Thesis

Kausale Entropische Kräfte: Intelligentes Verhalten, Dynamik und Strukturbildung

Causal Entropic Forces: Intelligent Behaviour, Dynamics and Pattern Formation

prepared by

Hannes Hornischer

from Peine

at the Max Planck Institut für Dynamik und Selbstorganisation

Thesis period:	15th May 2015 until 15th October 2015
Supervisor:	Dr. Marco G. Mazza
First referee:	Dr. Marco G. Mazza
Second referee:	Prof. Dr. Stephan Herminghaus

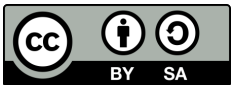

This Master's thesis by Hannes Hornischer is licensed under a
Creative Commons Attribution-ShareAlike 4.0 International License[1].

[1]http://creativecommons.org/licenses/by-sa/4.0/

Contents

1. Introduction

What are the underlying principles of intelligent behaviour? For that we first ask: How did complex organism with the potential of higher intelligence arise out of a process of evolution? One basic principle of evolution is survival, that is, organisms distance themselves from situations threatening their physical health. This requires the ability of processing information about the environment. For deer to flee from a predator, not only must it see, but it must also recognise the imminent threat. A connection between the amount of available information of the environment to an organism and its growth rate, or fitness, was suggested by Taylor et al. in 2007 [1]. Information about the system needs to be interpreted and used for predicting its future developement in order to identify threats and act accordingly, moving away from situations limiting the space of possible future options. By not only taking instantaneous maximization of options into account (such as a chemotactic bacterium following the gradient of a nutrient [2]) but instead considering longer future evolutions of the system, more complex situations can be assessed. The amount or diversity of possible future evolutions of a system can be quantified. A general definition of causal entropy is based on a dynamical version of the Boltzmann-Shannon entropy. That is, instead of considering the probability of macrostates, the causal entropy is based on the probability of a finite path in phase space.

In 2013, Wissner-Gross and Freer proposed a connection between maximization of causal entropy and intelligent behaviour [3]. This fundamental model can be applied to various fields and problems, such as game theory where it was possible to create a skilled artificial player in the game of Go using the principle of maximizing the amount of possible future moves [4]. Furthermore, this principle has already been used for modelling social cooperation in solving simple problems [3] for comparison with experiments made with various animal species in this regard [5–7]. A more general and basic approach to origins of collective and social behaviour was given [8]. Even the emergence of life and developement of our planetary system can be

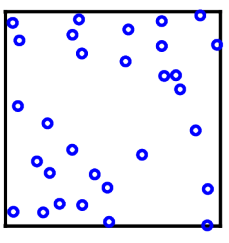

brought into direct connection with this model [9].

In this work we investigate the relationship between causal entropy and intelligent behaviour from the point of view of statistical mechanics by examining the dynamics of systems driven by a causal entropic force, maximizing their causal entropy. We dive into the topic of group behaviour and pattern formation in confined space. This includes the examination of steady state patterns in enclosed spaces, as well as the dynamics of particles in a bottleneck system as analogy to agent based evacuation scenarios [10–13]. Generally, in applying this model on bottleneck problems we see great potential for the field of protein folding [14, 15], more precisely allowing improvements to algorithms for Monte Carlo simulations of protein folding [16].

Our work is organized as follows. In the directly following section we will introduce the concept of the causal entropic force. A simple approach for a particle on a lattice with discrete timesteps will be introduced and examined in Chapter 2, where we both consider a square lattice as well as a bottleneck as geometries for the system. In Chapter 3 we derive a more general expression for the causal entropic force and introduce our model for continuous space and time. In Chapter 4 the dynamics of a single entropically driven particle in both a square and a bottleneck system will be examined. Furthermore we draw the analogy of this model to the statistical dynamics of polymers and compare numerical results with experimental data in Section 4.6. In Chapter 5 we consider many-particle systems and further analyse the formation of patterns of a large number of individually entropically driven particles in confined space in Section 5.3. Causal entropy maximization as model for evacuation problems will be examined in Section 5.4.

The figures in the bottom right corner of every odd page work as a flip book if the pages are turned rapidly. The animation is an example video sequence of pattern formation of many particles in a confined space and will be further discussed in Section 5.2.

The causal entropic force

We define entropy on the set of possible future evolutions of a system within a finite time horizon. This entropy, or causal entropy, is thus a quantity associated with the diversity of future options available to a system. By maximizing the causal entropy we maximize the diversity of options and therefore drive the system away from restricted states. Like a chess player thinking several steps ahead, keeping his

future options open. Thus, in phase space, moving away from restrictions such as an impending loss – which would drastically decrease the diversity or number of possible moves.

Figure 1.1 shows the light-cone representing the possible states a system can reach within a time horizon τ. Three future trajectories of the system are shown, all starting from the same initial state of the system $\mathbf{x}(0)$, its position in phase space at time $t = 0$. The restriction effectively narrows the accessible states in the future. Thus, by the causal entropic force maximizing its phase space volume the system is driven away from the restriction.

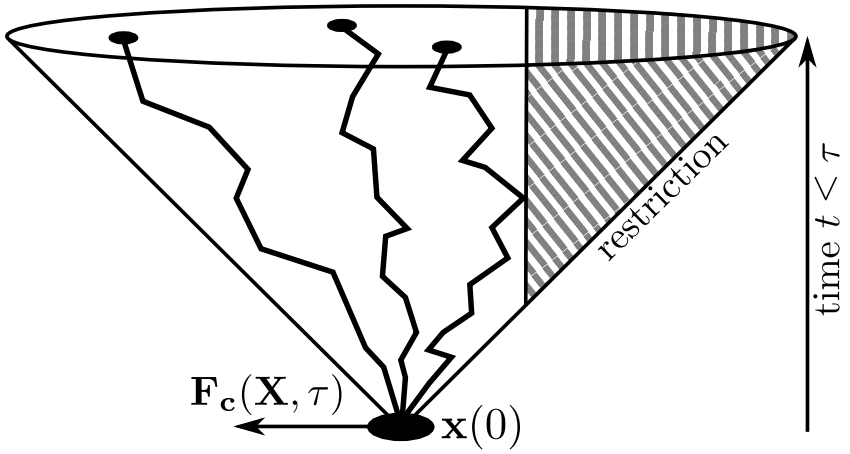

Figure 1.1.: Sketch of the system exploring phase space. $\mathbf{F_c}(\mathbf{X}, \tau)$ drives the system away from a restricted area. See also [3].

In this work we examine the behaviour of systems acted upon by such a causal entropic force $\mathbf{F_c}$ towards states of larger causal entropy. This force can formally be written

$$\mathbf{F}_c(\mathbf{X}_0, \tau) = T_c \nabla_{\mathbf{X}} S_c(\mathbf{X}, \tau)|_{\mathbf{X}_0} \,, \tag{1.0.1}$$

where S_c is the causal entropy, $\mathbf{X}$ the macrostate of the system, τ the maximum time horizon of the considered future evolution of the system and T_c a scaling factor which is convenient to call temperature or causal temperature.

In Chapter 3.1 we go into the details of the causal entropic force and causal entropy for a generic system. But first we use the general idea of maximizing the diversity of future option of a system in the following section, using discretized space and time.

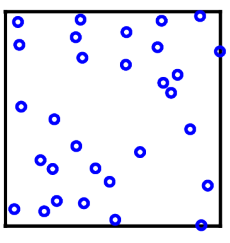

2. Discrete evolution: Theory and results

In this section we use the correspondence of causal entropy to the diversity of future options in a system's evolution. We directly define causal entropy on the diversity of possible trajectories, using two approaches with different quanitfications of this diversity in a simple system: A single particle moving in a two-dimensional lattice with discrete timesteps and only subject to the entropic force in Eq. (1.0.1). In Sec. 2.1 we count the number of possible future trajectories with τ steps, whereas in Sec. 2.2 we count the area covered by future trajectories. In Sec. 2.3 we discuss and compare the results of those approaches.

2.1. First approach

2.1.1. Method

Consider a point-like particle moving on a finite two-dimensional lattice bounded in both the x and y directions by walls. We study its motion under the influence of a causal entropic force. To calculate the entropic force in this system, we count the number of trajectories consisting of τ steps that are possible from the current position of the particle such that the trajectory does not intersect the wall. The particle will always take a step in the direction with the largest number of possible trajectories, i.e. towards the state which maximizes the total number of possible trajectories. If more than one direction have the same (maximum) number, the next step will be chosen randomly between those. The particle will always move a step – staying at its current field is not allowed. A typical sampling and calculation of the entropic force is illustrated in Fig. 2.1. Please note that the horizon is timewise, that is, the time we let a system evolve is fixed.

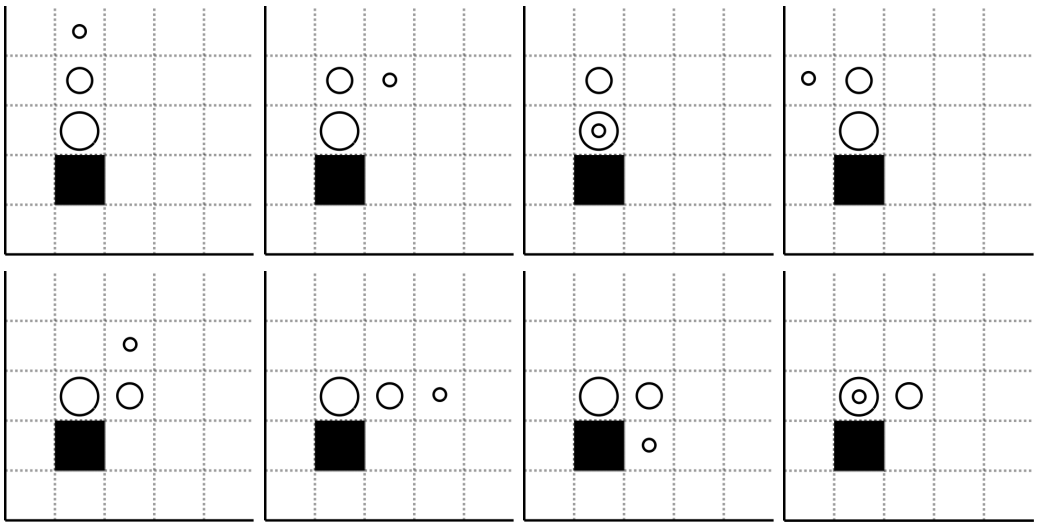

Figure 2.1.: Few examples of systematic counting of all possible trajectories for a particle (black square) in a two dimensional lattice close to two walls in an otherwise open system (here for horizon $\tau = 3$ steps). Circles of decreasing radius represent the sequence of steps taken by the particle.

In this case, the counting of possible trajectories for horizon $\tau = 3$ steps yields $n = 15$ possible paths in direction up and right, away from the walls, and $n = 9$ for down and left, towards the walls, as illustrated in Fig. 2.2. Since the smallest horizon we consider is 1, the particle will never try to take a step towards a wall. In the worst case it can only "sense" if there is a wall to avoid and otherwise perform a random walk.

In the following, when refering to a **path** or **trajectory**, we speak about actual paths an entropically driven particle takes. They shall not be confused with **sampling paths** or **- trajectories**, used for the calculation of the entropic force.

2.1.2. Numerical results

In Fig. 2.3 two trajectories of a driven particle in a $L \times L$, $L = 10$ square lattice are shown for the horizon $\tau = 5$.

The particle starts in the bottom left corner from where it moves towards the centre in both cases, but with slightly different trajectories. Closer to a wall the number of possible paths, and therefore the entropy, is smaller. The particle is then driven away from this restricted area towards the centre. Since the distance to the two closest walls is the same along the diagonal (at position $(0, 0)$, $(1, 1)$, ..) there

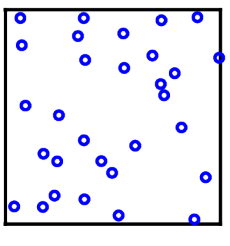

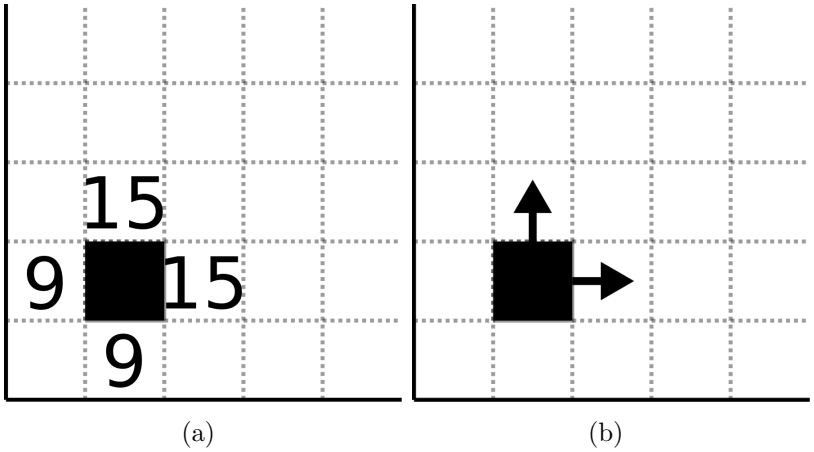

Figure 2.2.: (a) The number of possible paths for $\tau = 3$ steps. (b) Possible directions for the next step. Since there is more than one direction with maximum count, it will be randomly chosen between those two.

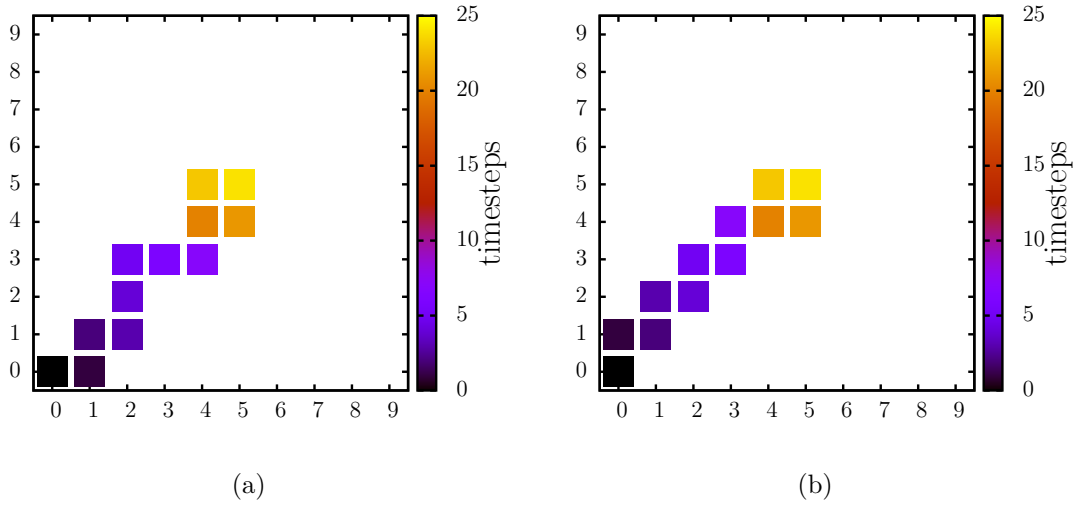

Figure 2.3.: Two trajectories for a particle. Horizon $\tau = 5$, box size $L = 10$, total runtime 25 steps.

is no preferred direction for the particle to move wherefore it randomly chooses a direction. In the centre, four fields are equidistant from the walls, therefore the particle stays in this area effectively performing a random walk.

For horizons $\tau = 4$ and $\tau = 6$ trajectories in the same environment are shown in Fig. 2.4.

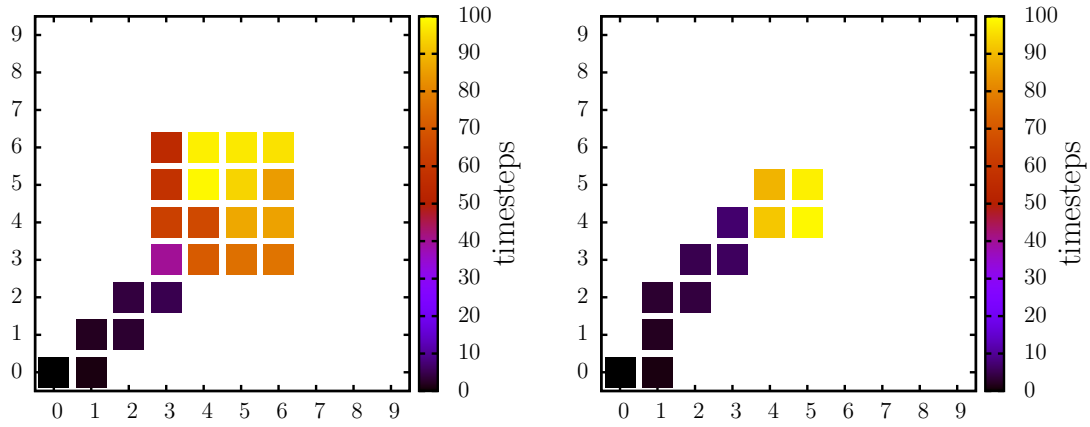

(a) (b)

Figure 2.4.: Trajectories for horizon $\tau = 4$ in (a) and $\tau = 6$ in (b). Box size $L = 10$, total runtime 100 steps. The inital position is at position $(0, 0)$, in the bottom left corner.

For horizon $\tau = 4$ the particle will be driven away from the walls towards the centre up to a minimum distance from the walls of 3 fields leading to a 4×4 area in which it moves around randomly. The horizon is just large enough for the entropic force to keep the particle at a minimum distance from the walls of 3 fields. For horizon $\tau = 6$, the behaviour does not change compared to $\tau = 5$ in Fig. 2.3 since the particle already "sees" the whole system, meaning the horizon is large enough for it to be repelled by the walls and to stay in the centre 4 fields.

We observe the particle being driven away from walls which restrict the accessible area and therefore the number of possible paths to take. However, the horizon determines the distance a particle will keep from the walls. In Fig. 2.5 this is shown for a driven particle with variable horizon in systems of size 5×5 and 10×10 respectively. The particle's average distance from the centre of the box is used to measure the performance of a particle.

We observe that for a small horizon the distance to the centre is largest and

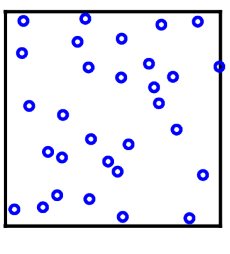

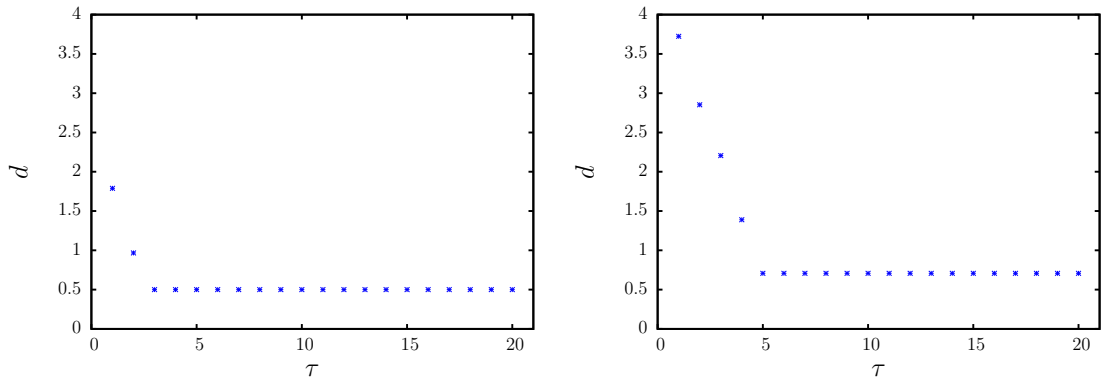

(a) Box size 5x5 (b) Box size 10x10

Figure 2.5.: Average steady-state distance to the centre of the box for different horizons in systems of size (a) $L = 5$ and (b) $L = 10$. Distance is averaged over 1000 steps after a transient of 100 steps. Initial position of the particle is at $(0, 0)$.

decreases for larger horizons to a minimum value. For $\tau = 1$ the particle performs a random walk since it can only sense one step ahead and therefore only the neighbouring fields, randomly choosing one direction while not colliding with the walls. For the 5×5 box the minimum distance is $d_{min} = 0.5$, for the 10×10 box $d_{min} = 0.7071 \approx 2^{-\frac{1}{2}}$. This is due to the geometry of the system together with the condition that a particle always needs to take a step and cannot rest at one field. In Fig. 2.6 we show how a particle in a $L \times L$ box for a horizon $\tau \leq L/2$ will move around the centre of the box for even and odd number of fields respectively. In Fig. 2.6(a) we see in grey the four fields a particle will move about, as we have observed earlier. The average distance is constant at $d_{min} = 2^{-\frac{1}{2}}$, all four fields are occupied with equal probability. In Fig. 2.6(b), for an odd system size, there is actually a centre field, but the particle is forced to move every step, and wherefore it switches between the centre field and a neighbouring field.

Figure 2.7 shows the average distances to the centre for variable horizon τ and box size $L \times L$. For increasing horizon the average distance to the centre decreases linearly. The area for large horizons and small box sizes, where the d is smallest, is the regime where the particle is able to stay in the centre as discussed earlier. The difference in behaviour between even and odd system sizes in that regime is not visible with the scale at the colour bar used in Fig. 2.7. For the sake of completeness this is illustrated in Fig. 2.8.

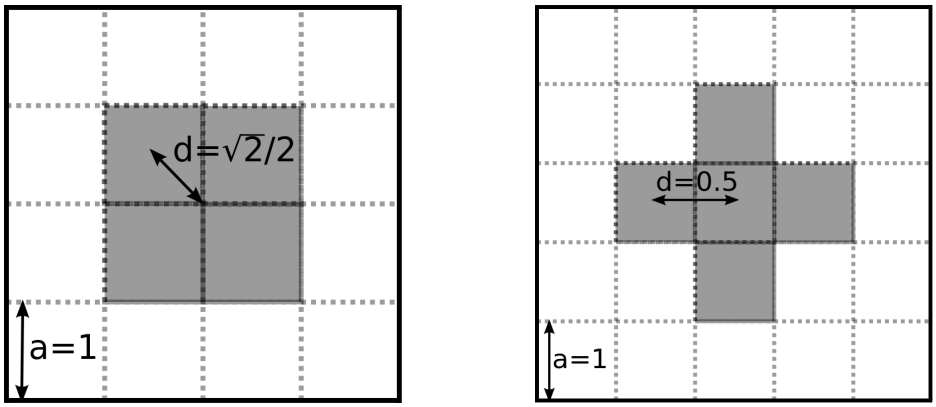

(a) Even box size (b) Odd box size

Figure 2.6.: Centre fields for a particle in a box of (a) even and (b) odd size in grey. For the even edge length the average distance is constantly $\sqrt{2}/2$, for odd size it is half of the time at the centre field with distance $d = 0$ and half of the time at a neighbouring field with $d = 0.5$ since it is forced to move every step.

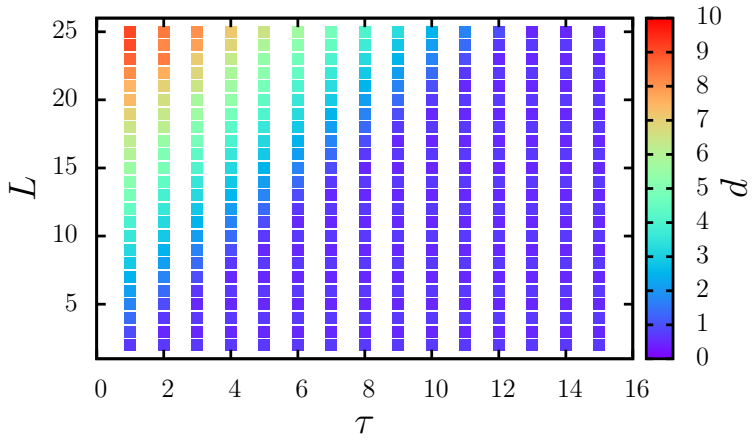

Figure 2.7.: Average distance d from the centre of a box for different horizons τ and box sizes L shown as three-dimensional plot in (a) and map in (b). Sampled time 10000 steps, transient time 500 steps, initial position $(0, 0)$.

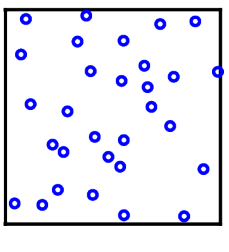

For large box sizes and small horizons the data are slightly noisy. In general the particle stays as far as possible away from the walls. The larger the system size the further away from the centre a particle can possibly be. This explains the increasing distance for small τ and increasing system size.

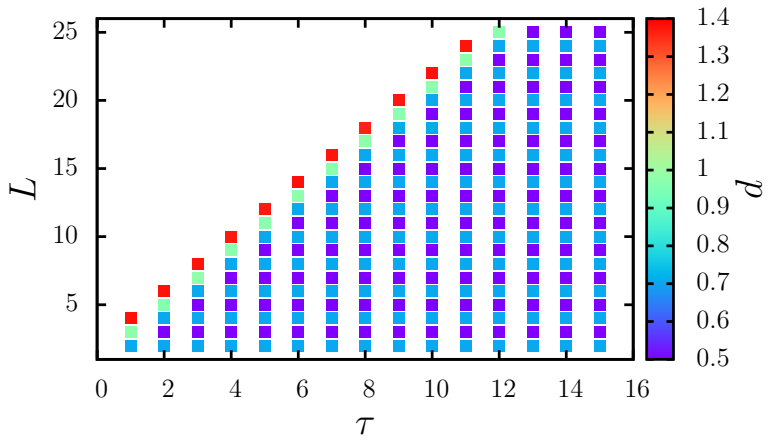

Figure 2.8.: Average distance d from the centre of a box for different horizons τ and box sizes L zoomed in in order to illustrate the deviant behaviour for even and odd box sizes in the regime of horizon larger than box size, respectively. Same data as shown in Fig. 2.7 (sampled time 10000 steps, transient time 500 steps, initial position $(0, 0)$).

The two minimum distances are now visible. All data with larger distances are not shown, therefore the whitespace in the top left corner.

We can consider the behaviour of the particle as quasi-deterministic. Except small differences in the trajectory for example when moving away from a corner as shown in Fig. 2.3 the qualitative outcome will always be the same. As soon as a particle is at a distance to all walls larger than its horizon it performs a uniform random walk within that distance.

2.1.3. Analytical results

We can view the trajectory of the particle as a random walk on a finite two-dimensional lattice. The horizon simply determines the minimum distance from

the walls a particle will keep after a transient time, i.e. long enough to be repelled by the walls. For infinite time the probability density distribution of the position of the particle will converge. In our system the probability for the particle to be at field x with i neighbouring fields will be

$$p(x) = \sum_i p_i \cdot \frac{1}{N_i} \tag{2.1.1}$$

where N_i denotes the number of neighbours of field i, which for this case is equivalent to the inverse probability of moving to field x. This problem can be viewed as a first order Markovian process. By creating a matrix of all transition probabilities we can find the steady state distribution which, after normalization, is just the probability density distribution of the particles position during a random walk. Appendix A.1 shows this in detail. The average distance to the centre can then be calculated using the probabilities and the distances d of every field to the centre:

$$d_{av} = \sum_x p(x) \cdot d(x) \tag{2.1.2}$$

The analytical results for average distances are shown in Fig. 2.9(a). The analytical

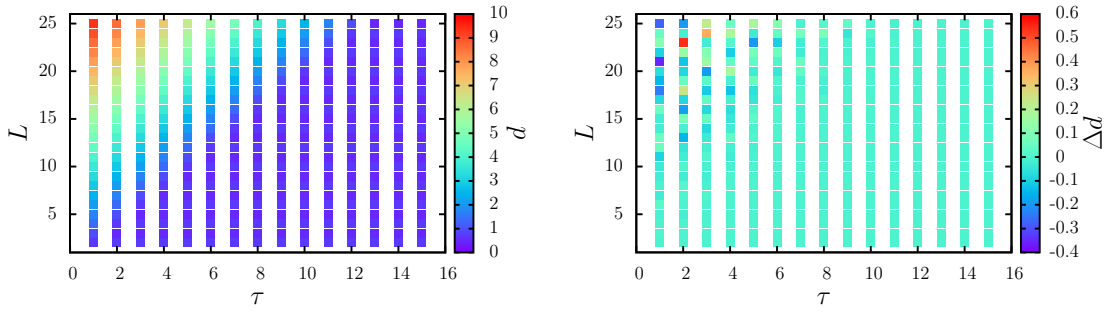

Figure 2.9.: (a): Analytical results for average distance d from the centre of a box for different horizons τ and box sizes $L \times L$. (b): Difference between analytical and numerical results. Difference in average distance $\Delta d = d_{analytical} - d_{numerical}$ from the centre of a box for different horizons τ and box sizes L.

model yields results that are very similar to computer simulations as shown in Fig.

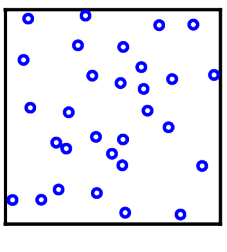

2.7. A comparison between the analytical model and simulations is shown in Fig. 2.9(b). The difference is negligible except for the regime with large horizon and box size. This is due to the fact that here the particle has a larger area in which it performs a random walk and therefore has a larger deviation from the expected value. The rather good match of theoretical and numerical data is a nice validation of the simulation.

The analytical results are valid for the case of a particle being able to remain on a field. In our simulation the particle was forced to move every timestep, therefore the densitiy distribution would alternate between two configurations. Like the king on a chessboard, the particle can only move from a black to a white field, therefore for one half of the fields the probability to be on is zero every step. The results can be viewed as the average over two steps after an infinite time, or for a system where a particle can rest at a field.

We observe the system moving away from restricted areas towards the centre i.e. towards a state of largest (causal) entropy i.e a state with largest amount of possibilities how to further evolve. In that sense entropy can be seen as a quantity for freedom. If we would interpret the particle as an intelligent being, its intellect would go with the horizon. For $\tau = 1$ it is smart enough not to bump into walls, for $\tau \gg 1$ it will keep as much distance to restricted areas as possible maximizing its freedom, maximizing its possibilities for the future.

This method becomes more and more computationally expensive, since the number of possible paths grows exponentially with the horizon. For an open infinte system the total number of paths is $N_{total} = 4^{\tau}$. Therefore, we now describe a different method where we do not fully sample the accessible space. Also we choose a different measurement for entropy (which is closer to what will be used later in this work when we move to a continuous representation of space and time) in order to have data that can be plausibly compared to the results of the simulations in continuous space and time.

2.2. Second approach

2.2.1. Method

Similarly as before we let the particle sample its environment, but now we statistically generate a large number of random trajectories instead of going over all

possible sampling paths. Also, now we do not count the number of paths per direction. Instead we sum over the number of fields each path contains, that is, the area each path covers. For the three paths in Fig. 2.10 the total area we would count is $A_{total} = 3 + 3 + 2 = 8$. The areas are summed up for the initial direction of the path. So for Fig. 2.10(a) the first step is up, for direction up we count the area $A_{up} = 3$. Statistically the area of a path initially moving towards a restricted area, like a wall, will be smaller and therefore giving information about the accessible phase space (here consisting only of position-space). In this way we can relate the area covered by sampling paths to (causal) entropy as introduced before. This method of sampling phase space is closer to what we will later use for continuous systems. Thus making it comparable with results from different approaches.

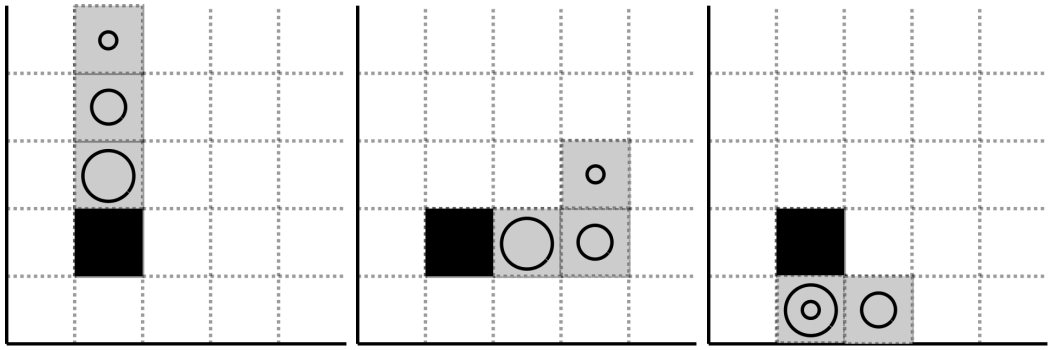

Figure 2.10.: Schematic illustration: Sampling accessible phase space using (three) random walks, counting the area of each path.

For the sampling shown in Fig. 2.10 the total area A for each direction D is the sum of the areas a_i of every sampling path i, whose first step is in direction D.

$$A(\tau, D) = \sum_i a_i \quad . \tag{2.2.1}$$

From this we calculate a weight W

$$W(D) = \frac{A(\tau, D)}{\sum_D A(\tau, D)} \, , \tag{2.2.2}$$

$$\sum_D W(D) = 1 \, . \tag{2.2.3}$$

We then would have the following values (assuming those three paths would consti-

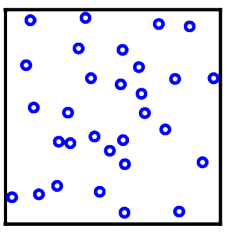

tute the whole sampling):

$$A(\tau, \uparrow) = 3 \tag{2.2.4}$$
$$A(\tau, \rightarrow) = 3 \tag{2.2.5}$$
$$A(\tau, \downarrow) = 2 \tag{2.2.6}$$
$$A(\tau, \leftarrow) = 0 \tag{2.2.7}$$
$$\sum_D A(\tau, D) = 8 \tag{2.2.8}$$
$$W(\uparrow) = 0.375 \tag{2.2.9}$$
$$W(\rightarrow) = 0.375 \tag{2.2.10}$$
$$W(\downarrow) = 0.25 \tag{2.2.11}$$
$$W(\leftarrow) = 0 \tag{2.2.12}$$
$$\sum_D W(D) = 1 \tag{2.2.13}$$

The largest area is in the direction $\uparrow$ and $\rightarrow$. Hence one of these will be chosen randomly for taking a step.

2.2.2. Results: Box

First, we again consider a single particle in a two-dimensional, square lattice with discrete timesteps, and only subject to the entropic force. Again as a measure of performance we take the average distance from the centre d, averaged over 5000 steps after a transient of 500 steps. Figure 2.11 shows the average distance from the centre for different horizons τ for a particle in a 5×5 and 10×10 box, respectively. In both systems, for small horizons, the distance is large and decreasing as τ increases to a minimum where it first stagnates. Contrary to our previous method d starts to grow again when further increasing τ. That is, the particle is not as likely to stay in the centre anymore. In the 5×5 system (Fig. 2.11(a)) for $\tau \geq 35$ it even has a larger distance than when it performs a random walk at $\tau = 1$, that is, it prefers moving close to the walls. For small τ the behaviour in mostly a random walk, as soon as the horizon is large enough for the particle to properly see the walls it stays quite central, in (a) approaching $d_{min} \approx 0.5$, in (b) $d_{min} \approx 0.8$ which is around the minimum found and discussed in the previous method. Concerning the behaviour for large τ, note that in (a) the whole system in only $5 \times 5 = 25$ fields large. For

such high horizons the system can easily be covered by every trajectory. Sampling trajectories initially going towards a wall will therefore sample an area very similar to sampling trajectories initially going away from a wall. The entropic force hence increases, causing the particle to change behaviour and preferences. In (b) the total number of fields is 100 wherefore this effect is weaker, however there is a trend visible in growing distance for larger horizon.

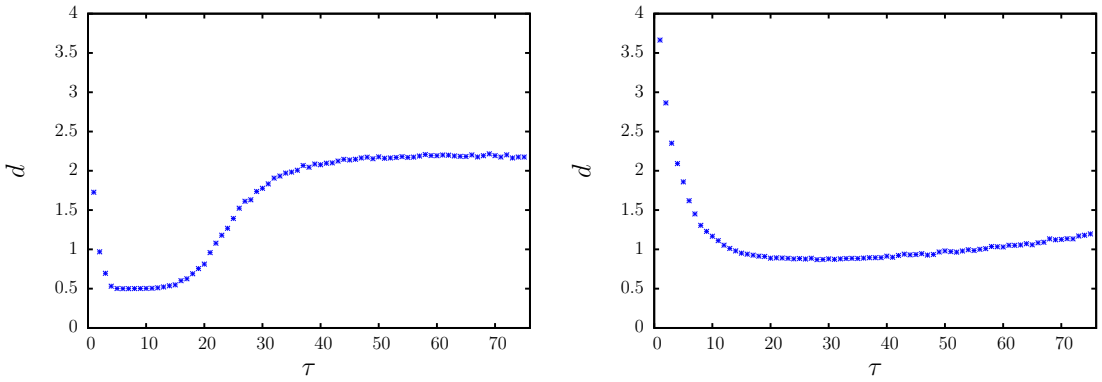

(a) 5x5 (b) 10x10

Figure 2.11.: Average distance to the centre of the box for different horizons in systems with (a) $L = 5$ and (b) $L = 10$. [Distance averaged over 5000 steps after transient time 500 steps, initial position $(0, 0)$, sampled paths per step: 50000]

Figure 2.12 shows the dependence of d on τ and system size L.

For large L and small τ, d is relatively large and decreases smoothly for smaller L and larger τ respectively. The dark blue region indicates a large set of parameters where the particle stays in the centre. For small systems and large horizons in the bottom right corner there is a light blue area were the particle shows a change in behaviour congruent with what was already observed in Fig. 2.11(a).

In order to understand the behaviour in this regime we calculate the probability density of the particle's position. Figure 2.13(a) shows the case for $\tau = 1$ (when the particle performs a random walk). There are three kinds of fields with different occupation probabilities: In the corners (two neighbours), at the walls (three neighbours) and in the central area (four neighbours). As a comparison Fig. 2.13(b) shows the analytical solution for this scenario (see Sec. A.1 in the appendix for details on the analytical method). This gives the exact occupation probabilities p_c,

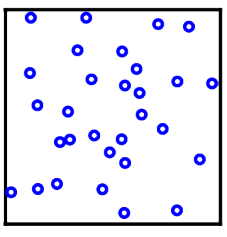

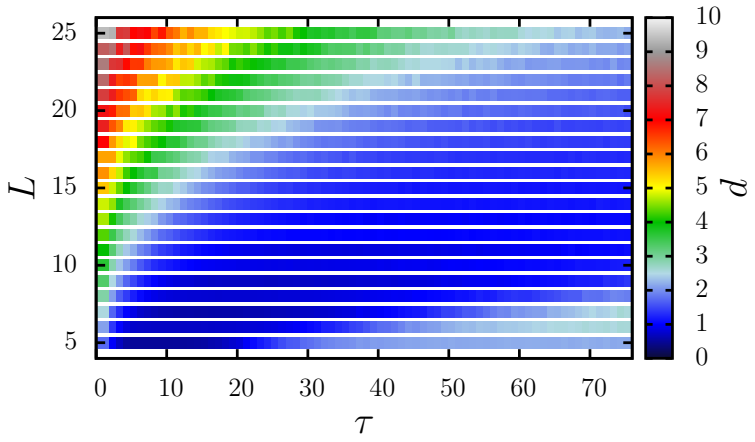

Figure 2.12.: Average distance from the centre of a box d for different horizons τ and box sizes L. [Distance averaged over 5000 steps after transient time 500 steps, initial position $(0, 0)$, sampled paths per step: 50000]

p_w, p_m for corner, wall and central area, respectively,

$$p_c = 0.025 = \frac{1}{40} \tag{2.2.14}$$

$$p_w = 0.0375 = \frac{3}{80} \tag{2.2.15}$$

$$p_m = 0.05 = \frac{1}{20} \tag{2.2.16}$$

$$p_{total} = 4 \cdot p_c + 12 \cdot p_w + 9 \cdot p_m = 1 \quad . \tag{2.2.17}$$

The occupation probability is linearly related to the number of neighbouring fields by

$$p_c = \frac{2}{4} \cdot p_m \quad \text{and} \tag{2.2.18}$$

$$p_w = \frac{3}{4} \cdot p_m \quad . \tag{2.2.19}$$

Be aware of the different colour scale in Fig. 2.13(c) and (d). Figure 2.13(c) shows the occupation probability for $\tau = 10$. Around this horizon a minimum average distance is reached (as shown and discussed in Fig. 2.11(a)). The probability to stay in the centre field is around $p \approx 0.5$ whereas its neighbouring fields have $p \approx 0.125$.

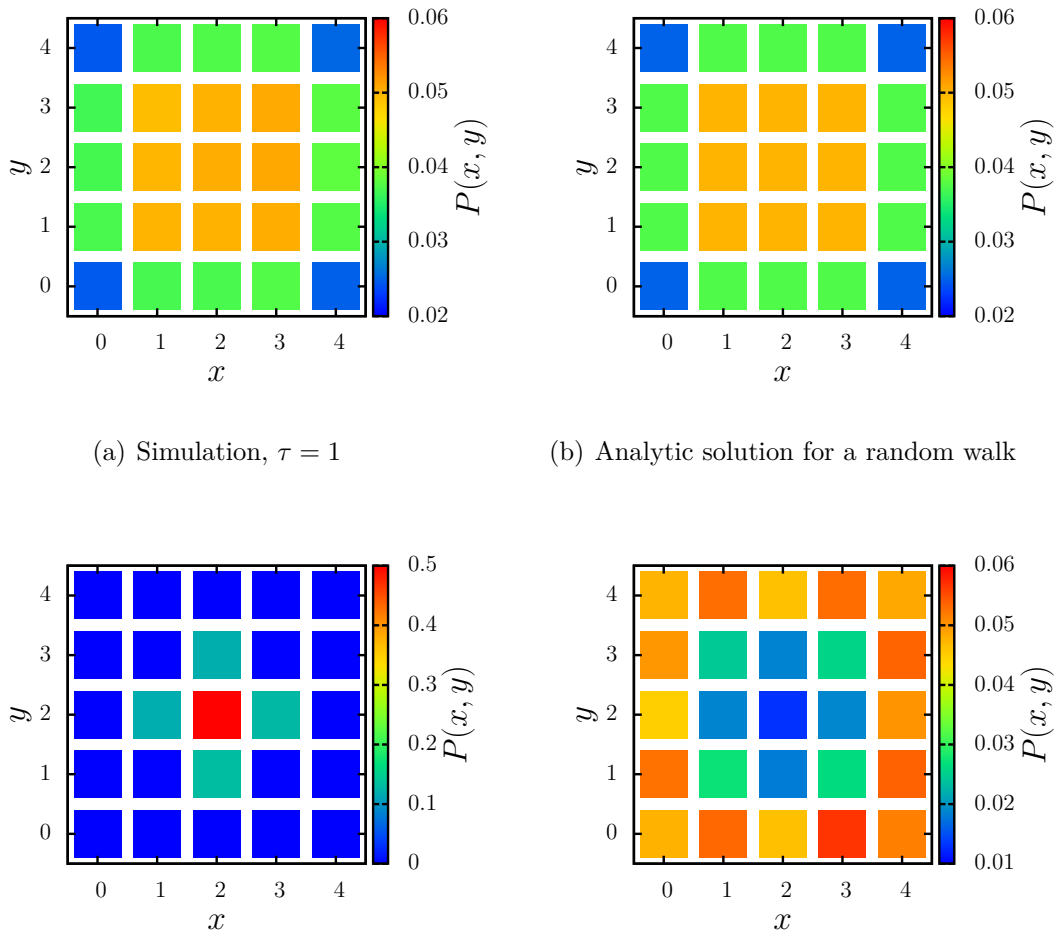

(a) Simulation, $\tau = 1$

(b) Analytic solution for a random walk

(c) Simulation, $\tau = 10$

(d) Simulation, $\tau = 40$

Figure 2.13.: Occupation probability for a particle in a 5x5 box for (a) $\tau = 1$ and (b) its analytical solution. In (c) $\tau = 10$ and in (d) $\tau = 40$. Be aware of the different colour scale. [Occupation probability sampled using 10000 steps after transient time 500 steps, initial position $(0, 0)$, sampled paths per step: 50000]

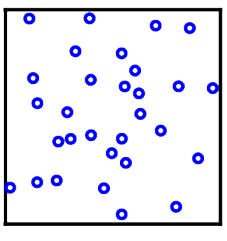

The particle switches between the centre and the neighbouring fields thus showing a behaviour we would expect from the previous method. However, for $\tau = 40$ when the average distance is even larger than in the diffusive case of $\tau = 1$ the behaviour differs dramatically as shown in Fig. 2.13(d). The occupation probability along the wall is much higher than the centre fields. For a sufficiently large horizon, such that one trajectory could fill the entire system, the positions close to the wall or the corners seem more attractive than the centre. If a particle randomly moves starting from the centre, it will most likely reflect from the wall and cross its own path. Hence the total area is smaller than when it starts from a corner. In the latter case the particle has a larger chance of moving towards the centre and other corners because two directions are immediately restricted and so it easily moves to unexplored areas. This might explair the tendency to stay close to the walls. However, if the horizon is even larger, so that almost all trajectories cover the whole system, every direction would be equally favorable and therefore we would observe behaviour equivalent to a random walk. For a particle in a 5×5 box this is shown in Fig. 2.14, where the data for $\tau \in [1, 70]$ are the same as in Fig. 2.11(a). For $\tau = 1$, the particle performs a random walk. The performance then increases, that is, the particle finds the centre. Then it enters the regime where the wall is more favorable. When further increasing τ the average distance to the centre d then converges to the level of the random walk marked with a solid line. As expected, the particle performs a random walk for $\tau \to \infty$ since every trajectory, covering the whole system, will indicate the same (maximum) entropy for every position. Walls lose their influence on the particle.

For $\tau \sim L$ the behaviour for this method qualitatively matches the previously examined approach of counting all possible trajectories - for even smaller τ, the behaviour agrees quantitatively with the previous approach. As soon as the horizon approaches the system size $\tau \sim L^2$ we observe a different behaviour which can be explained. In general for larger horizons this method exhibits larger deviations from the expected values and a stochasticity due to the finite sampling. We now apply this method to one class of problems or systems we want to examine in this thesis, a bottleneck system.

2.2.3. Results: Bottleneck

Bottleneck problems can be found in various fields in physics. In a geometrical sense, such as in evacuation scenarios where agents need to pass through a narrow exit, also in the sense of a bottleneck in an energy landscape in the context of protein folding.

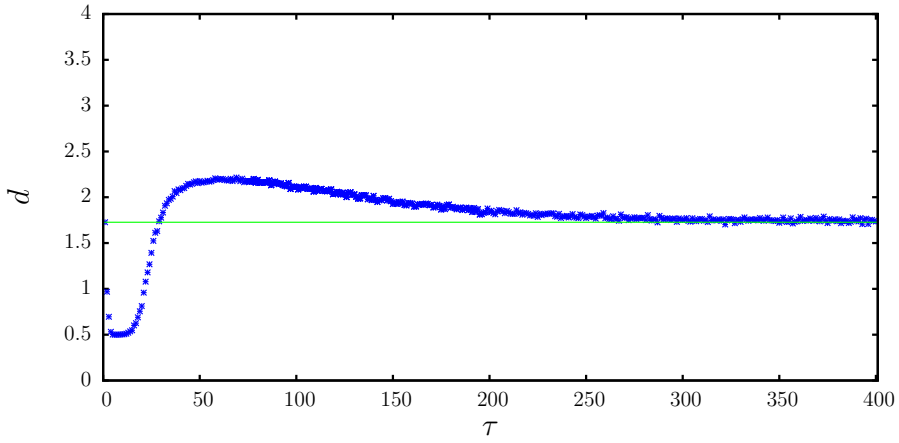

Figure 2.14.: Average distance to the centre of the box for high horizons in system with $L = 5$. [Distance averaged over 5000 steps after transient time 500 steps, initial position $(0, 0)$, sampled paths per step: 50000]

We find great importance and relevance in studying this class of problem and thus shall now examine the behaviour of a particle in a bottleneck-system. Figure 2.15 shows the system in which we let an entropically driven particle evolve. If not stated otherwise we will always consider a small box of size $s_x = s_y = 5$ and a large box $S_x = S_y = 21$ connected by a bottleneck of variable length l_{BN}. Since the larger box contains a larger area it is entropically more favorable to be occupied. The particle starts in the smaller (less favorable) box and starts moving around. If it is "smart" enough, it will move through the bottleneck into the big box. In general, as soon as a particle reaches the first field of the big box after the bottleneck (marked in grey in Fig. 2.15) the simulation is successful in entering the big box. It is most likely (despite the slight stochasticity of this sampling method) to remain in the large box.

Figure 2.16 shows the average time to reach the big box t_{fp} (a first passage time) for different horizons τ and bottleneck-lengths l_{BN}. Every data point is averaged over 1000 simulations. If a particle takes longer than 25000 steps to succeed, the whole set of simulations for those parameters counts as fail and no data point is shown. For $\tau = 1$, (so for a random walk) the particle succeeds for all bottleneck-lengths. Then there is a gap where only for $l_{BN} = 0$ the particle succeeds, the success-time increases with increasing τ up to $\tau = 4$. For $\tau > 4$ the success-time decreases and finally reaches a plateau. The magnitude of the plateau increases with longer l_{BN}. Close inspection of the curves for $l_{BN} \in \{0, 1, 2\}$ reveals that there is a shallow minimum. For $l_{BN} = 0$ this dip is at $\tau \simeq 15$, for $l_{BN} = 1$ at $\tau \simeq 20$ and for

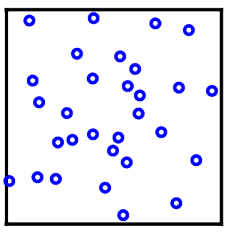

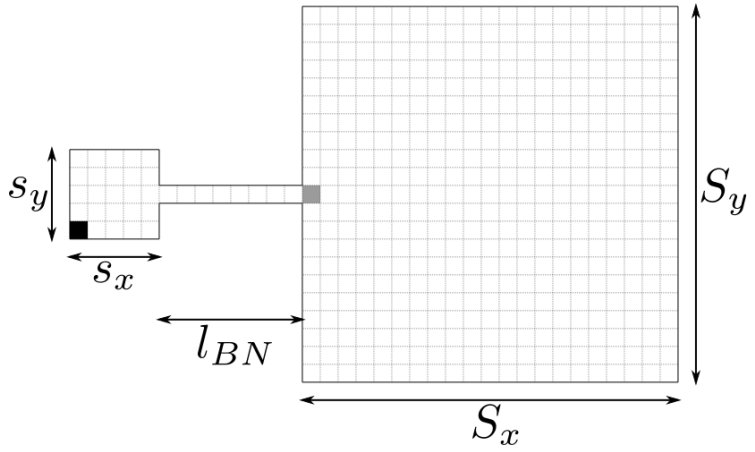

Figure 2.15.: Geometry of discrete bottleneck potential. Initial position of the particle is in the lower left corner of the small box, marked with a black field. Marked in grey is the field which in the following simulation needs to be reached for the particle to be counted as "reached the big box" or success.

$l_{BN} = 2$ at $\tau \simeq 23$. For simulations with $l_{BN} > 2$ there is an interval for $\tau > 1$ where success-times were larger than the simulation time. In this regime the particle feels the small box as favorable, more favorable than the bottleneck and simultaneously is too "short sighted" to perceive the big box. Therefore, it is reasonable to stay in the small box.

The small dip before finally converging, visible for short bottlenecks, originates from the same effects as we discussed previously: As soon as the horizon is large enough the corners are more favorable than the centre. Concerning the dip, first the particle would move towards the central area from where it easily enters the bottleneck. For a larger horizon the corners will be more favorable, causing the particle to move there with higher probability.

For large horizons at some point the particle will succeed when it can see far enough to rate the big box as more favorable. In general, the longer the bottleneck, the longer it takes the particle to succeed.

For $\tau = 1$ (the particle performs a random walk) we can calculate an analytical success time. For that, again the whole system can be translated into a Markovian process. See the appendix A.2 for details. The results together with the numerical results are shown in Fig. 2.17.

We find that first passage time linearly increases with l_{BN} and the analytical

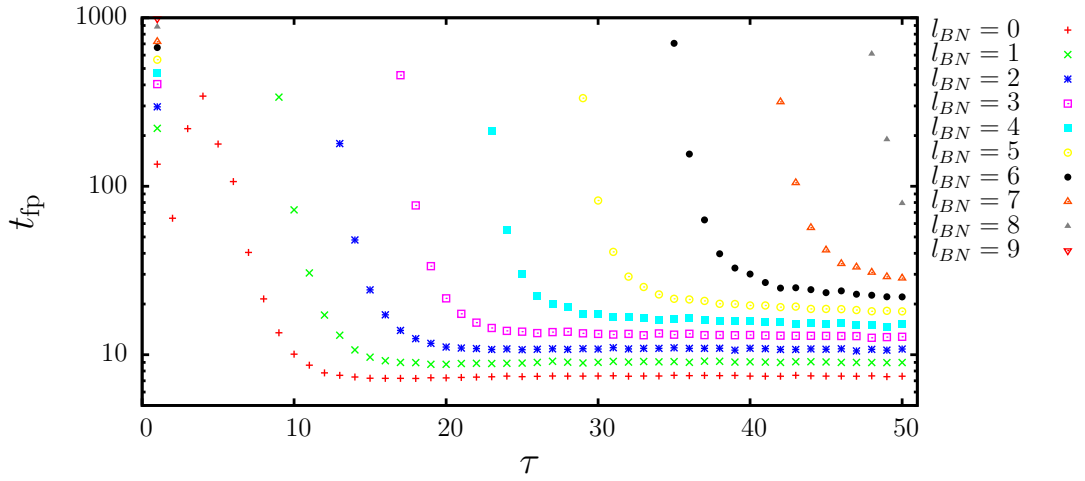

Figure 2.16.: Average time for a particle to reach the big box t_{fp} for different horizons τ and bottleneck-lengths l_{BN}. [Averaged over 1000 simulations, sampled paths per step: 50000, maximum runtime $t_{max} = 25000$]

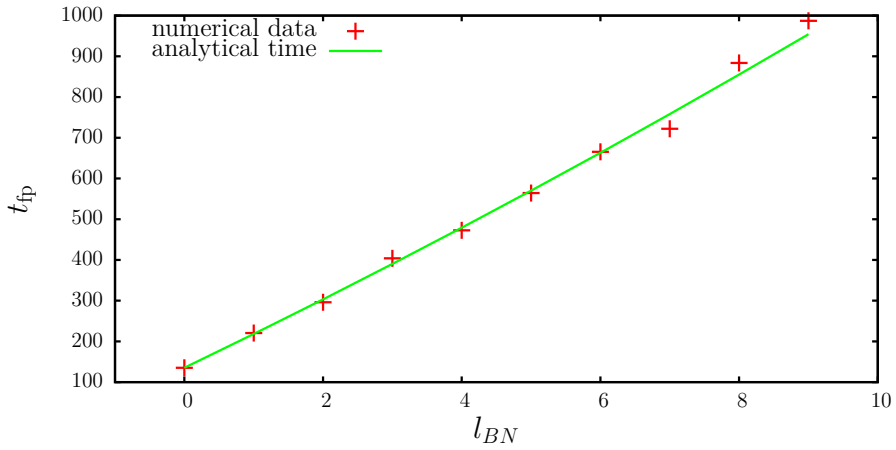

Figure 2.17.: Average time for a particle to reach the big box t_{fp} for horizon $\tau = 1$ (i.e a random walk) and different bottleneck-lengths l_{BN}. [Numerical data same as in Fig. 2.16: Averaged over 1000 simulations, sampled paths per step: 50000, maximum runtime $t_{max} = 25000$]

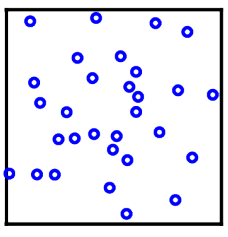

results (solid line) match well with the numerical data (crosses). For larger l_{BN} there is a deviation between the two curves which we ascribe to larger error bars in the numerical calculations.

For large horizon, in Fig. 2.16 the average first passage time into the big box t_{fp} reaches a plateau. Those times are shown in Fig. 2.18 together with the theoretical minimum number of steps necessary Clearly the theoretical minimum number of

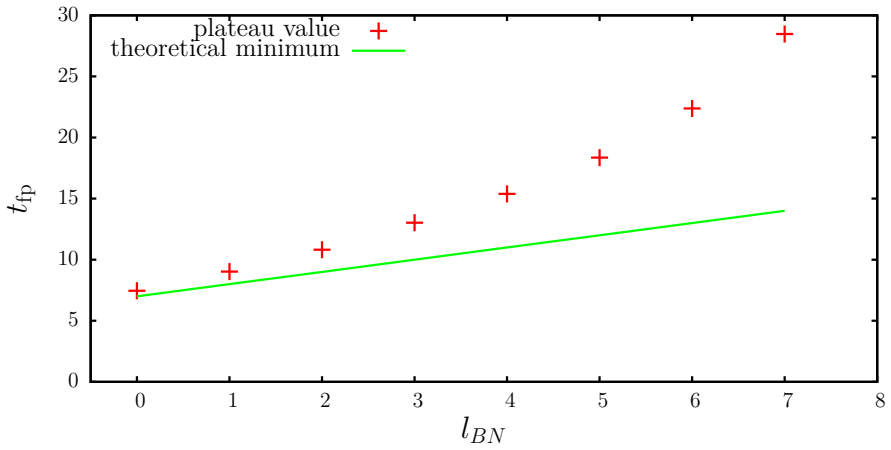

Figure 2.18.: Asymptotic time for a particle to reach the big box t^*_{fp} for large horizons versus bottleneck-length l_{BN}. [Data same as in Fig. 2.18, time averaged over all times after converging]

steps (crosses) increases linearly with l_{BN} with slope one. The ideal performance (line) is close to the minimum steps and increases for longer l_{BN}.

2.3. Conclusions

Using the first approach where we counted the number of possible sampling paths, we observed a particle moving towards the centre of a box or square lattice if the horizon was at minimum as large as half of the side length of the box. For smaller horizon it would keep τ steps distance from walls, performing a random walk within a square area around the centre. The average distance from the centre d for different system sizes L and horizons τ could be reproduced by a random-walk-based theoretical approach.

With the second appreach, counting the area covered by each sampling path, we observed a similar behaviour. However for a relatively large horizon around $\tau \approx L^2$

the particle finds the proximity of walls entropically favorable and thus moves towards the walls, until the horizon is large enough to fill the entire system. At this point the particle starts performing a random walk since all directions seem equivalent. Furthermore, we explored the first passage time of a particle in a bottleneck system. For a random walk a particle succeeded within finite time. For increasing τ first the particle would not succeed, then succeed with decreasing first passage times until it reached a plateau. Again we analytically calculated the behaviour for a random walk and obtained matching results. It is remarkable that for for small horizons a random walk produces the best success times. In this case of a small horizon the entropic approach makes the bottleneck "scary" to the particle.

In order to move to more general systems and including momentum, in the following section we derive an expression for the causal entropic force for a system with a continuous representation of space and time.

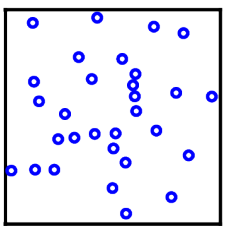

3. Continuous evolution: Theory

In this section we will first derive the equation for the entropic force in Sec. 3.1, we then discuss how to sample the path probabilities in Sec. 3.2 based on [3]. We then further explain and discuss the implementation in Sec. 3.3. In Sec. 3.4 we introduce the model and discuss some of its parameters.

3.1. Derivation of the causal entropic force

Consider the standard definition of entropic force $\mathbf{F}$ with respect to the present macrostate $\mathbf{X}_0$, that is, the state of the system including its environment

$$\mathbf{F}(\mathbf{X}_0) = T\boldsymbol{\nabla}_{\mathbf{X}} S(\mathbf{X})|_{\mathbf{X}_0} \,, \tag{3.1.1}$$

with reservoir temperature T and entropy S of the macrostate $\mathbf{X}$.

Now, we define the causal path entropy S_c of macrostate $\mathbf{X}$ on the set of all possible paths through phase space within a finite time τ:

$$S_c(\mathbf{X}, \tau) = -k_{\mathrm{B}} \int \Pr(\mathcal{X}_\tau|\mathbf{x}(0)) \ln \left[\Pr(\mathcal{X}_\tau|\mathbf{x}(0))\right] \mathcal{D}\mathcal{X}_\tau \,, \tag{3.1.2}$$

with conditional probability $\Pr(\mathcal{X}_\tau|\mathbf{x}(0))$ of the occurence of a path $\mathcal{X}_\tau$ starting from the initial (micro)state or position in phase space $\mathbf{x}(0)$, where k_{B} is Boltzmann's constant and

$$\Pr(\mathcal{X}_\tau|\mathbf{x}(0)) = \int_{\xi_\tau} \Pr(\mathcal{X}_\tau, \xi_\tau|\mathbf{x}(0)) \mathcal{D}\xi_\tau \,, \tag{3.1.3}$$

that is, the conditional probability of a path $\mathcal{X}_\tau$ is determined by the integral over all possible evolutions of the open system's environment ξ_τ during the time interval τ. The integrals in Eq. (3.1.2) and (3.1.3) are path integrals.

The entropic force can then be rewritten

$$\mathbf{F}_c(\mathbf{X}_0, \tau) = T_c \boldsymbol{\nabla}_{\mathbf{X}} S_c(\mathbf{X}, \tau)|_{\mathbf{x}_0} \tag{3.1.4}$$

where T_c is the causal path temperature which determines the amplitude of the force and therefore the tendency of the system to evolve towards states of higher causal entropy. In the following we will refer to causal entropic force $\mathbf{F}_c$ simply as force $\mathbf{F}$ and causal (path) entropy S_c as entropy S for the sake of simplicity. If we restrict ourselves to position-space coordinates $q_j(0)$ we can express the force in the following way:

$$F_j(\mathbf{X}_0, \tau) = T_c \frac{\partial S_c(\mathbf{X}, \tau)}{\partial q_j(0)}\bigg|_{\mathbf{x}_0} , \tag{3.1.5}$$

and using Eq. (3.1.2)

$$\begin{aligned} F_j(\mathbf{X}_0, \tau) &= -T_c k_{\mathrm{B}} \frac{\partial}{\partial q_j(0)} \int \Pr(\mathcal{X}_\tau|\mathbf{x}(0)) \ln\big[\Pr(\mathcal{X}_\tau|\mathbf{x}(0))\big] \mathcal{D}\mathcal{X}_\tau \qquad (3.1.6) \\ &= -T_c k_{\mathrm{B}} \int \frac{\partial}{\partial q_j(0)} \Pr(\mathcal{X}_\tau|\mathbf{x}(0)) \ln\big[\Pr(\mathcal{X}_\tau|\mathbf{x}(0))\big] \mathcal{D}\mathcal{X}_\tau \\ &= -T_c k_{\mathrm{B}} \int \frac{\partial \Pr(\mathcal{X}_\tau|\mathbf{x}(0))}{\partial q_j(0)} \ln\big[\Pr(\mathcal{X}_\tau|\mathbf{x}(0))\big] + \\ &\qquad \Pr(\mathcal{X}_\tau|\mathbf{x}(0)) \cdot \left[\frac{1}{\Pr(\mathcal{X}_\tau|\mathbf{x}(0))} \cdot \frac{\partial \Pr(\mathcal{X}_\tau|\mathbf{x}(0))}{\partial q_j(0)}\right] \mathcal{D}\mathcal{X}_\tau \\ &= -T_c k_{\mathrm{B}} \Bigg\{ \int \frac{\partial \Pr(\mathcal{X}_\tau|\mathbf{x}(0))}{\partial q_j(0)} \ln\big[\Pr(\mathcal{X}_\tau|\mathbf{x}(0))\big] \mathcal{D}\mathcal{X}_\tau + \\ &\qquad \underbrace{\int \frac{\partial \Pr(\mathcal{X}_\tau|\mathbf{x}(0))}{\partial q_j(0)} \mathcal{D}\mathcal{X}_\tau}_{=0} \Bigg\} \qquad (3.1.7) \\ &= -T_c k_{\mathrm{B}} \int \frac{\partial \Pr(\mathcal{X}_\tau|\mathbf{x}(0))}{\partial q_j(0)} \ln\big[\Pr(\mathcal{X}_\tau|\mathbf{x}(0))\big] \mathcal{D}\mathcal{X}_\tau \, . \qquad (3.1.8) \end{aligned}$$

We can assume deterministic behaviour within one interval $[t, t+\epsilon]$. Therefore a conditional path probability can be decomposed into the probabilities of its intervals in the following way:

$$\Pr(\mathcal{X}_\tau|\mathbf{x}(0)) = \left[\prod_{n=1}^{N} \Pr(\mathcal{X}_\epsilon|\mathbf{x}(t_n))\right] \Pr(\mathcal{X}_\epsilon|\mathbf{x}(0)) \, , \tag{3.1.9}$$

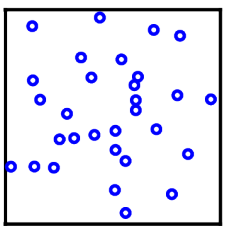

where $\mathcal{X}_\epsilon$ denotes a path of length ϵ (starting from whichever initial conditions are given) and $\tau = N\epsilon$. Accordingly, we can express the gradient of the probability as

$$\frac{\partial \Pr(\mathcal{X}_\tau|\mathbf{x}(0))}{\partial q_j(0)} = \left[\prod_{n=1}^{N} \Pr(\mathcal{X}_\epsilon|\mathbf{x}(t_n))\right] \frac{\partial \Pr(\mathcal{X}_\epsilon|\mathbf{x}(0))}{\partial q_j(0)} \tag{3.1.10}$$

Since $\mathcal{X}_\epsilon$ can be seen as the path from $q_j(0)$ to $q_j(\epsilon)$ in one step, the gradient in probability of jumping from $\mathbf{x}(0)$ to $\mathbf{x}(\epsilon)$ with respect to $q_j(0)$ is equal to the negative gradient in probability of jumping from $\mathbf{x}(0)$ to $\mathbf{x}(\epsilon)$ with respect to $q_j(\epsilon)$:

$$\frac{\partial \Pr(\mathcal{X}_\epsilon|\mathbf{x}(0))}{\partial q_j(0)} = -\frac{\partial \Pr(\mathcal{X}_\epsilon|\mathbf{x}(0))}{\partial q_j(\epsilon)} \tag{3.1.11}$$

Now, by choosing the ϵ sufficently smaller than and spatial or kinetic variation of the internal forces $h(x)$

$$\epsilon \ll \sqrt{\frac{m_j}{|\boldsymbol{\nabla}_{\mathbf{q}(0)} h_j(\mathbf{x}(0))|}}\,, \tag{3.1.12}$$

$$\epsilon \ll \frac{1}{|\boldsymbol{\nabla}_{\mathbf{p}(0)} h_j(\mathbf{x}(0))|}\,, \tag{3.1.13}$$

we can reasonably Taylor expand and express the position $q_j(\epsilon)$ as follows:

$$q_j(0) = q_j(0) + \frac{p_j(0)}{2m_j}\epsilon + \frac{f_j(0) + h_j(0)}{2m_j}\epsilon^2\,, \tag{3.1.14}$$

where $f_j(t)$ denotes a random Gaussian force with

$$\langle f_j(t)\rangle = 0 \tag{3.1.15}$$

$$\langle f_j(t) f_{j'}(t')\rangle = \frac{m_j k_\mathrm{B} T_r}{\epsilon^2}\delta_{ij}\delta(t-t')\,, \tag{3.1.16}$$

and where $\delta(t)$ is the Dirac δ-function, and δ_{ij} is the Kronecker delta. Thus we find

that $\Pr(\mathcal{X}_\epsilon|\mathbf{x}(0))$ is Gaussian in $q_j(\epsilon)$. Therefore we can write

$$\Pr(\mathcal{X}_\epsilon|\mathbf{x}(0)) \sim \exp\left(-\frac{1}{2}\frac{(q_j(\epsilon)-\langle q_j(\epsilon)\rangle)^2}{\langle q_j^2(\epsilon)\rangle - \langle q_j(\epsilon)\rangle^2}\right) \tag{3.1.17}$$

$$\Rightarrow \frac{\partial \Pr(\mathcal{X}_\epsilon|\mathbf{x}(0))}{\partial q_j(\epsilon)} = \frac{q_j(\epsilon)-\langle q_j(\epsilon)\rangle}{\langle q_j^2(\epsilon)\rangle - \langle q_j(\epsilon)\rangle^2}\Pr(\mathcal{X}_\epsilon|\mathbf{x}(0))$$

$$= \frac{2f_j(0)}{k_\mathrm{B}T_r}\Pr(\mathcal{X}_\epsilon|\mathbf{x}(0))\ . \tag{3.1.18}$$

Using this last result Eq. (3.1.11) takes the form

$$\frac{\partial \Pr(\mathcal{X}_\tau|\mathbf{x}(0))}{\partial q_j(0)} = \left[\prod_{n=1}^{N}\Pr(\mathcal{X}_\epsilon|\mathbf{x}(t_n))\right]\frac{2f_j(0)}{k_\mathrm{B}T_r}\Pr(\mathcal{X}_\epsilon|\mathbf{x}(0))\ . \tag{3.1.19}$$

With (3.1.8) we then obtain

$$F_j(\mathbf{X}_0,\tau) = -\frac{2T_c}{T_r}\int f_j(0)\Pr(\mathcal{X}_\tau|\mathbf{x}(0))\ln\left[\Pr(\mathcal{X}_\tau|\mathbf{x}(0))\right]\mathcal{D}\mathcal{X}_\tau. \tag{3.1.20}$$

Once we find a way to estimate the probabilites $\Pr(\mathcal{X}_\tau|\mathbf{x}(0))$ we can explicitly compute the causal entropic force $F_j(\mathbf{X}_0,\tau)$.

3.2. Sampling of path probabilities

We use M Brownian trajectories through phase space to sample $\Pr(\mathcal{X}_\tau|\mathbf{x}(0))$ with a finite time horizon τ. Every sampling trajectory starts from the current system state $\mathbf{x}(0)$. A phase space volume is assigned to each sampling trajectory:

$$\Omega_i \sim \frac{1}{\Pr(\mathcal{X}_{\tau,i}|\mathbf{x}(0))}\ , \tag{3.2.1}$$

assuming a uniform probability for all paths within a neighbourhood of a sampled path $\mathcal{X}_{\tau,i}$, $i<M$. The normalization condition implies

$$\sum_i^M \Omega_i \Pr(\mathcal{X}_{\tau,i}|\mathbf{x}(0)) = 1 \quad \Rightarrow \quad \Omega_i = \frac{1}{M\Pr(\mathcal{X}_{\tau,i}|\mathbf{x}(0))}. \tag{3.2.2}$$

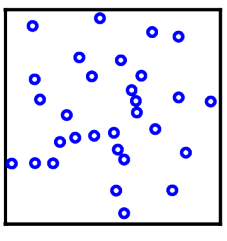

Thus, our estimate of the force in Eq. (3.1.20) is

$$F_j(\mathbf{X}_0,\tau) = -\frac{T_c}{T_r}\int f_j(0)\Pr(\mathcal{X}_\tau|\mathbf{x}(0))\ln\Big[\Pr(\mathcal{X}_\tau|\mathbf{x}(0))\Big]\mathcal{D}\mathcal{X}_\tau \tag{3.2.3}$$

$$\begin{aligned}
&\approx -\frac{2T_c}{T_r}\left\langle \sum_i f_{ij}(0)\frac{1}{M\Omega_i}\ln\left(\frac{1}{M\Omega_i}\right)\Omega_i\right\rangle \\
&=\frac{2T_c}{T_rM}\left\langle \sum_i f_{ij}(0)\ln(M\Omega_i)\right\rangle \\
&=\frac{2T_c}{T_rM}\left\{\underbrace{\left\langle \sum_i f_{ij}(0)\ln(M)\right\rangle}_{=0}+\left\langle \sum_i f_{ij}(0)\ln(\Omega_i)\right\rangle\right\} \\
&=\frac{2T_c}{T_rM}\left\langle \sum_i f_{ij}(0)\ln(\Omega_i)\right\rangle ,
\end{aligned} \tag{3.2.4}$$

now we add a vanishing term,

$$F_j(\mathbf{X}_0,\tau) =\frac{2T_c}{T_rM}\left\{\left\langle \sum_i f_{ij}(0)\ln(\Omega_i)\right\rangle - \left\langle \ln\langle\Omega_i\rangle\cdot\sum_i f_{ij}(0)\right\rangle\right\} \tag{3.2.5}$$

$$\begin{aligned}
&=\frac{2T_c}{T_rM}\left\langle \sum_i \Big(f_{ij}(0)\ln(\Omega_i)\Big) - \sum_i \Big(f_{ij}(0)\ln\langle\Omega_i\rangle\Big)\right\rangle \\
&=\frac{2T_c}{T_rM}\left\langle \sum_i \Big\{f_{ij}(0)\ln(\Omega_i) - f_{ij}(0)\ln\langle\Omega_i\rangle\Big\}\right\rangle \\
&=\frac{2T_c}{T_rM}\left\langle \sum_i \Big\{f_{ij}(0)\Big(\ln(\Omega_i) - \ln\langle\Omega_i\rangle\Big)\Big\}\right\rangle \\
&=\frac{2T_c}{T_rM}\left\langle \sum_i f_{ij}(0)\ln\left(\frac{\Omega_i}{\langle\Omega_{i'}\rangle}\right)\right\rangle .
\end{aligned} \tag{3.2.6}$$

Many possible choices are available to quantify the phase space volume Ω_i of the sampling trajectories. We choose the radius of gyration:

$$\mathcal{R}_i \equiv \Omega_i = R^2_{\mathrm{gyr},i} = \frac{1}{N}\sum_{k=1}^{N}(\mathbf{r}_k - \mathbf{r}_{\mathrm{mean}})^2 , \tag{3.2.7}$$

with $N = \frac{\tau}{\delta t}$ the number of steps per sampling path. It contains the information of how elongated a trajectory is. Statistically speaking, closer to an obstacle trajectories will be more "folded" and shorter, causing a smaller $\mathcal{R}$. In open space however

the trajectory is more likely to be elongated, causing a larger $\mathcal{R}$. The information about proximity of obstacles is conserved under this choice of phase space discretization, and therefore it retains the relevant information required by our investigations. The Gaussian noise of the sampling trajectory for time $t = 0$ is given by $f_{ij}(0)$, that is the force applied on the particle during its first step.

Effectively the entropic force is calculated by letting non-interacting Brownian particles evolve through phase space for a fixed duration τ, then weigh their first step using its phase space volume $\mathcal{R}$. The first step is determined by the initial position in phase space and the random Brownian force applied to the particle $f_{ij}(0)$. In the end we take the sum over all weighted first steps. This is schematically shown in Fig. 3.1 with the first step in the small ellipse and what is used for calculating $\mathcal{R}$ in the large ellipse.

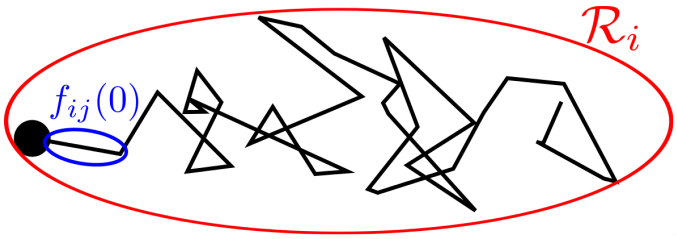

Figure 3.1.: Schematic of a sampling trajectory with first step (small blue ellipse) and part used as weight marked in large red ellipse.

Figure 3.2(a) shows an example of a sampling trajectory close to a wall. It encounters an obstacle, such as as wall, and is therefore more likely to cross its own previous steps again. Statistically it will be more compressed, producing a smaller $\mathcal{R}$ and resulting in weighting the first step $f_{ij}(0)$ towards an obstacle less than a step towards open space. This in total will generate a force directed away from the obstacle.

3.2.1. Connection between sampling trajectory and polymers

An ideal polymer chain experiences a force between its two ends

$$\langle \vec{f} \rangle = -k_{\mathrm{B}} T \frac{3\langle \vec{R} \rangle}{N l^2} \,, \tag{3.2.8}$$

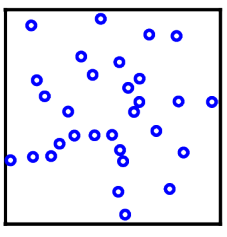

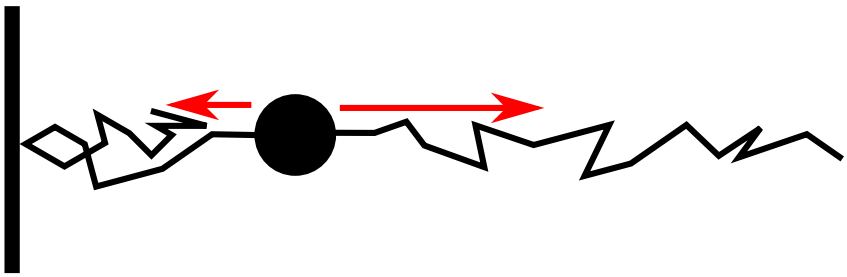

(a)

Figure 3.2.: Sketch of a particle close to a wall with two exemplary sampling paths. The path towards the wall is reflected and in total more compressed compared to the path towards the right without any restricted areas. The latter one has a larger radius of gyration and is therefore weighted stronger. In total this generates a force away from the wall.

where T is the temperature of the chain, $\vec{R}$ is the distance between the two ends of the polymer with N chain segments, each of length l. This force originates from the polymers bias towards states of larger conformational entropy, caused by thermal fluctuations acting on its chain segments. Thus, similar to a sampling trajectory generating a force away from a restriction, a polymer under spatial confinement statistically will expand and thereby exert a force onto the confinement pushing itself away from it [17–19]. We can interpret a sampling trajectory, consisting of $N = \frac{\tau}{\delta t}$ uncorrelated random steps an a non-self-avoiding ideal chain of N freely jointed segments – an ideal polymer. Thus an (causal) entropically driven particle can be viewed as a particle with a number of ideal polymers attached to it (see Fig. 3.3(b)), being repelled by any restricted area.

We use this analogy in Sec. 4.6 where we compare results of an experiment with DNA molecules with results of simulations with equivalent setup.

3.2.2. Position- and momentum-space – $F_{\mathcal{P}}$ and $F_{\mathcal{M}}$

The phase spaces of most systems in this thesis consists of two position and two momentum dimensions per particle. We decided to examine those two cross-sections of phase space of the sampling trajectories seperately and analyse their effects on the evolution of the system. If we explicitly refer to the radius of gyration for a certain set of dimensions, position or momentum, we will add this information as an index $\mathcal{R}_{\mathcal{P}}$ and $\mathcal{R}_{\mathcal{M}}$, respectively. Accordingly, if we distinguish between simulations

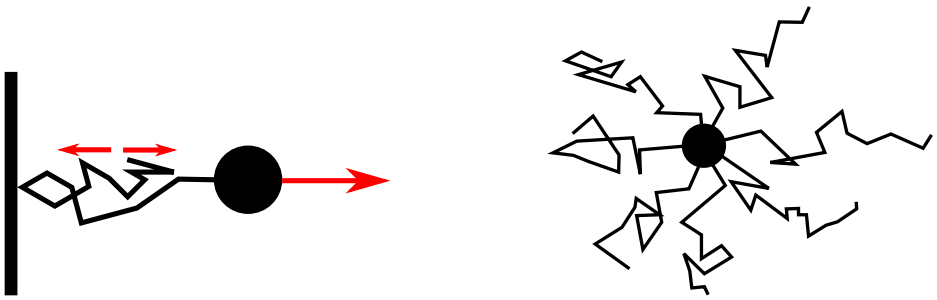

(a) (b)

Figure 3.3.: (a) Sketch of a particle close to a wall with a sampling path compressed at the wall. In analogy to samplings paths as polymers, two arrows indicate the expansion of the polymer, thus generating a force away form the wall. (b) Sketch of a particle with several sampling trajectories.

where we use the entropic force calculated using position- and momentum-space and refer to them as $F_{\mathcal{P}}$ and $F_{\mathcal{M}}$, respectively.

For position-space the radius of gyration $\mathcal{R}_{\mathcal{P}}$ is intuitive since it is equivalent to the moment of inertia. The set of positions between two steps can be viewed as a number of point particles of equal mass and the moment of inertia is taken relative to the centre of mass, that is, the average position of all points. The more spread out a trajectory and therefore its steps or positions, the larger $\mathcal{R}_{\mathcal{P}}$, the larger the weight for the first step of this particular trajectory.

However, in momentum-space $\mathcal{R}_{\mathcal{M}}$ will show reciprocal behaviour. After a collision with an obstacle the orthogonal part of the momentum will be inverted, causing the data points to be spread out in phase space. Figure 3.4 shows an example of two trajectories experiencing the same sequence of Gaussian noise, one with a reflection, the other without. Both position and momentum-space are shown. Figure 3.4(a) shows the position of a moving particle in an open environment while in Fig. 3.4(b) its momentum is given. Figure 3.4(c) shows the evolution of a particle colliding with a wall which is illustrated as a vertical black line. Its momentum-space in Fig. 3.4(d) shows a large horizontal jump from negative to positive values as the collision occurs. Please note that the lines do not indicate the actual trajectory of the particle but connects the coordinates between two consecutive timesteps. This is the reason why in Fig. 3.4(c) it might seem as if the particle did not touch the wall.

In momentum-space, collisions with an obstacle will dramatically increase $\mathcal{R}_{\mathcal{M}}$.

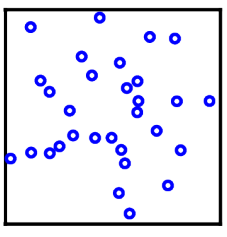

For open space where with no or few collisions the points will be rather close to each other resulting in a small $\mathcal{R}$. Given our choice of radius of gyration as method for quantification of the phase space volume, in the following for momentum-space the calculated force will be inverted. Thereby an obstacle will statistically cause large $\mathcal{R}_\mathcal{M}$ thus having resulting in a repulsive effect on driven particles.

Generally a trajectory with large $\mathcal{R}_\mathcal{P}$ will produce relatively small $\mathcal{R}_\mathcal{M}$ and vice versa.

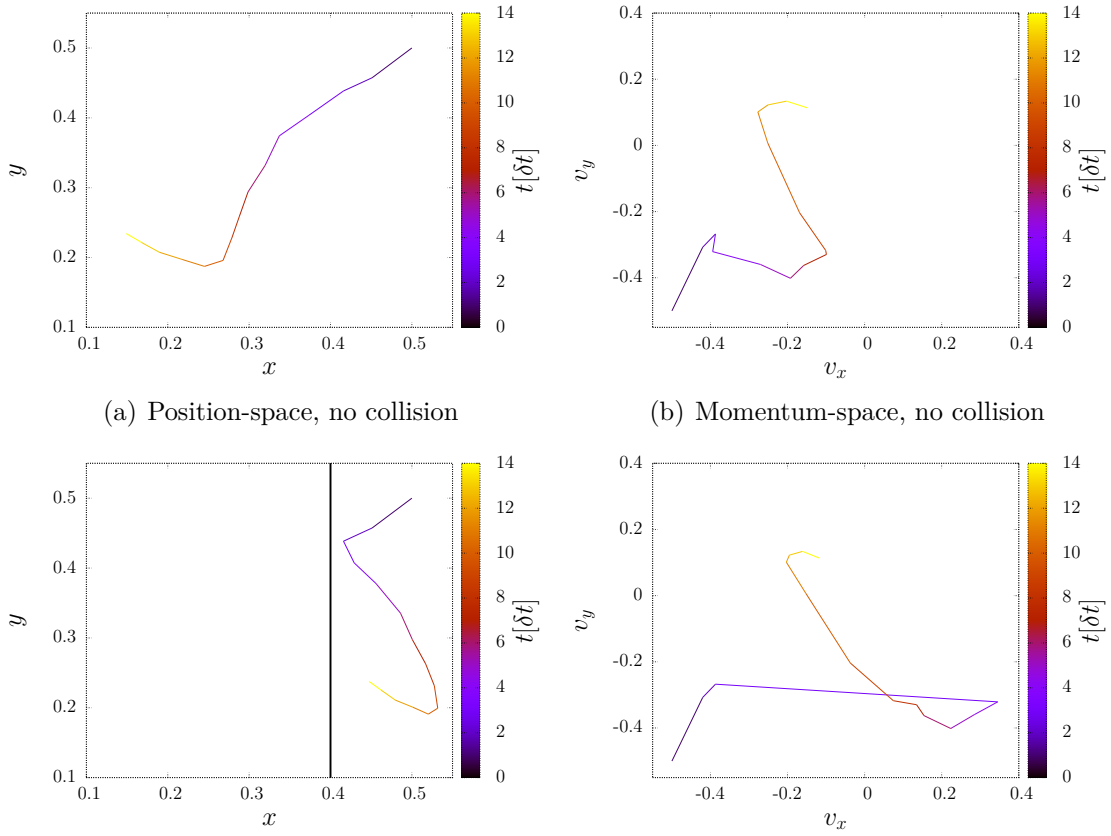

(a) Position-space, no collision

(b) Momentum-space, no collision

(c) Position-space, collision

(d) Momentum-space, collision

Figure 3.4.: Position-(a),(c) and momentum-space (b),(d) of two trajectories, (a),(b) in an open environment and (c),(d) experiencing a collision with a wall.

3.3. Implementation of the method

The Brownian trajectories used for sampling obey the Langevin equation

$$m\dot{\vec{v}} = -\gamma\vec{v} + \xi(t) + h(\vec{x}) \ , \tag{3.3.1}$$

where $\xi(t)$ is a Gaussian noise, $h(\vec{x})$ represents the walls or other external forces and the mass $m = 1$. Again, the two relevant quantities of each sampled trajectory are the first step containing the information of direction and the radius of gyration of the whole trajectory used to weight the first step. The total number of steps per sampling trajectory $n = \tau/\delta t$ needs to be large enough such that the environment will be sufficiently explored. At the same time n cannot be arbitrarily large for the follwing reasons. Statistically, a first step of a sampling trajectory towards a wall will always result in a smaller $\mathcal{R}_{\mathcal{P}}$, causing a repulsion. Upon increasing n, the influence of the first step decreases thus requiring more sampled trajectories in order to observe statistical effects, that is, a repulsive force away from restricted areas. In this thesis we let a sampling trajectory explore the environment with the total of $n = 15$ steps, $\tau = 1.5$, $\delta t = 0.1$. For exploration of a large area this comparably small number of steps can be compensated through spatially large steps. In order to maintain an accurate interaction with the walls despite large steps, in case of a collision a step will be divided into smaller steps.

Figure 3.5 shows a sampling of an environment with every trajectory behaving according to Eq. (3.3.1). Illustrated are 500 sampling trajectories of a point particle close to a wall, that is, the initial position of every trajectory close to a wall. The colour bar parametrizes time along the trajectory. Trajectories facing the wall are more likely to be shorter, resulting in a smaller $\mathcal{R}_{\mathcal{P}}$ and in total will produce a repulsion from the wall. Thus the entropic force will be directed away from the wall. In order to get a qualitative idea of how the force depends on the distance from an obstacle we show in Fig. 3.6 the force on a particle generated by an infinitely long wall. The qualitative behaviour for this geometry is of interest. We calculate the entropic force resulting from taking into account only the position subspace of phase space $\mathcal{P}$, or the momentum subspace $\mathcal{M}$. We also consider the components of the entropic force parallel and perpendicular to the walls. The forces $F_{\mathcal{P}\parallel}$ and $F_{\mathcal{M}\parallel}$ are zero for all values of distance from the wall.

For large distances all forces considered vanish, while closer to the origin $F_{\mathcal{P}\perp}$ and $F_{\mathcal{M}\perp}$ have smooth maxima indicating a repulsive force. Close to the wall there is a

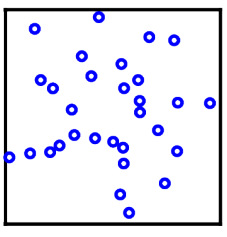

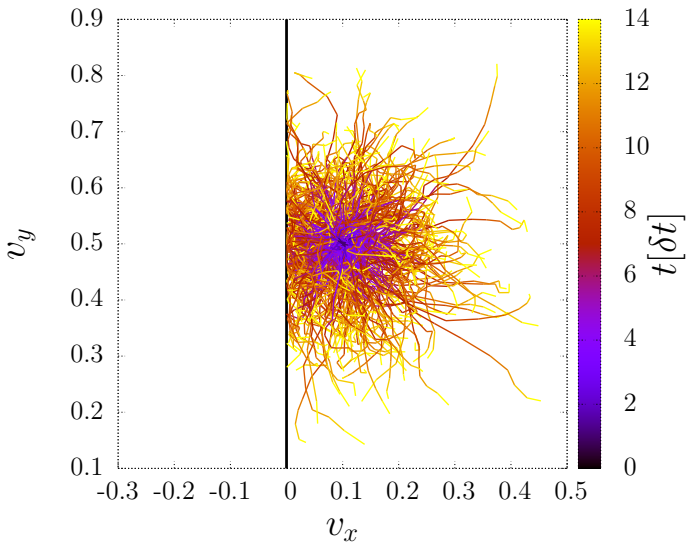

(a)

Figure 3.5.: 500 sampling trajectories for a particle close to a wall with initial position (0.1,0.5)

small regime of attraction to the wall, until for distances almost zero also $F_{\mathcal{P}\perp}$ and $F_{\mathcal{M}\perp}$ become zero (see Fig. 3.6(b) for an enlarged view).

The behaviour $\lim_{d\to\infty} F = 0$ is expected, since as soon as an obstacle is further away than the extent of the area covered by the sampling paths, it is not detected, hence it cannot influence the particle. The repulsion is also as expected: Trajectories are effectively shortened by the constrains imposed by the wall causing the repulsion.

The vanishing force for the particle close to the wall is also easily explained. For a particle right at the wall all of its sampling trajectories will take their first step away from the wall. If the first step is towards the wall, it is reflected immediately, which is equivalent to a first step away from the wall. Statistically the following steps of each trajectory will be the same causing the calculated entropic force to cancel out.

Concerning the small attractive regime for $d \leq 0.05$ we observe an effect similar to what we discussed in Sec. 2.2.2 with a particle on a square lattice preferring the edges of the system for large horizons. In a continuous system for a particle sufficiently close to a wall the radius of gyration of sampling trajectories with first steps towards the wall will statistically be larger. Assuming that the radius of gyration is smallest if the sampling trajectory crosses itself at around $\tau/2$, the proximity of a wall will restrict the number of such $\tau/2$-stage crossings. Close to a wall, in direction towards

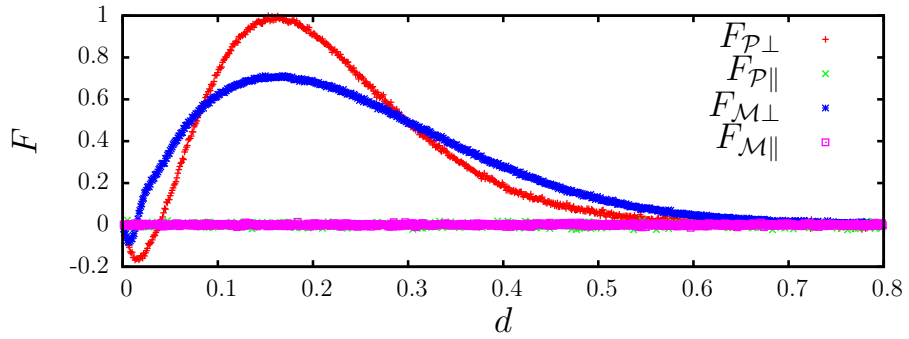

(a)

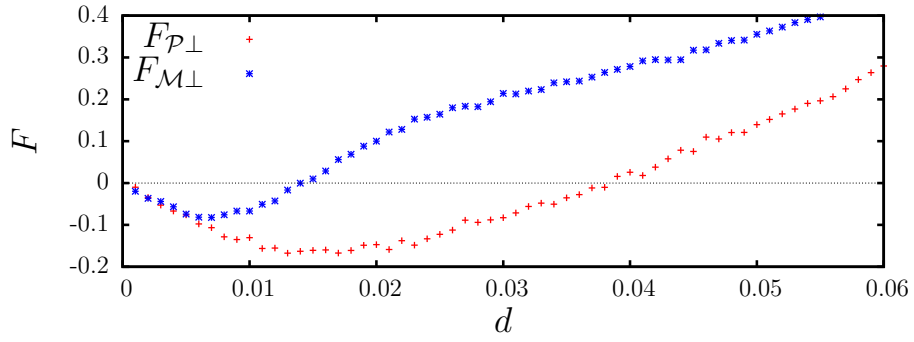

(b) magnification of (a) close to the origin

Figure 3.6.: Entropic force calculated using position-space and momentum-space of sampling trajectories, respectively, depending on distance to an infinte wall. The force parallel to the walls is fluctuating around zero. [Averaged over 10^6 trajectories, $\gamma = \frac{0.25}{\delta t}$, $\tau = 1.5$, $\delta t = 0.1$. Force was normalized to have its maximum value at 1.]

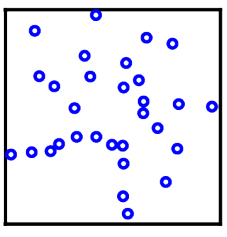

it no such crossing can occur since the sampling trajectory would be reflected or move along the wall (see Fig. 3.7(a)). However in free space such crossings can occur towards any direction (see Fig. 3.7(b)). The wall eliminating this event thus lets $\mathcal{R}$ of trajectories with first steps towards it statistically be larger. We conclude therefore that very close to a wall the entropic force will be weakly attractive.

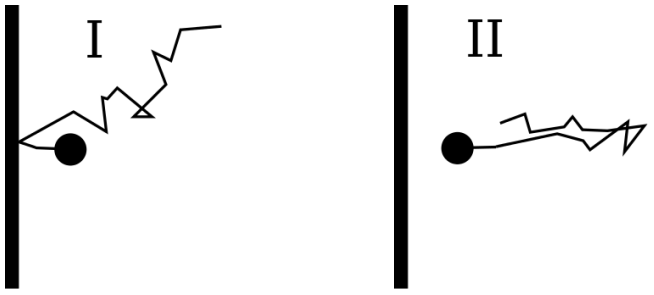

(a) (b)

Figure 3.7.: Schematic of two sampling trajectories of a particle close to a wall with (a) the first step towards the wall and (b) the first step away.

3.4. Model equation

In this section we will give illustrative evolutions of entropically driven particles and discuss their dependence on the temperatures T_r and T_c.

After calculating the entropic force we can apply it to the driven particle according to the following equation of motion

$$m\dot{\vec{v}} = -\gamma\vec{v} + \vec{F}_C(t) + h(\vec{x}) \ , \tag{3.4.1}$$

as introduced in the previous section with drag γ, mass $m = 1$ and walls and system forces $h(\vec{x})$. We replace the Gaussian noise with the entropic force $\vec{F}_C(t)$. We can now let an entropically driven particle run freely in a system. Figure 3.8(a) shows an entropically driven particle in a box using momentum-space for calculating the entropic force. In Fig. 3.8(b) a set of sampling trajectories is shown. The driven particle in Fig. 3.8(a) moves straight towards the centre of the box where it then stays. It successfully detects the walls and moves away from them, ultimately finding the most favorable position in the centre of the box. Figure 3.9 shows two trajectories with different T_r.

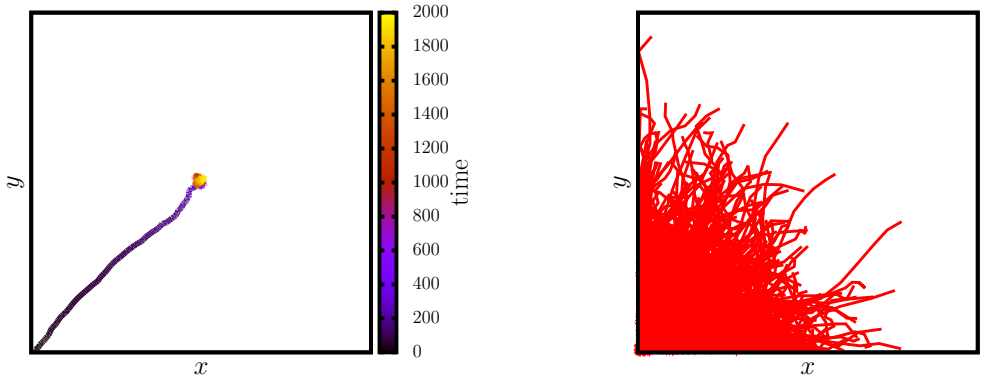

(a) (b) Sampling trajectories for the initial position

Figure 3.8.: (a): A particle in a box, using momentum-space of sampling trajectories for calculating the entropic force. (b): Sampling trajectories for the initial position. [$T_r = 0.02$, $\frac{T_c}{T_r} = 1.25$, $L = 1$, $\delta t = 0.1$, $\tau = 1.5$, $\gamma = \frac{0.25}{\delta t}$, initial position $(0.1, 0.1)$, using momentum-space]

In order to develope an intuition of the influence of the parameters T_r and $\frac{T_c}{T_r}$, we will examine the qualitative change in behaviour by varying those parameters indepentently, while keeping all other parameters fixed.

3.4.1. Influence of T_r

We put a particle in a box of size $L = 1$ with initial position $(0.1, 0.1)$ and let it evolve according to Eq. (3.4.1). Figure 3.9(a) shows a simulation with $T_r = 0.005$ and Fig. 3.9(b) with $T_r = 0.015$. Sampling paths from the initial position are given in the small insets. In both cases the particle starts moving straight away from the corner. For $T_r = 0.005$ at $t = 250$ it starts to move upwards in a diffusive manner. For $T_r = 0.015$ it reaches the centre and moves in the same manner diffusive manner around it. In Fig. 3.9(a) the particle moves away from the walls until the sampling trajectories do not reach them anymore and therefore do not produce any repulsion. The particle then performs a random walk staying at a minimum distance from the walls at all times. The particle in Fig. 3.9(b) has a T_r large enough so that its sampling trajectories are sufficiently long to keep the particle relatively confined in the centre, at maximum distance from all walls. Figure 3.10(a) shows the average net displacement $\langle d_{net} \rangle = \langle |\vec{r}(\tau) - \vec{r}(0)| \rangle$ of a sampling trajectory depending on T_r. The average net distance of a sampling path scales with its average travelled distance. Therefore we conclude that the distance from which a particle is able to

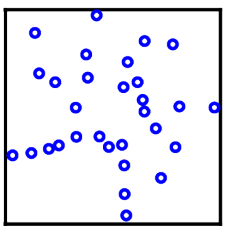

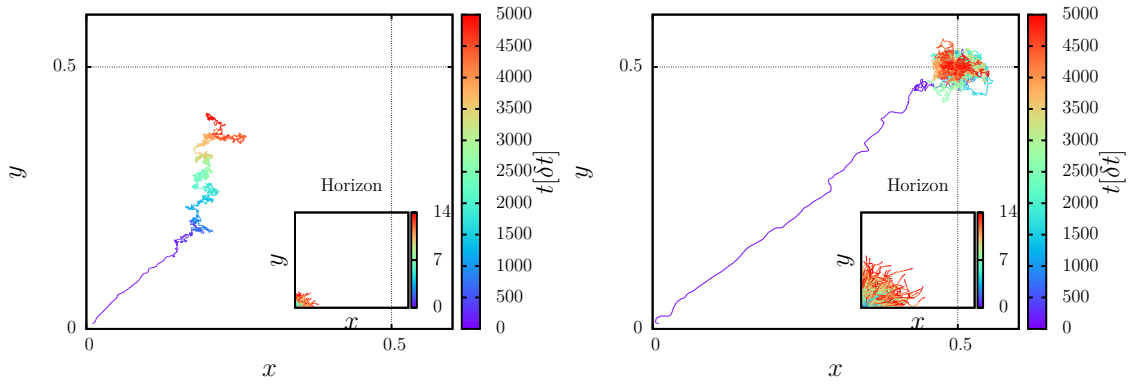

(a) $T_r = 0.005$ (b) $T_r = 0.015$

Figure 3.9.: A particle in a box for (a): $T_r = 0.005$ and (b): $T_r = 0.015$. The dotted lines mark the centre of the box. [$\frac{T_c}{T_r} = 10$, $L = 1$, $\delta t = 0.1$, $\tau = 1.5$, $\gamma = \frac{0.25}{\delta t}$, initial position $(0.1, 0.1)$, using $F_{\mathcal{M}}$]

detect the walls depends linearly on T_r. Figure 3.10(b) shows an exemplary set of sampling paths.

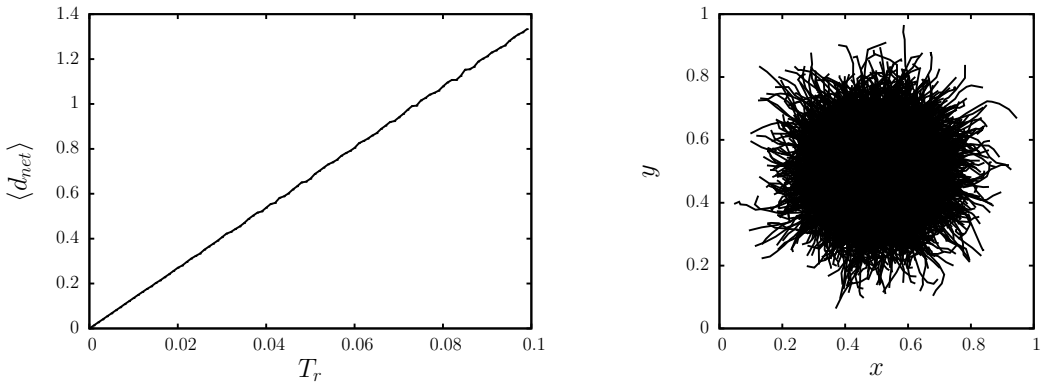

(a) (b) $T_r = 0.01$

Figure 3.10.: (a): Average end to end distance of a sampling trajectory depending on T_r. b): Sampling paths for $T_r = 0.01$. [sampled paths per data point: 10000, $\delta t = 0.1$, $\tau = 1.5$, $\gamma = \frac{0.25}{\delta t}$]

3.4.2. Influence of T_c/T_r

We also consider the influence of T_c through the dimensionless number $\frac{T_c}{T_r}$ as it appears in Eq. (3.2.6). Figure 3.11(a) shows a particle in box for $\frac{T_c}{T_r} = 1$ which

moves towards the centre where it stays relatively confined. Figure 3.11(b) shows the same system for $\frac{T_c}{T_r} = 30$ which also moves towards the centre, but it has comparably larger steps and is not as confined to the centre as in Fig. 3.11(a). It experiences a stronger entropic force.

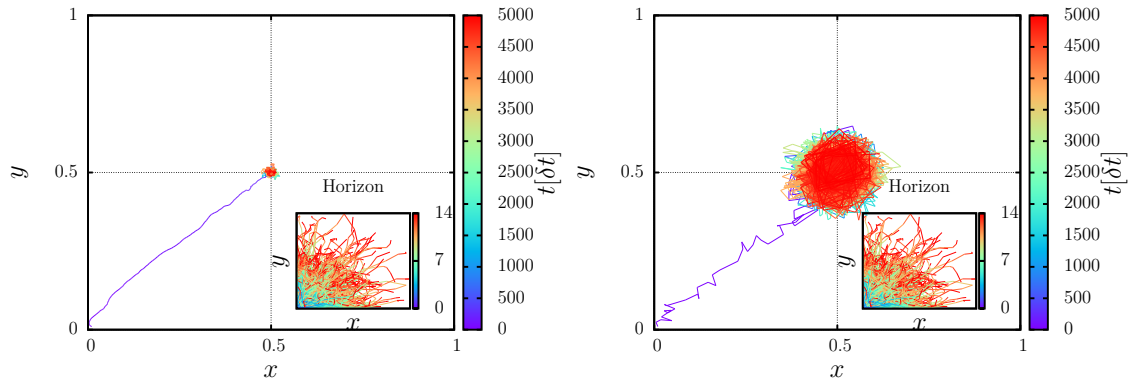

(a) $\frac{T_c}{T_r} = 1$ (b) $\frac{T_c}{T_r} = 30$

Figure 3.11.: A particle in a box for (a):$\frac{T_c}{T_r} = 1$ and (b):$\frac{T_c}{T_r} = 30$. The dotted lines give the coordinates of the centre of the box. [$T_r = 0.03$, $L = 1$, $\delta t = 0.1$, $\tau = 1.5$, $\gamma = \frac{0.25}{\delta t}$, using $F_{\mathcal{M}}$]

3.4.3. Model parameters

In the simulations in this thesis we keep most parameters fixed. We list in table 3.1 all parameters including the value used if not explicitly stated otherwise.

	commonly used value	
δt	0.1	timestep
τ	1.5	time horizon of sampling trajectories
γ	$\frac{0.25}{\delta t}$	drag
N_{sample}	5000	number of sampled paths per step

Table 3.1.: List of parameters. Given values are used in all simulations shown, if not explicitly stated otherwise.

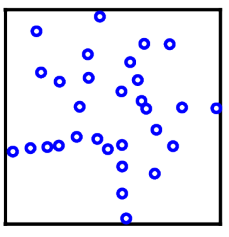

4. Continuous evolution: Single particle dynamics

First we will examine how well a particle performs in reaching the centre of a box. We use the average distance of a particle from the centre of the box d as quantity for measuring its performance. We will show a phase-diagram of d depending on T_r and $\frac{T_c}{T_r}$ and some exemplary path of entropically driven particles. In Sec. 4.1 this is shown using the position-space of sampling trajectories for calculating $\mathcal{R}$ and therefore the entropic force. Analogously in Sec. 4.2 this is done using momentum-space of the sampling trajectories for calculating the entropic force. In Sec. 4.4 we examine the performance of a particle in a bottleneck system and finally compare it to the results of the simulations on a lattice.

4.1. Particle in a box, using $F_{\mathcal{P}}$

We consider an entropically driven particle in a box of size $L = 1$ and let it move for $t = 3 \cdot 10^4 \delta t$. After a transient of $N_{transient} = 10^4$ steps we calculate its distance d from the centre of the box and finally average over time. Figure 4.1 shows $\langle d \rangle$ for different T_r and $\frac{T_c}{T_r}$. Upon increasing T_r we can distinguish four regions:

1. The blue region for small T_r and large $\frac{T_c}{T_r}$,
2. a purple region for increasing T_r,
3. a green region, and finally
4. the orange region covering the whole diagram for $T_r > 0.06$.

Except for the blue to the purple transition, all other transitions are rather steep.

In region 1 the particle has such a small horizon that it will gain some distance from the walls, then diffuse and due to limited sampling time, not fully explore the system. In region 2 the particle finds the centre and stays there. Region 3 indicates that the particle manages to find the centre of one wall and stays there at distance $d \approx 0.5$. In region 4 the particle stays at the corner at distance ($d \approx 0.7 \approx \sqrt{0.5}$).

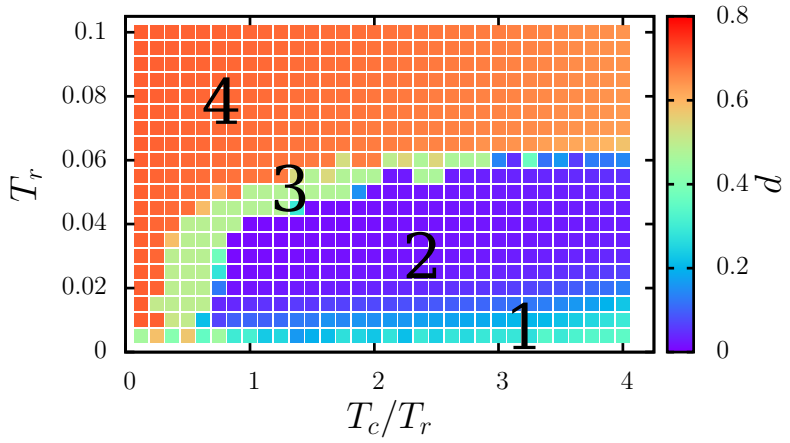

Figure 4.1.: The average distance of a particle from the centre of the box for variable T_r and $\frac{T_c}{T_r}$. Region numbers are displayed for each corresponding regime. [$L = 1$, total runtime $t = 3000\ \delta t$, transient time $t_{transient} = 1000\ \delta t$, using $F_{\mathcal{P}}$]

Figure 4.2 shows six trajectories for points in the phase-diagram, giving the horizon as insets. In Fig. 4.2(a)-(d)we increase T_r while keeping the ratio $\frac{T_c}{T_r} = 1$; they correspond to a vertical cut through the phase diagram (Fig. 4.1). Figures 4.3(a) and (b) give two trajectories in the right area of the phase diagram for $\frac{T_c}{T_r} = 4$. In Fig. 4.2(a) a trajectory for parameters in region 1 is shown. The particle moves away from the corner and starts moving around in a diffusive manner. T_r and therefore the horizon are much smaller than the box such that the particle stops detecting the presence of walls long before it reaches the centre. In Fig. 4.2(b) the particle with parameters in region 2 of Fig. 4.1 succeeds in reaching the centre. It starts in the bottom left corner where it first moves along the walls until it moves towards the centre in a curved trajectory. Initially it is not repelled by the wall but instead moves around in the corner until by chance it gains sufficient distance from the walls such that it is repelled. It first reaches this distance from the vertical wall, which

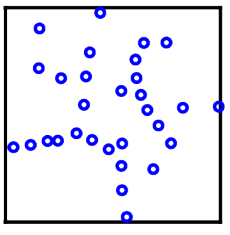

is why it experiences for some time stronger repulsion in the x direction. Therefore the trajectory to the centre is bent. A trajectory in region 3 of Fig. 4.1 is shown in Fig. 4.2(c). The particle moves around in the bottom left corner until at some point it reaches a distance to the left wall such that it is repelled. It then stays in the centre at the bottom wall. The horizon is large enough for the sampling trajectories to cover the entire system. With equal probability the particle could have moved along the vertical wall up and stayed at the left wall. Figure 4.2(d) shows a particle in region 4 for even larger horizon, which never leaves the bottom left corner. In Fig.4.3(a) a trajectory in region 1 for $\frac{T_c}{T_r} = 4$ is shown. The particle moves straight away from the corner and then moves within the system in almost ballistic fashion, feeling a repulsion of the walls and keeping a certain distance from them. The distance is roughly the length of the radius of the set of sampling trajectories. Figure 4.3(b) shows a particle in region 4 for $\frac{T_c}{T_r} = 4$ where the particle remains in the corner as observed in Fig. 4.2(d), but this time covering a larger area in the corner. We conclude that region 2 corresponds to the most efficient combination of parameterns to find the centre of the box.

4.2. Particle in a box, using $F_{\mathcal{M}}$

Now we study an entropically driven particle in a box, similarly to the previous section, but this time we use the radius of gyration of the points of a sampling trajectory in momentum-space. Figure 4.4 shows the phase diagram of the average distance of a particle from the centre d for variable T_r and $\frac{T_c}{T_r}$. We can identify three regions:

1. The blue region for $T_r \lesssim 0.1$,
2. the purple region for $0.1 < T_r \lesssim 0.06$, and
3. the orange region for $T_r \gtrsim 0.06$.

Region 1 takes values from $d = 0.4$ to $d = 0.2$ smoothly increasing with increasing $\frac{T_c}{T_r}$. Region 2 uniformly shows values around $d < 0.05$. In region 3 for small $\frac{T_c}{T_r}$ we observe distances up to $d = 0.75$, and for increasing $\frac{T_c}{T_r}$ it decreases to $d = 0.06$.

Figure 4.5 shows three trajectories with parameters taken from the phase-diagram in Fig. 4.4. It shows a vertical cut through the phase diagram for $\frac{T_c}{T_r} = 2$ with a trajectory for each region. In Fig. 4.5(a) the particle moves away from the corner

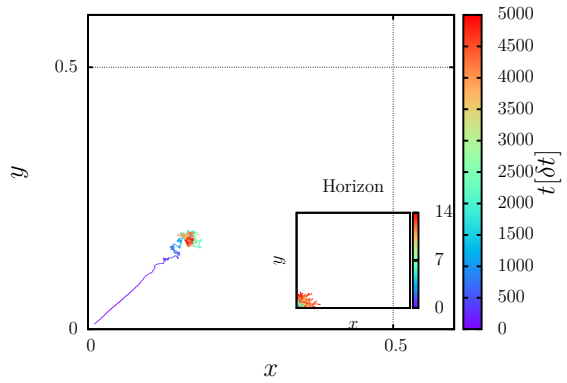

(a) $\frac{T_c}{T_r} = 1$, $T_r = 0.005$, blue region

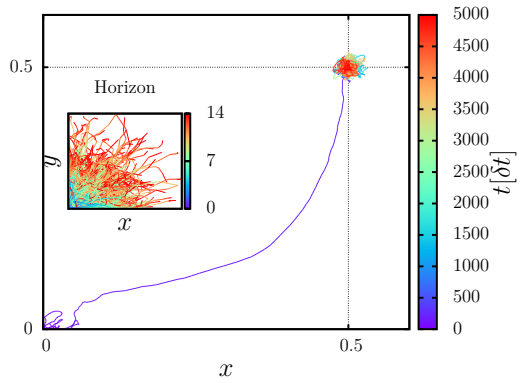

(b) $\frac{T_c}{T_r} = 1$, $T_r = 0.03$, purple region

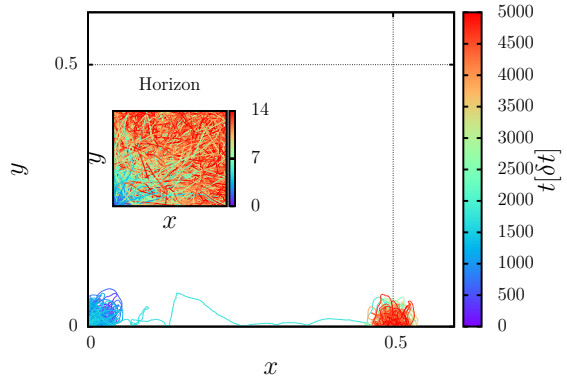

(c) $\frac{T_c}{T_r} = 1$, $T_r = 0.05$, green region

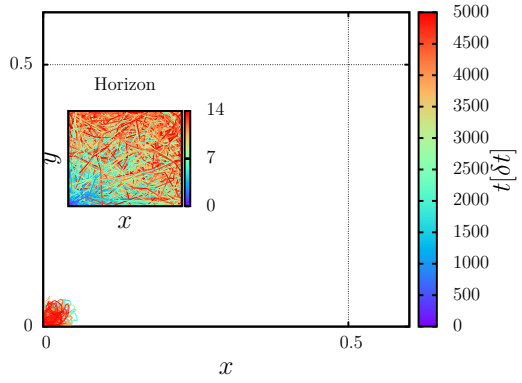

(d) $\frac{T_c}{T_r} = 1$, $T_r = 0.07$, orange region

Figure 4.2.: Typical trajectories for a particle in a box and different sets of parameters in the phase diagram of Fig. 4.1. [$L = 1$, using $F_{\mathcal{P}}$]

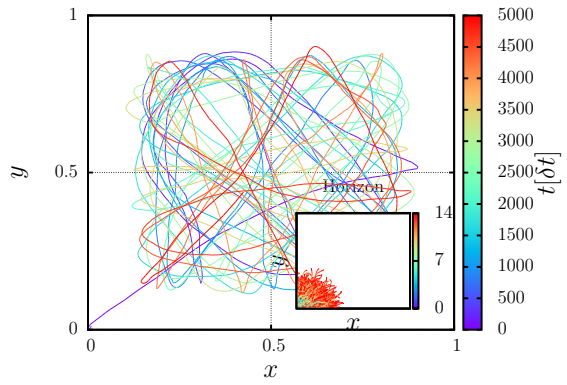

(a) $\frac{T_c}{T_r} = 4$, $T_r = 0.01$, blue region

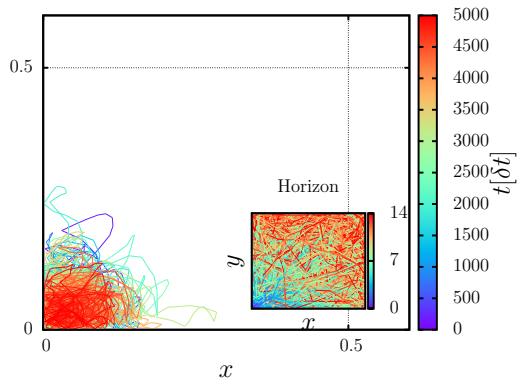

(b) $\frac{T_c}{T_r} = 4$, $T_r = 0.07$, orange region

Figure 4.3.: Typical trajectories for a particle in a box and different sets of parameters in the phase diagram of Fig. 4.1. [$L = 1$, using $F_{\mathcal{P}}$]

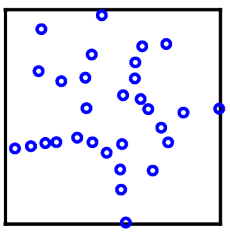

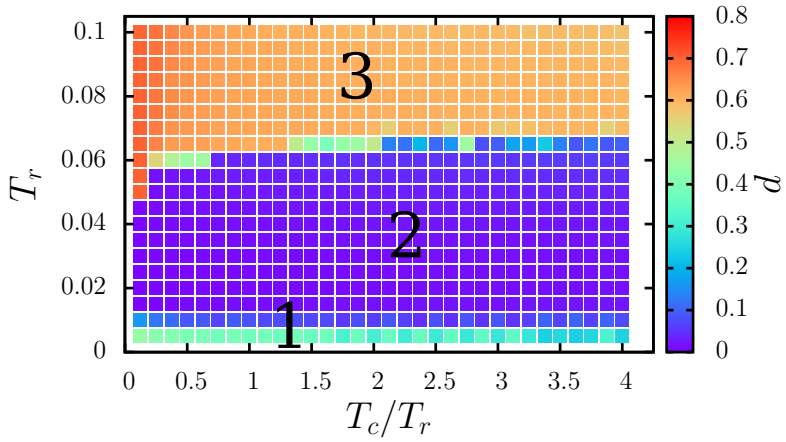

Figure 4.4.: The average distance of a particle from the centre of the box for variable T_r and $\frac{T_c}{T_r}$.[$L = 1$, total runtime $t = 3000$, transient time $t_{transient} = 1000$, using $F_{\mathcal{M}}$]

until it cannot detect the walls any longer and then moves around in a diffusive manner. For increasing $\frac{T_c}{T_r}$ the particle experiences stronger entropic forces. As soon as the influence of the walls vanishes, the entropic force decreases to a non-zero value with random orientation due to finite sampling. With larger $\frac{T_c}{T_r}$ this random noise increases and therefore determines the stepsize of the random walk the particle then performs. If we assume it is diffusing, increasing $\frac{T_c}{T_r}$ corresponds to an increasing diffusion coefficient. This explains the smooth decrease from $d = 0.4$ to $d = 0.2$ for increasing $\frac{T_c}{T_r}$, since the particle then randomly explores larger areas of the system and statistically moves closer around the centre. For infinite sampling time every horizontal line in the phase diagram would have the exact same value d.

Figure 4.5(b) shows the particle moving towards the centre. For $T_r = 0.03$ the horizon is large enough to produce a repulsion from all walls forcing the particle to remain confined in the centre of the box. A trajectory in region 3 is shown in Fig. 4.5(c). The horizon is large enough for the sampling trajectories to be larger than the system size, covering the entire box. The particle remains in its inital corner, slightly moving around but constantly feeling an attraction to the walls.

The transition from region 2 to 3 in Fig. 4.4 at $d = 0.06$ is steep and is due to too large a horizon relative to the system's size. Both for position- and momentum-space we observed the particle preferring proximity to the walls for a horizon significantly

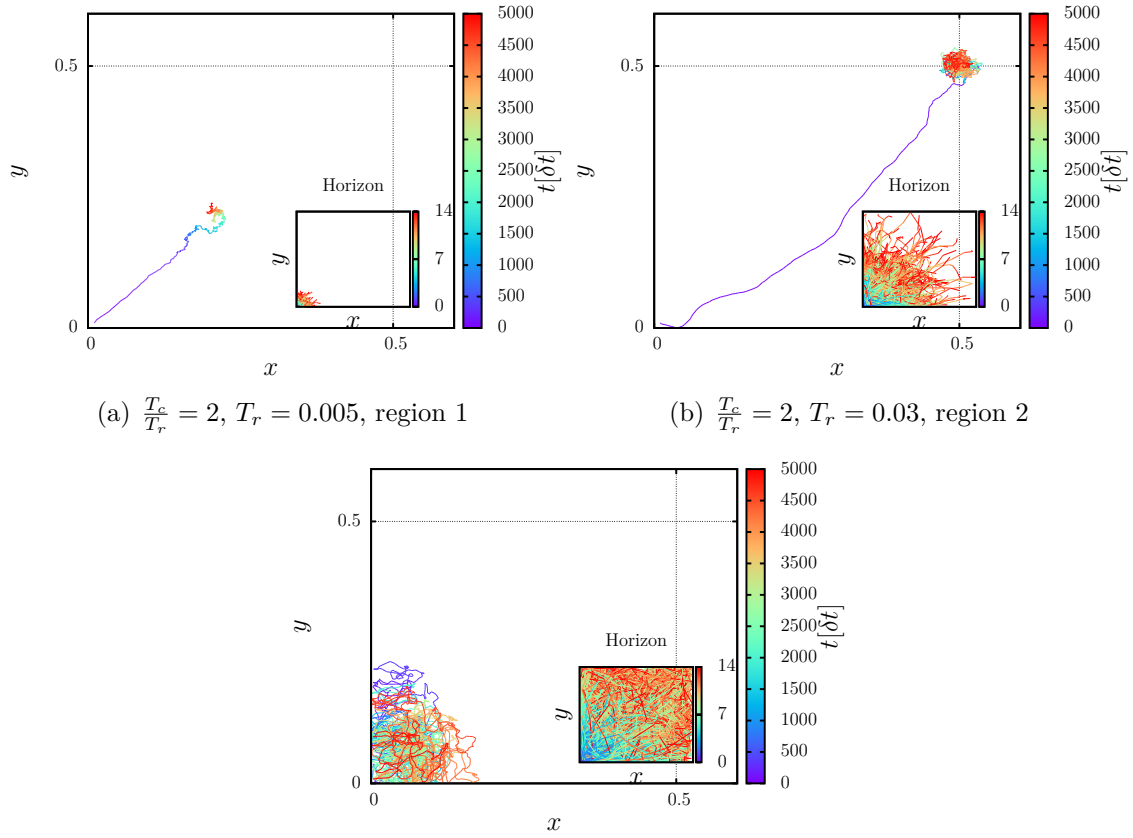

(a) $\frac{T_c}{T_r} = 2$, $T_r = 0.005$, region 1

(b) $\frac{T_c}{T_r} = 2$, $T_r = 0.03$, region 2

(c) $\frac{T_c}{T_r} = 2$, $T_r = 0.08$, region 3

Figure 4.5.: Three trajectories in a box for constant T_c and changing T_r as a cut through the phase diagram. Note that this is still a box with $L = 1$, it is zoomed in. [Using $F_{\mathcal{M}}$]

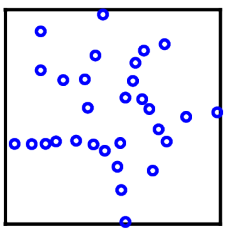

larger than the system's size. This we also observed for a particle on a square lattice in Sec. 2.2.2.

In Fig. 4.4 the transition between success in reaching the centre and staying in the corner is constant around $T_r = 0.06$ as soon as $\frac{T_c}{T_r}$ is sufficient large. For $\frac{T_c}{T_r}$ too small the entropic force is so weak that the deviation in behaviour (region 3 reaching down to $T_r = 0.05$) is due to insufficient sampling times.

To quantify the relative importance of the horizon to the relevant length-scale in the system we introduce the Prandtl number $\mathscr{P}$ as ratio between viscous and thermal diffusion rate which directly translate to the ratio of the effective size l_H of the sampling horizon and the system's size L.

$$\frac{1}{\mathscr{P}} \equiv \frac{\text{thermal diffusion rate}}{\text{viscous diffusion rate}} = \frac{k_\mathrm{B} T_r}{\gamma \frac{\sigma}{\delta t}} \frac{1}{L} = \frac{l_H}{L} \,, \tag{4.2.1}$$

where σ denotes the diameter of a particle. In this section we treat the particle as point-like, however the dynamics do not change for a particle-size much smaller than the box. It is convenient to set $k_\mathrm{B} = 1$ and choose $\sigma = 0.004 = \frac{\delta t}{\gamma}$ such that we can directly use the value of T_r from the diagram in Fig. 4.4 to define a critical ratio which we call Λ

$$\frac{1}{\mathscr{P}_\text{critical}} \equiv \Lambda = \frac{l_{H,\text{critical}}}{L} = \frac{0.06}{1} = 0.06 \,. \tag{4.2.2}$$

We can expect a behaviour where the particle prefers being close to a wall for $\frac{l_H}{L} < \Lambda$ and a behaviour where the particle persistently feels a repulsion of walls for $\frac{l_H}{L} > \Lambda$. The critical Prandtl number and $l_{H,\text{critical}}$ correspond to the parameters at the transition between region 2 and 3, or the transition between the two described behaviours, respectively.

4.3. Brief conlusion

In the previous two sections we examined how efficiently a single particle in a box reaches the centre depending on T_r and $\frac{T_c}{T_r}$. Figure 4.1 and 4.4 show the phase diagram for position- and momentum-space, respectively. We identified different regions and their characteristics in performance. The most striking difference in behaviour lies in the region of position-space in Fig. 4.1 for $T_r < 0.06$ and $\frac{T_c}{T_r} < 0.7$ where a particle sticks to a walls. This originates from the different interaction with

walls of the two methods, as discussed in Sec. 3.3.

Figure 3.6 shows the entropic force experienced by a particle close to a wall for position- and momentum-space. Using position-space, there is a larger interval of distances where a particle is attracted to the wall than with momentum-space. This most certainly causes the difference in performance of the two methods. For momentum-space theoretically there also exists this domain, however even the smallest values $\frac{T_c}{T_r}$ considered in the calculations of the phase-diagram caused fluctuations strong enough to let a particle move away from walls. Only for $T_r < 0.04$ we can identify parts of this region.

In the following section we let a particle explore a bottleneck system. In order to exclude wall effects as far as possible we exclusively use momentum-space for this type of system.

4.4. Particle in a bottleneck, using $F_{\mathcal{M}}$

We now let an entropically driven particle move in a bottleneck system. Figure 4.6 shows such system for a bottleneck of length $l_{BN} = 0.6$. The small box in which the particle starts at position $(0.36, 0.01)$ is of size $l_x = l_y = 0.3$ whereas the large box has a side length of $L_x = L_y = 1.0$. In Fig. 4.6 the starting position is marked with a red cross. A simulation will be counted as successful if the particle reaches the large box, that is, it enters the large box at the position marked with a green circle at $x = l_x + l_{BN}$. As discussed in the previous sections when examining the behaviour of a particle in a box for position- and momentum-space respectively, the general behaviour for simple systems is the same for both methods. However, using $F_{\mathcal{M}}$, the particle is less likely to get stuck at a wall or a corner. Therefore in this section we will exclusively use momentum-space for calculating the entropic force.

Figure 4.7 shows a typical trajectory of an entropically driven particle, including its speed which was averaged over 20 simulations. The color bar indicates time and a set of sampling trajectories is shown in the inset.

Starting from the corner, the particle accelerates towards the centre of the small box where it slows down until at $x \approx 0.2$ it discovers the bottleneck and what is behind. It speeds up until entering, then slows down again since the sampling trajectories going diagonally up right and down right now do not contribute that much again. However while approaching the large box the speed increases again. Right after entering it again slows down and around $x = 5.5$ accelerates while gaining

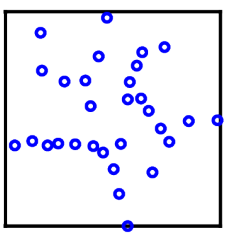

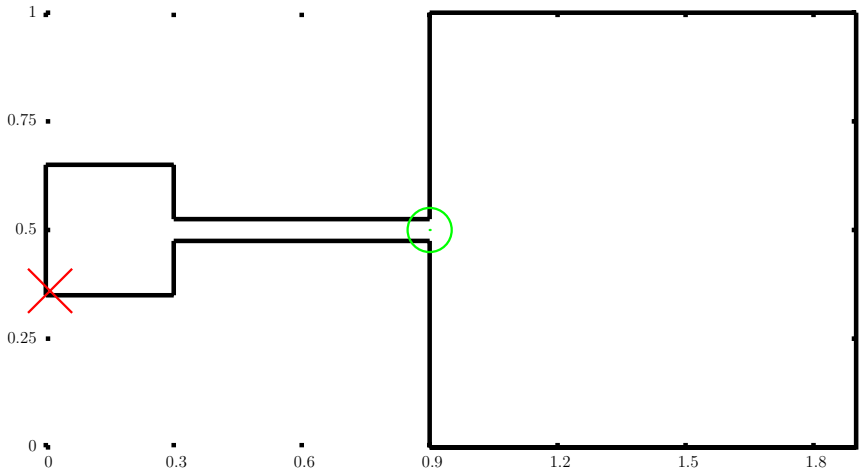

Figure 4.6.: The bottleneck potential for bottleneck-length $l_{BN} = 0.6$. The initial position of the particle for every simulation in the small box marked with a red cross, the entrance to the big box and position used for sampling the first passage time marked with a green circle. For all simulations the size of the small box is $l_x = l_y = 0.3$, of the large box $L_x = L_y = 1.0$ and the width of the bottleneck $w_{BN} = 0.025$.

some distance from the walls and therefore feeling their repulsion. Then its speed gradually decreases as it moves towards the centre of the large box where it then stays. The speed in vertical direction fluctuates around zero, except in the beginning around $x = 0$ to $x = 0.15$ when it moves upwards from the corner.

Despite an entropically unfavourable bottleneck the particle succeeds in reaching the large box. We want to emphasize that there is no artificial incentive given, the particle succeeds only due to detecting the entropically favorable area in the large box.

Displayed in Fig. 4.8 are the average success or first-passage times to the large box t_{fp} depending on the sampling horizon determined by T_r and the length of the bottleneck l_{BN}. For every data point we averaged over 100 simulations. If one of those simulations were to take longer than a maximum of $t_{max} = 30000\ \delta t$, all simulations for this set of parameters would be stopped and we would consider the simulations for those parameters as failures. That means that they do not appear as data points in Fig. 4.8. Simulations were performed for all bottleneck-lengths $l_{BN} \in \{0.0, 0.1, .., 0.9, 1.0\}$ and horizons $T_r \in \{0.005, 0.01, .., 0.065, 0.07\}$. Every missing point in Fig. 4.8 indicates a failure – either the particle could not succeed or it took the particle longer than the maximum time. Note that in the latter case

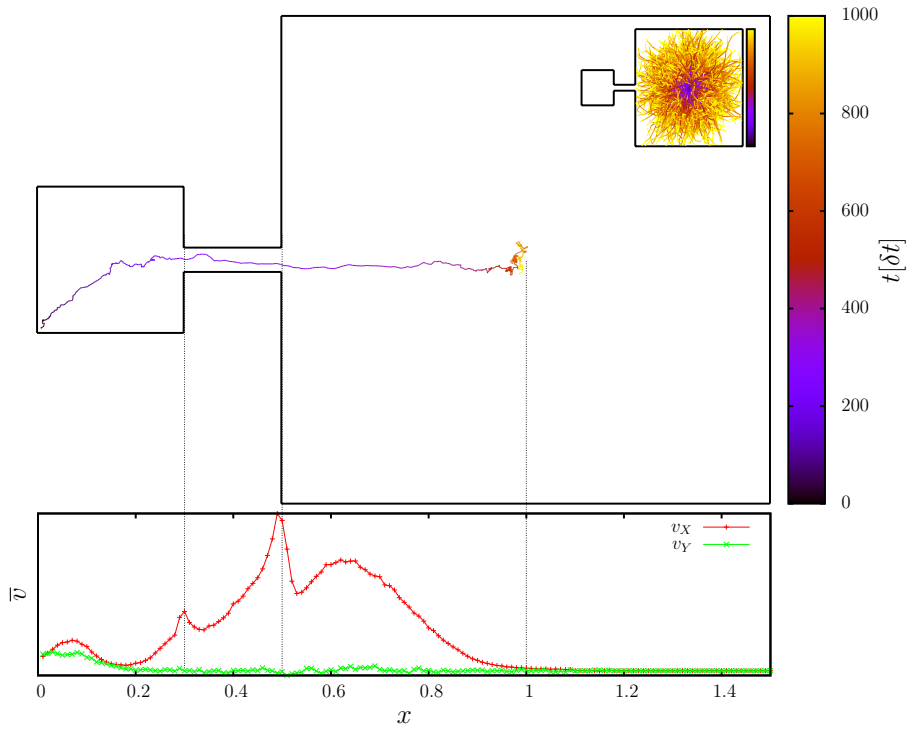

Figure 4.7.: Top: Example trajectory for same set of parameters as used for finding the velocity profile. Bottom: Average velocity profile of a particle. [$T_r = 0.015$, $\frac{T_c}{T_r} = 4$, using $F_{\mathcal{M}}$, velocity profile averaged over 20 simulations]

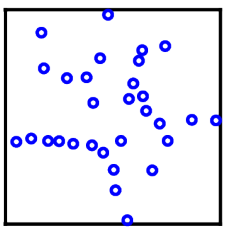

the average time was not necessarily larger than the maximum time, but its variance was large enough such that within the 100 simulations in at least one simulation the particle would have taken longer than the maximum time to succeed.

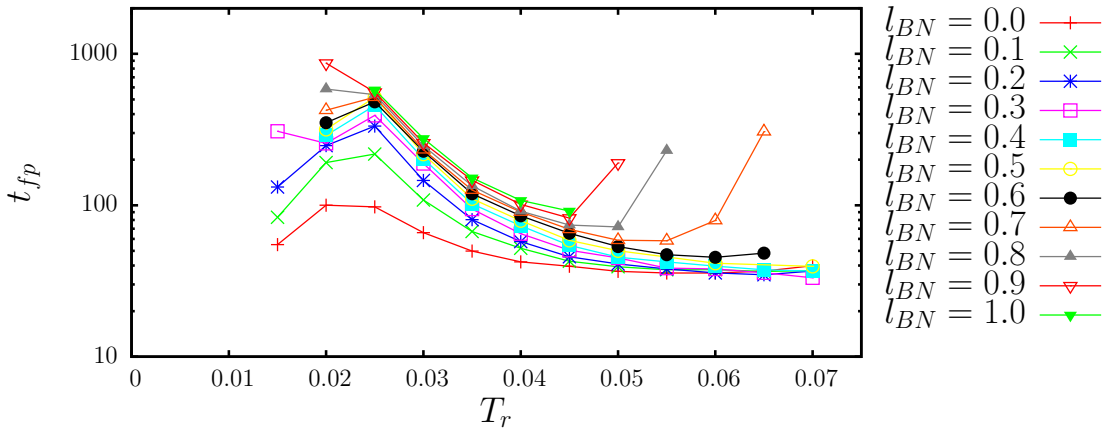

Figure 4.8.: Average first passage or success time t_{fp} depending on T_r and bottleneck-length l_{BN}. Initial position is in the bottom left corner of the small box at $(0.01, 0.36)$. Every data point is averaged over 100 simulations. If a single simulation in a set took longer than $t = 30000\ \delta t$, the simulation for those parameters was stopped and skipped (do not appear in plot). So every data point indicates full success rate. Using $F_{\mathcal{M}}$.

First, we will describe the behaviour for $l_{BN} < 0.4$. For $T_r \leq 0.01$ the particle always fails. It succeeds for $T_r = 0.015$ with increasing t_{fp} for increasing T_r up to a maximum at $T_r = 0.025$. With further increasing T_r the first passage times decrease and reach a plateau. In general t_{fp} increases with longer bottleneck l_{BN}. Concerning the simulations with larger l_{BN} they first succeed for $T_r = 0.02$. For larger T_r instead of monotonously decreasing the show a drastic increase ($l_{BN} = [0.7, 0.8, 0.9]$) or fail ($l_{BN} = 1.0$).

For small $T_r \leq 0.01$ the particle does not enter the big box since as soon as the particle approaches the bottleneck, the opposed wall is so far that the particle does not detect it via sampling. Thus, in that direction the particle feels no repulsion anymore in contrast to the bottleneck. The small peak around $T_r = 0.025$ can be explained by looking at the behaviour of the particle for those parameters. Figure 4.9 shows example trajectories for horizons $T_r = [0.015, 0.02, 0.025]$. While for $T_r = 0.015$ (Fig. 4.9(a)) the particle first moves towards the centre of the small box and then approaches the exit. For larger T_r (Fig. 4.9(b) and (c)), the particle stays close

to the walls. From that position fewer sampling paths enter the bottleneck and are therefore less likely to detect the large box. Statistically it takes longer times for the particle to sufficiently detect the large box and ultimately succeed – despite the larger horizon.

As approximated in equation (4.2.2) the ratio between size of horizon and system needs to be smaller than $\Lambda = 0.06$ for the particle to move towards the centre. For the small box in this system the temperature T_r determining the size of the sampling horizon needs to be chosen such that the size of the horizon l_H is smaller than

$$l_{H,\text{critical}} = \Lambda \cdot L = 0.06 \cdot 0.3 = 0.018 \,. \tag{4.4.1}$$

This is consistent with what we observe in Fig. 4.9: For $T_r = 0.015$, corresponding to $l_H = 0.015 < l_{H,\text{critical}}$ the particle moves towards the centre of the small box whereas for $T_r = 0.02$, corresponding to $l_H = 0.02 > l_{H,\text{critical}}$ the particle moves along the walls.

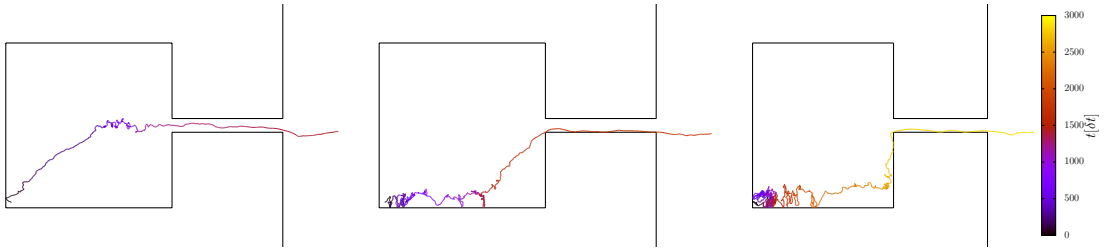

(a) $T_r = 0.015$, $l_H = 0.015$ (b) $T_r = 0.02$, $l_H = 0.02$ (c) $T_r = 0.025$, $l_H = 0.025$

Figure 4.9.: For three temperatures $T_r = [0.015, 0.02, 0.025]$ a particle leaving the small box. $[\frac{T_c}{T_r} = 1$, using $F_{\mathcal{M}}]$

In the following we will briefly examine the behaviour of the system at different points in Fig. 4.8 by showing example trajectories of entropically driven particles for those parameters.

Figure 4.10 shows a trajectory for $l_{BN} = 0.2$ and $T_r = 0.005$ in the region of failing simulations. The particle moves towards the centre of the small box and stays there. Its horizon is so small that as soon as it moves further towards the bottleneck it does not detect the left wall anymore, thus only feeling a repulsion of the bottleneck.

Figure 4.11 shows a particle with $T_r = 0.02$ moving along the bottom wall of the small box towards the bottleneck and continuing through the bottleneck until it reaches the centre of the large box. The dashed lines indicate the exact centre

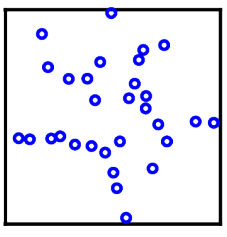

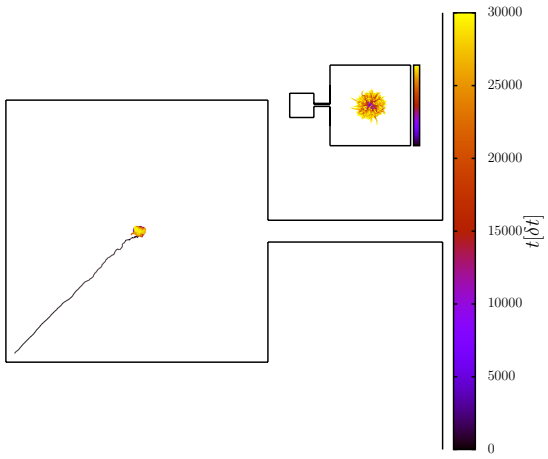

Figure 4.10.: The particle stays in the small box. $[T_r = 0.005,\ \frac{T_c}{T_r} = 1]$

of the large box. Concerning the small box the horizon is larger than the critical horizon $l_H > l_{H,\text{critical}}$ (see Eq. 4.4.1).

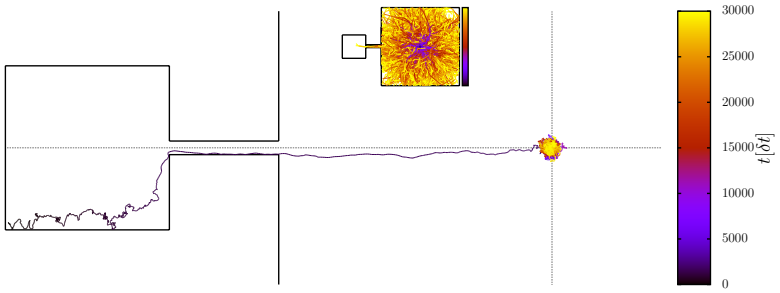

Figure 4.11.: The particle reaches the large box. $[T_r = 0.02,\ \frac{T_c}{T_r} = 1]$

A simulation with much larger horizon corresponding to $T_r = 0.06$ is shown in Fig. 4.12. The particle moves relatively straight towards the bottleneck and ends up close to the centre of the large box. However, it moves around a point close to the centre, slightly shifted towards the bottleneck. The sampling paths cover the entire system and detect the small box, causing this shift. Also the entropic force is stronger than the simulation given in Fig. 4.11 for example. Except T_r, all parameters are the same in both simulations. Due to larger T_r the sampling paths are on average larger, producing a larger $\mathcal{R}$ which comes in as a factor in Eq. (3.2.6).

Figure 4.13 shows a particle for $l_{BN} = 1$ and $T_r = 0.06$, parameters for which the

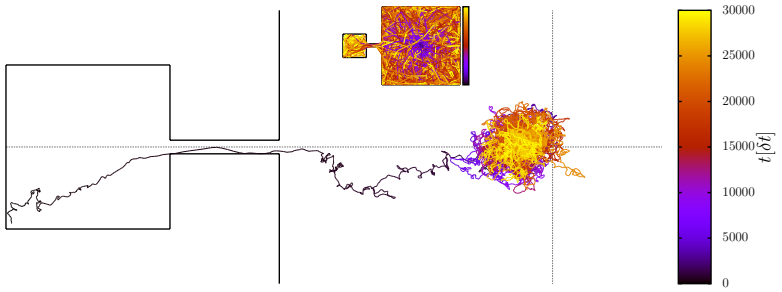

Figure 4.12.: The particle reaches the large box. $[T_r = 0.06,\ \frac{T_c}{T_r} = 1,\ l_{BN} = 0.2]$

simulation fails after a drastic increase of t_{fp} for increasing T_r in Fig. 4.8. After entering the bottleneck, the particle stops before entering the large box and stays there. Due to its large horizon, which easily covers the entire system from its final position within the bottleneck, largest entropy is found in the centre of the system. We already observed the final position moving closer to the small box for larger T_r in Fig. 4.12. For larger l_{BN} this position eventually shifts into the bottleneck. This causes the simulation to fail in reaching the large box. Entropically speaking, the particle does not see the necessity of entering the large box. For a large box of

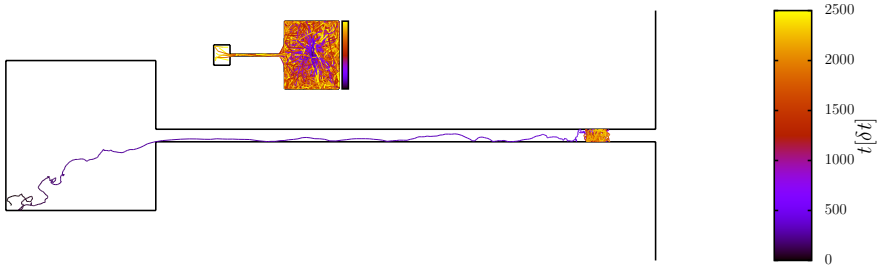

Figure 4.13.: The particle gets stuck in the bottleneck. $[T_r = 0.06,\ \frac{T_c}{T_r} = 1,\ l_{BN} = 1]$

infinite size the particle would not get stuck but always succeed. Figure 4.14 shows the success or first passage times to the large box t_{fp} for different T_r and l_{BN}, but for a system with $L_x = L_y = \infty$. For $T_r < 0.045$ the data correspond to the data in Fig. 4.8. Though for $T_r > 0.45$ the first passage times do not increase but instead decreases monotonically. This negative slope is the same for all l_{BN}, the curves are parallel to each other. This is due to fact, that for this system the walls of the large box do not produce any repulsion anymore. In Fig. 4.8, a particle with a

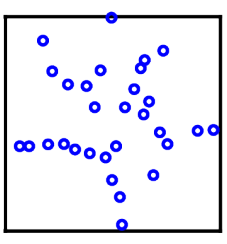

large horizon was, despite considering the large box as most favorable, repelled by its walls.

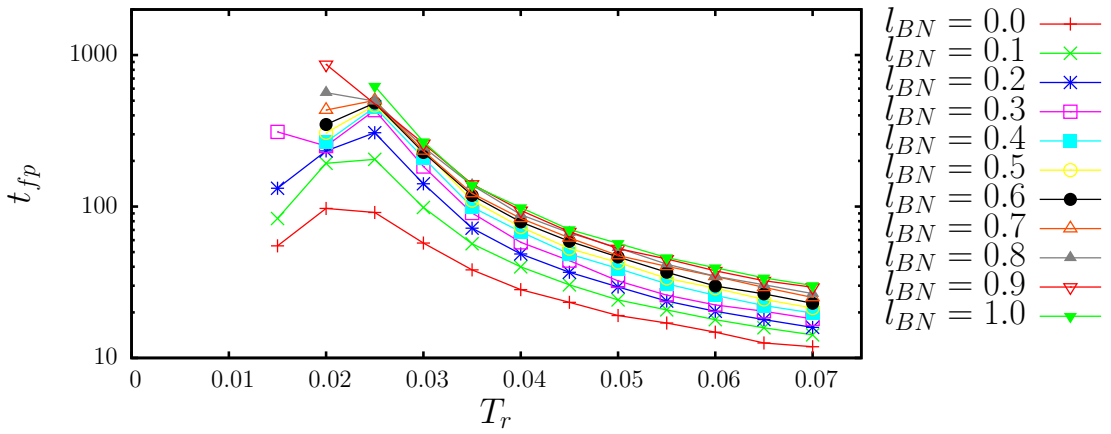

Figure 4.14.: The same simulations as shown in Fig. 4.8 but with a large box of infinte size. Average success time t_{fp} depending on T_r and bottleneck-length l_{BN}. Initial position is in the bottom left corner of the small box at $(0.01, 0.36)$. Every data point is averaged over 100 simulations. If a single simulation in a set took longer than $t = 30000\ \delta t$, the simulation for those parameters was stopped and skipped (do not appear in plot). Every shown data point indicates full success rate. Using $F_{\mathcal{M}}$.

4.5. Comparison of results from continuous and discrete systems

We now compare the results of a particle in a bottleneck system in a spatially discrete system (Fig. 4.15(c)) with the continuous case for both the large box of size $L_x = L_y = 1$ (Fig. 4.15(a)) and $L_x = L_y = \infty$ (Fig. 4.15(b)). For a purely random motion, which was not included in the continuous simulation yet intuitive, statistically the particle succeeds in finding the large box in any case after finite time.

For small horizons in all simulations the particle does not succeed since it perceives the bottleneck as an unfavourable area only, and stays in the small box. In the continuous case the behaviour of the particle changes at $T_r = 0.02$ when it starts moving along the walls of the small box (see Fig. 4.9), causing the success time to increase up to a maximum at $T_r = 0.025$ before steadily decreasing for larger

T_r. This effect did not occur in the discrete simulation. We did not observe, in the discrete simulations, the effect in the continuous simulations for $L_x = L_y = 1$ that for large T_r and l_{BN} the particle stays in the bottleneck (see Fig. 4.13). For large horizons both the first passage time for the discrete simulations and the continuous for $L_x = L_y = \infty$ in Fig. 4.15(b) decrease in the same manner, and the curves for different l_{BN} are parallel to each other.

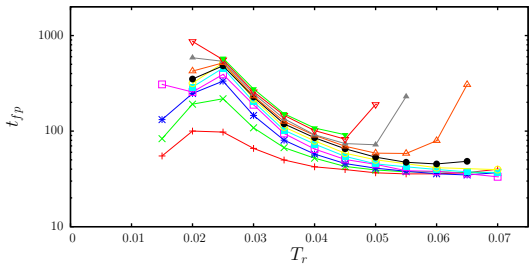

(a) Continuous (see Fig. 4.8)

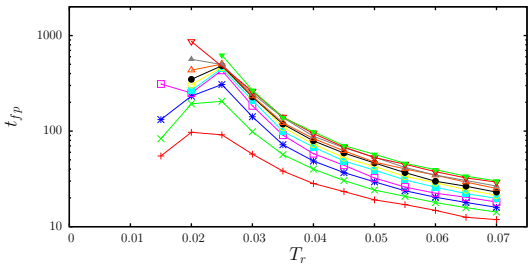

(b) Continuous, large box infinitely large (see Fig. 4.14)

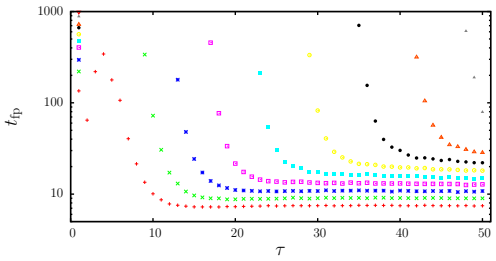

(c) Discrete (see Fig. 2.16)

Figure 4.15.: Average success times of a particle in a bottleneck system for different horizons and lengths of the bottleneck. Results of the continuous and the discrete simulations for comparison.

4.6. Entropically driven particle as DNA molecule

We can interpret an entropically driven particle as the centre of mass of a polymer and thus compare its dynamics with experiments. In 2002 Turner, Cabodi and Craighead [20] examined the dynamics of DNA molecules confined by nanopillars but in proximity to an entropically more favorable area. Figure 4.16(a) shows their experimental setup where the area with nanopillars is entropically less favorable due to the restricted degrees of freedom. They observe that strands of DNA are

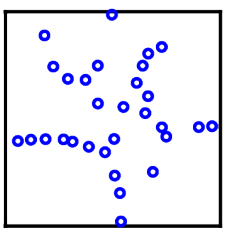

strongly pulled into the area free of nanopilllars as soon as an end of the DNA strand reaches into it. In their experiment the entropic force originates from a gradient in configuration entropy. In the interpretation of our driven particle as centre of mass of a polymer, its sampling trajectories correspond to polymer configurations. Thereby for this setup the causal entropy can be associated with the configuration entropy of a DNA molecule.

Figure 4.16(b) shows our numerical setup. A field of pillars in which an entropically driven particle moves towards the right, towards an empty area. We collect the times t_{fp} the particle takes to reach the entropically favorable area, starting at a distance d from it. We used simulations with initial position of the particle $d = n \cdot 0.001$, $n \in [1, \infty]$, increasing n until the particle did not succeed within a maximum time, that is, the entropic force was too weak for the particle to move into the direction of the open area.

Figure 4.16(c) and (d) show the experimental results from Turner et al.[20] and our numerical results, respectively. Shown is the distance from the entropically favorable area as a function of its first passage time. The fit is a square-root dependence, which was predicted by Turner et al.. Our numerical setup matches the experimental setup qualitatively, the dimensions and ratios of distances are different, also due to long simulation times our results are relatively noisy. However we were able to qualitatively reproduce experimental results, which gives us confidence in the validity of the polymer-analogy of our model.

4.7. Conclusions

We analysed the dynamics of a single particle in a box for both position- and momentum-space driven entropic forces and identified a difference in behaviour. Using position-space, particles find the proximity of walls entropically favorable if they initially are close enough, as discussed in Sec. 4.3. We then examined the first passage times for a particle in a bottleneck system and found similar results as in the discrete case, discussed more elaborate in Sec. 4.5. Also we briefly compared experimental results of the dynamics of DNA strands between two areas of different configurational entropy with our numerical results of an equivalent setup. The qualitatively matching results give us confidence in the polymer-analogy of our model.

The next step is to explore the dynamics of many particle systems where all

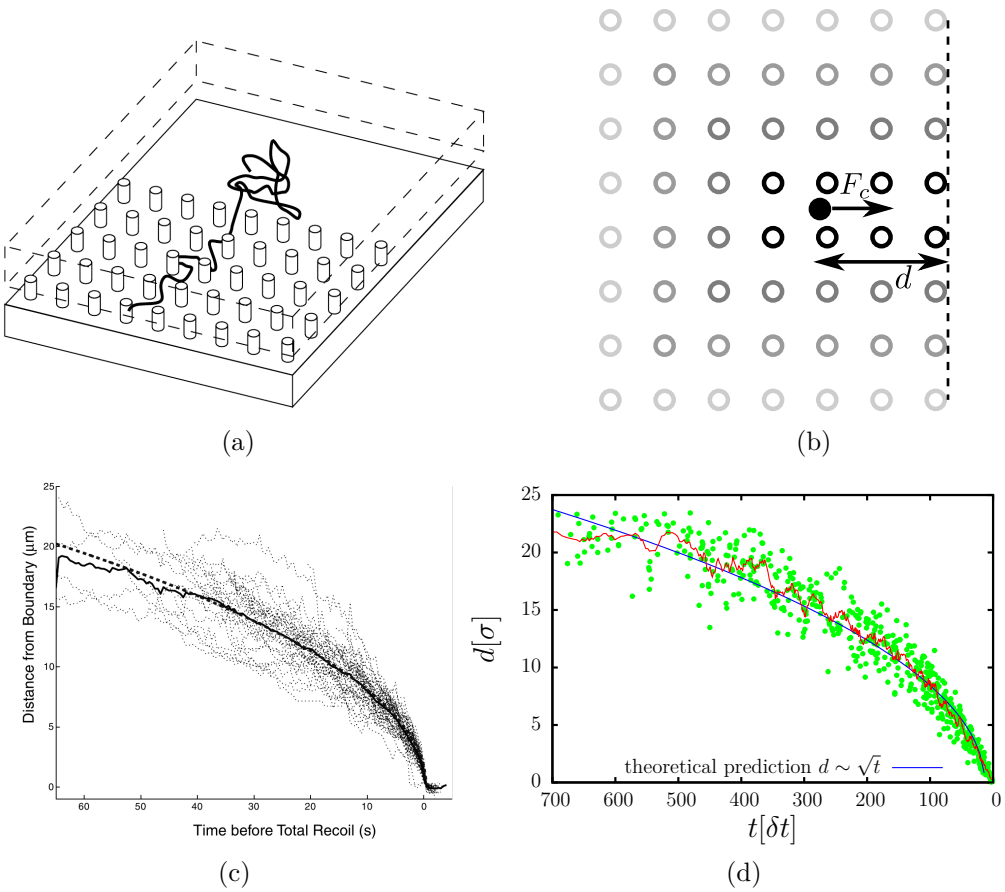

Figure 4.16.: (a): Sketch of the experimental setup used in [20]. "The fluidic device consists of a quasi-two-dimensional gap between a floor and ceiling approximately 60 nm in height. Some regions of the device are populated with nanopillars". (b): Sketch of the numerical setup. [Diameter of pillars: σ, distance between two pillars $d_p = 4\sigma$, $\gamma = \frac{0.75}{\delta t}$, using $F_{\mathcal{M}}$]. (c): Experimental results from [20] and (d) our numerical results for time before total recoil, that is, time until the entire DNA strand or our entropically driven particle fully reaches the entropically favorable area. (a) and (c): Reprinted figures with permission from S. W. P. Turner, M. Cabodi and H. G. Craighead, Phys. Rev. Lett. 88, 128103 (2002). Copyright 2015 by the American Physical Society.

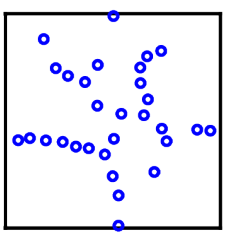

particles are subject to the entropic force.

5. Continuous evolution: Many-particle dynamics

In this section we will examine the dynamics of multiple entropically driven particles in a confining box. Particles will still interact with the walls as point particles. Particles interact with each other as elastic spheres of cross-section σ following Eq. 5.1.1.

We use two different types of interaction, A and B, which differ in the way the entropic force acting on a single particle is calculated. In Sec. 5.1 type A interaction is introduced and the resulting particle dynamics examined. We then introduce type B interaction in Sec. 5.2 which leads to the emergence of patterns. Their origin and characteristics are discussed thereafter.

For both interaction types we again examine the dynamics of a number of particles in a bottleneck system in Sec. 5.4, directly relating those simulations to evacuation scenarios.

Concerning particles in a box we examine three system sizes, for the ratio $\mathcal{S}$ between the size of a square box $L \times L$ and the approximate diameter of the area explored by the sampling paths $2r_{\text{sample}}$. We keep fixed the size of particles σ relative to r_{sample}.

- $\mathcal{S} = \frac{l}{2r_{\text{sample}}} = 0.5$ ($T_r = 0.015$, $L = 20\sigma$),
- $\mathcal{S} = \frac{l}{2r_{\text{sample}}} = 1$ ($T_r = 0.015$, $L = 40\sigma$),
- $\mathcal{S} = \frac{l}{2r_{\text{sample}}} = 1.5$ ($T_r = 0.015$, $L = 60\sigma$),

which are illustrated in Fig. 5.1.

Both position- and momentum-space will be used and examined seperately. For better differentiation, we use red and blue in the plots for position- and momentum-space, respectively. In all simulations the particles are given random initial positions,

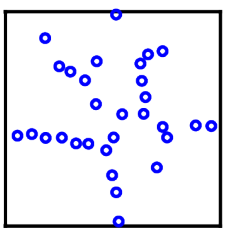

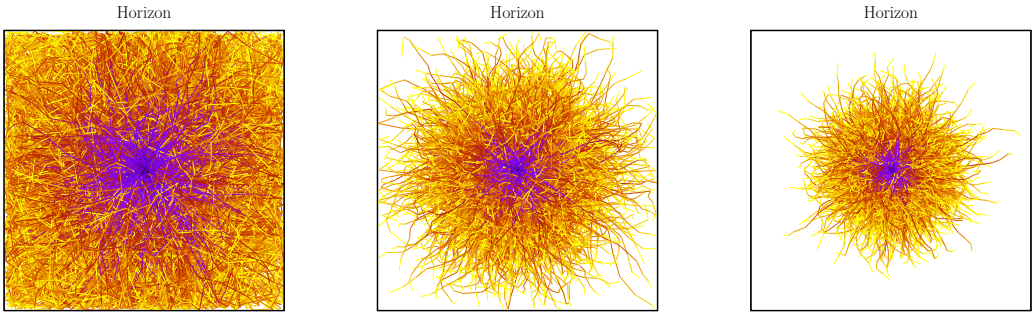

(a) $\mathcal{S} = 0.5$, $L = 20\sigma$ (b) $\mathcal{S} = 1.0$, $L = 40\sigma$ (c) $\mathcal{S} = 1.5$, $L = 60\sigma$

Figure 5.1.: A set of sampling paths for a particle in the centre of the three system sizes used in this thesis, respectively.

but paying attention that the particles do not overlap, and have zero initial total momentum.

5.1. "Blind agents" (Type A)

Type A particles do not detect other particles while sampling, that is, entropically any particle assumes being in an empty system. Sampling trajectories will not interact with other particles. However if two particles i and j touch each other they interact through a repulsive linear force

$$\vec{F}_{ij} = \begin{cases} -k(\sigma - |\vec{x}_j - \vec{x}_i|)\vec{e}_{ij} \text{ , if } |\vec{x}_j - \vec{x}_i| < \sigma \\ 0 \text{ , otherwise.} \end{cases} \tag{5.1.1}$$

If we interpret the particles as intelligent entities, the sampling trajectories are their eyes; they try to maximize the free area around them, avoid walls but are blind to other entities for this interaction type. Figure 5.2(a) shows four particles and Fig. 5.2(b) the sampling trajectories for the red particle. The three green particles do not influence the sampling trajectories.

Figure 5.3 illustrates the temporal evolution of 20 entropically driven type A particles in a box of size $L = 20\sigma$, the particles' initial positions have been chosen randomly with no particles touching and initially no momentum. The timestep in given in the title of each figure, the frames indicate the walls. At timestep $n = 20$ the particles move closer to the centre, at $n = 50$ they already reached it. At timestep

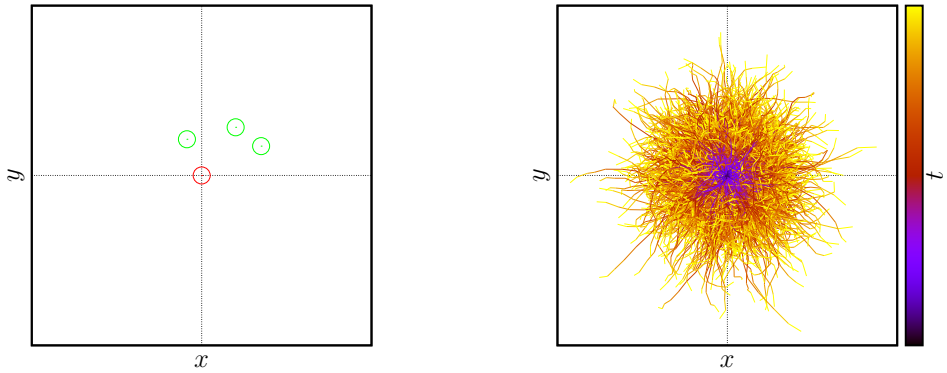

(a) (b)

Figure 5.2.: Type A interaction. (a): Four particles. (b): Sampling trajectories of the red particle.

$n = 75$ they exhibit a different configuration, showing that they constantly move around.

Every particle in general behaves as if it was alone in the system, being repelled by the walls and move towards the centre. All particles form a cloud, frequently bump into each other, never reaching an equilibrium state since all try to reach the same spot in the centre.

In Fig. 5.4 the final states of 20 particles in different systems are shown, both for position-space (left column, (a), (d), (g)) and momentum-space (right column, (b), (e), (h)). By final state we mean the steady state the system evolves to after a sufficiently long time. Every row contains a different system size and its respective horizon (small plot in the very right). In (a) ($\mathcal{P}$, $L = 20\sigma$) the particles move to the centre where they bump into each other and push each other away from the centre continuously. Four particles are stuck on the walls. (d) ($\mathcal{P}$, $L = 40\sigma$) shows essentially the same behaviour: Most particles are in the centre, two are stuck at the centre of the upper wall. For the largest system in (g) ($\mathcal{P}$, $L = 60\sigma$) the particles even after a long time do not fully move to the centre as soon as they reached a distance of size around the maximum length of they sampling paths. Not directly visible in this plot, the particles come to stop and very slowly diffuse, as it is the case in (a) actively bump into each other. One particle is stuck on the bottom wall at about $x = 0.5$, also not in the centre as it is the case for the two previously described simulations. In panels (b), (e) and (h) momentum-space $\mathcal{M}$ is used and the behaviour is qualitatively the same as when using $\mathcal{P}$, except that we do not

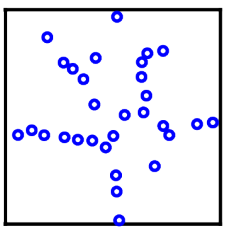

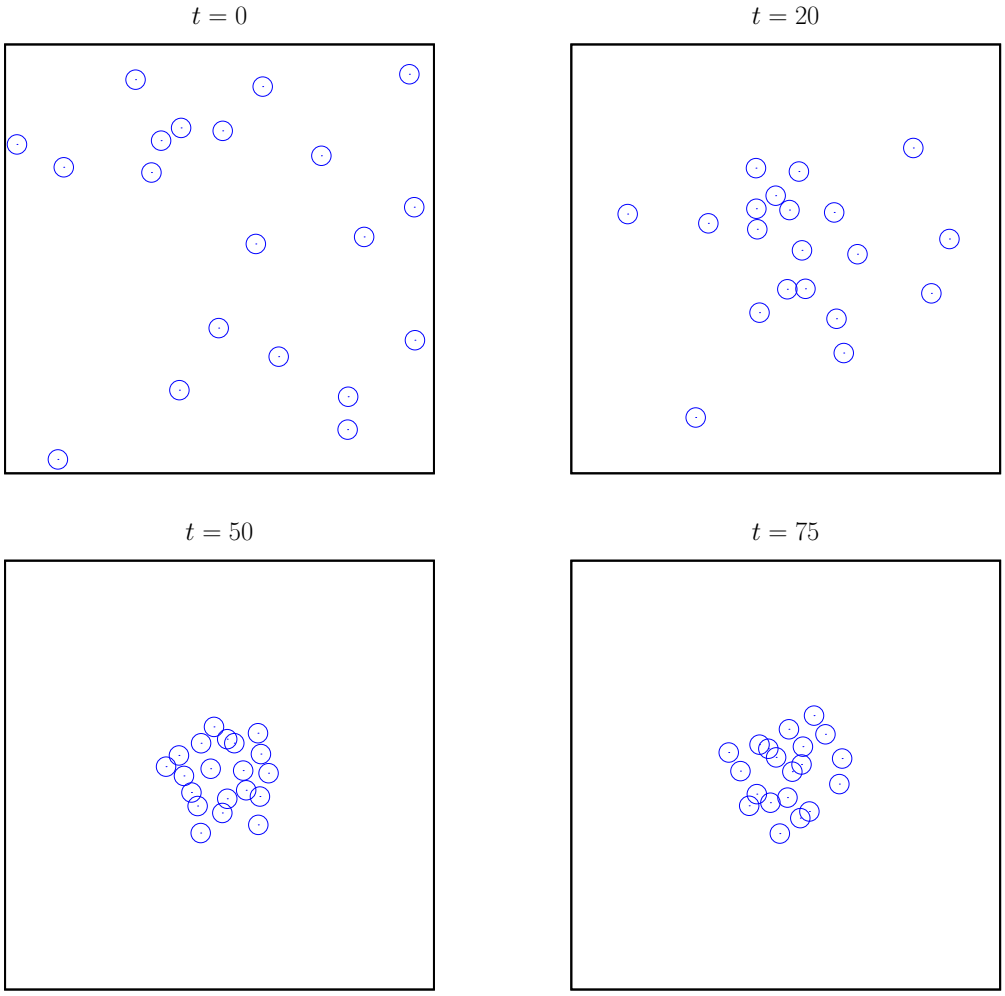

Figure 5.3.: Four snapshots of 20 particles moving in a box. [Type A interaction. Timesteps illustrated: $n \in [0, 20, 50, 75]$. $L = 20\sigma$, $T_r = 0.01$, $\frac{T_c}{T_r} = 0.5$, using $F_{\mathcal{M}}$]

observe particles getting stuck at a wall. Also in (h) they are closer to the centre than in panel (g).

The phenomenon of particles stuck at a wall when using $F_{\mathcal{P}}$ was already discussed in section 4.1. All particles stuck to the walls for the shown simulations initially happened to be so close to the walls that the entropic force was attractive. Note that the particles at a wall still maximize their distances from all other restrictions. In (a) and (d) they are at the centre of the wall whereas in (g) at maximum distance from the left wall, keeping in mind that its horizon is considerably smaller than the box.

The behaviour of the particles in (h), being more confined to the centre compared to (g), can be explained by looking at the way phase space is sampled. If a sampling path is reflected by a wall and we consider momentum-space, its radius of gyration $\mathcal{R}$ (which we use for quantifying phase space volume of a sampling path) increases dramatically. Therefore even if at the last step of a path a reflection from a wall occured it will have significant effect on $\mathcal{R}$. Using position-space a reflection in the last step of a otherwise stretched out path will make little difference to $\mathcal{R}$. To significantly feel the walls the particle would need to be closer to a wall.

The general behaviour of systems with type A interaction is always like just observed, we will not gain any new insights for other sets of parameters. However later in this thesis we will examine escape scenarios where this interaction type will be used again. We now move on to a different type of interaction.

5.2. "Seeing agents" (Type B)

Type B particles can detect other particles while sampling. The position of all other particles is kept fixed for the entire sampling time. If we interpret the particles as intelligent entities, type B particles see other particles and will assume they stay where they are in that moment. While sampling they have hard-core interactions, that is, if a sampling trajectory collides with a particle it is reflected in a manner equivalent to a collision with a wall. This applies only to sampling trajectories. If two seeing particles collide they still interact via a linear repulsive force as introduced in Eq. (5.1.1).

Figure 5.5 illustrates the sampling. Sampling paths are shown for the red particle at position (1,1), for the same configuration as in the type A case shown in Fig. 5.2. It is visible how every particle hinders the sampling paths from reaching the area

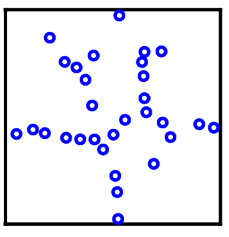

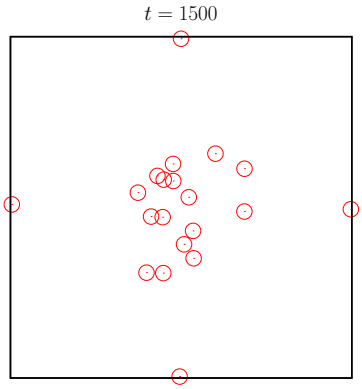

(a) Position-space, $L = 20\sigma$

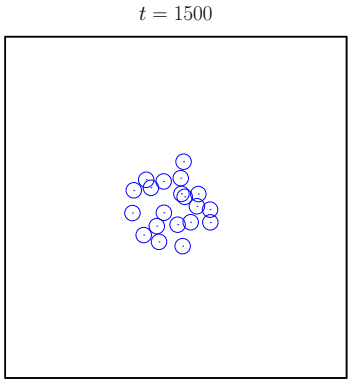

(b) Momentum-space, $L = 20\sigma$

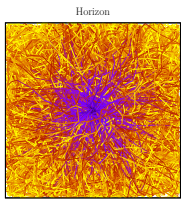

(c) Horizon $L = 20\sigma$

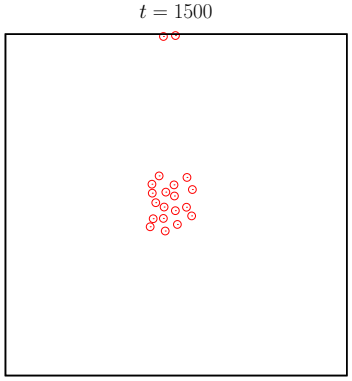

(d) Position-space, $L = 40\sigma$

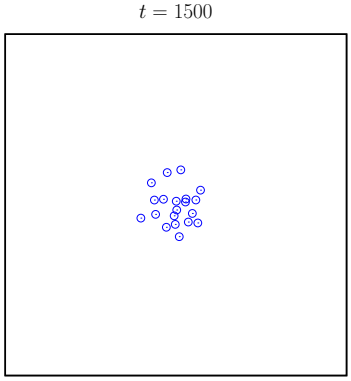

(e) Momentum-space, $L = 40\sigma$

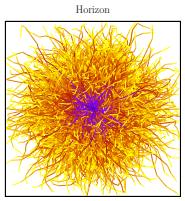

(f) Horizon $L = 40\sigma$

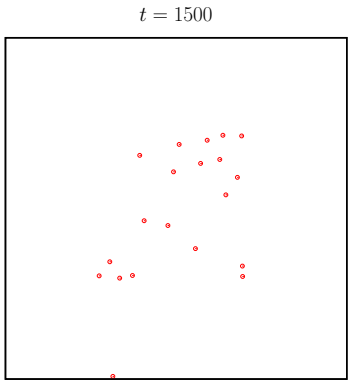

(g) Position-space, $L = 60\sigma$

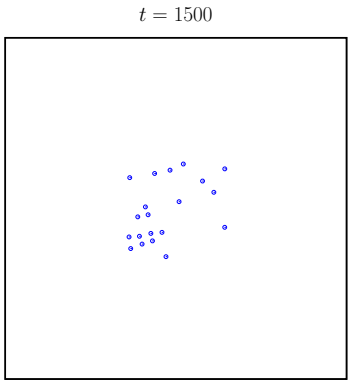

(h) Momentum-space, $L = 60\sigma$

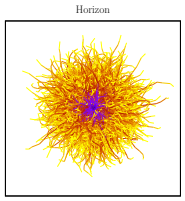

(i) Horizon $L = 60\sigma$

Figure 5.4.: 20 particles in systems of different sizes for position-space $\mathcal{P}$ and momentum-space $\mathcal{M}$. [$\mathcal{P}$: $\frac{T_c}{T_r} = 0.5$, $\mathcal{M}$: $\frac{T_c}{T_r} = 4$. $T_r = 0.015$]

behind it.

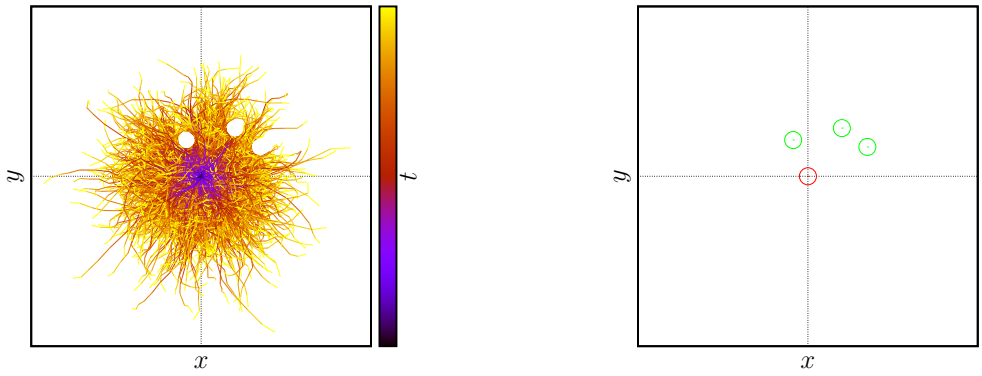

(a) (b)

Figure 5.5.: Type B interaction. (a): Sampling trajectories of the red particle. (b): The positions of the particles at time of sampling. [$T_r = 0.01$]

A typical evolution of a system using type B interaction is shown as an animation of figures in the bottom right corner of every odd page when rapidly turning the pages of this thesis. The shown figures are at times $t \in \{0, 4, 8, \dots\}$ (At page n the figure shows the system at time $t = \frac{n-1}{2} \cdot 4$). Figure 5.6 shows configuration of the system at selected times. The initially randomly distributed particles reach a steady state where they form lines. Some particles move towards the centre then together take a rhombic shape. The lines in general touch the wall at the central part. Note that (g) is at $t = 400\ \delta t$ and (h) at $t = 1500\ \delta t$, showing that this conformation does not change anymore except for small fluctuations around the steady-state positions. However single particles still can move around, as for example in (g) the single particle in the top right area or in (h) the one in the top left area. We want to emphasize that patterns do not form due to an artificially implemented potential, as for instance the Lennard-Jones potential with an attractive region. Pattern formation solely exists due to the entropic force.

We will now introduce some quantities and methods to quanitatively characterise the system's behaviour and evolution.

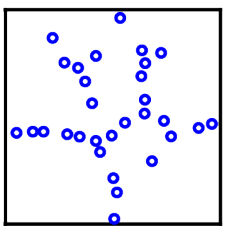

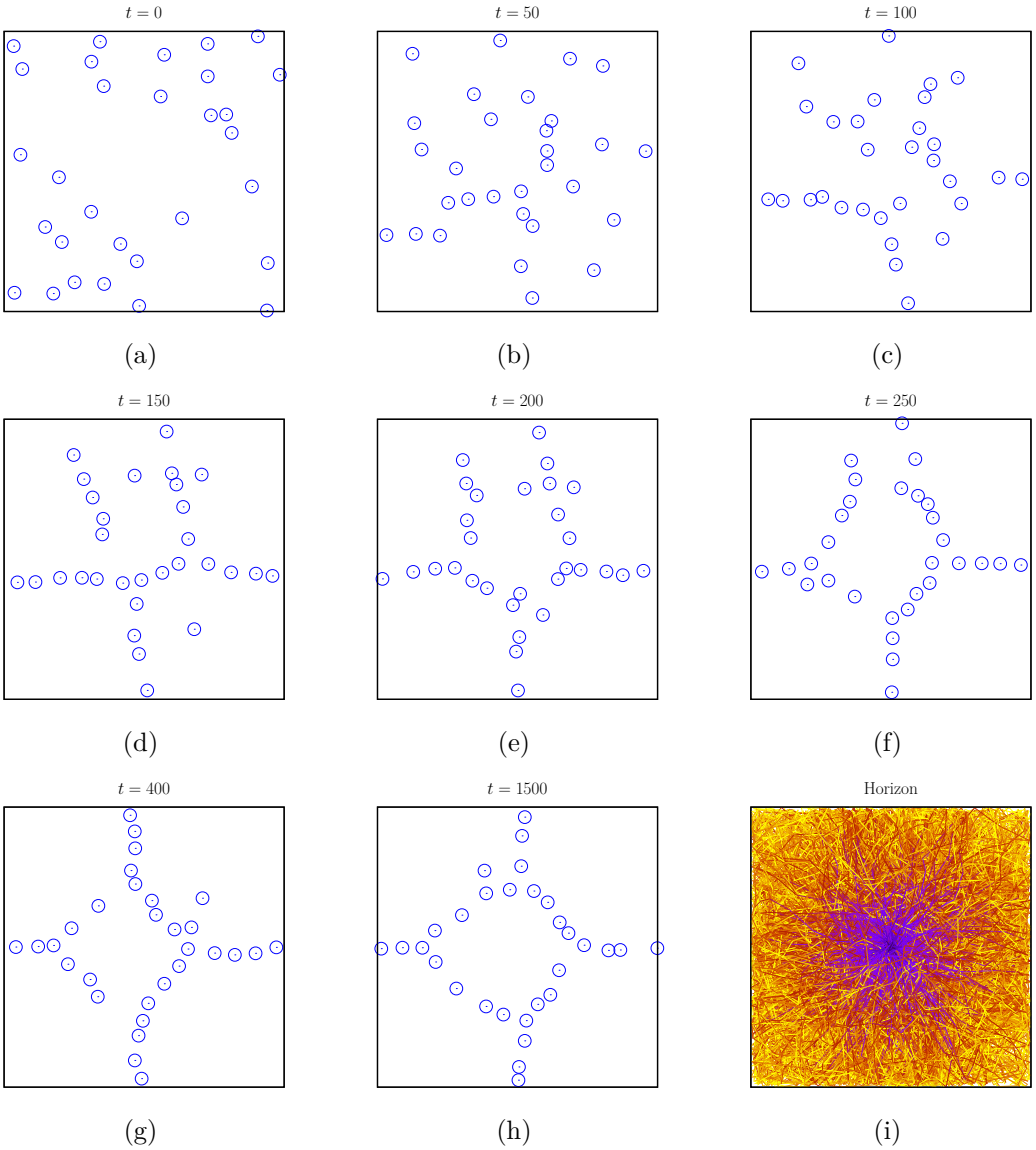

Figure 5.6.: Evolution of a system with type B interaction using $F_{\mathcal{M}}$. $[\frac{T_c}{T_r} = 4, T_r = 0.015, N = 30]$

5.2.1. Alignment factor

To detect the formation of lines as observed in Fig. 5.6 we use the alignment factor A

$$A(t) \equiv \left\langle 1 - \cos^2(\theta) \right\rangle , \tag{5.2.1}$$

where θ is the angle between the vectors connecting particle i to two neighbouring particles i_j (see Fig. 5.7(a)). We average A over all particles, where for every particle we include only its local neighbourhood within radial distance r_n (see Fig. 5.7(b)).

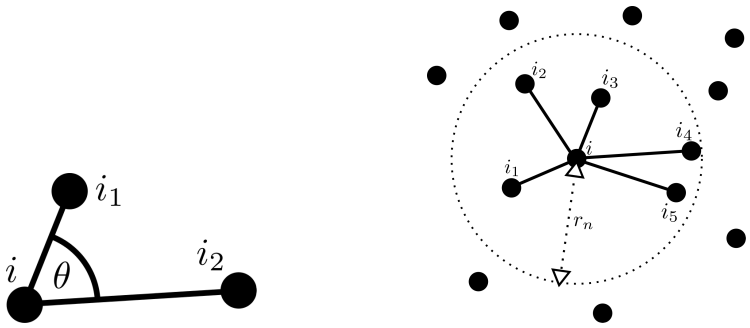

Figure 5.7.: (a): The angle θ between the connecting vectors of particle i to its two neighbours i_1 and i_2. (b): Particle i and five particles within its neighbourhood radius.

The alignment factor can vary between $A = 0$ which corresponds to a perfectly aligned system as shown is Fig. 5.8(a), and $A = 1$, corresponding to a system with exclusively perpendicular connecting vectors, shown in Fig. 5.8(b).

Figure 5.9 shows the alignment factor for the system in Fig. 5.6. Every data point is averaged over 25 snapshots. We observe the alignment factor decreasing from initially $A = 0.57$ to an average value around $A = 0.37$. Theoretically an unordered system would result in $A = 0.5$, but due to walls and finite size effects in our system the initial value is slightly increased. From Fig. 5.9 we can conclude that at $t = 200$ large parts of the system already formed lines. This can be confirmed by examining Fig. 5.6(d)-(f).

The alignment factor allows us to estimate the transient time of a system.

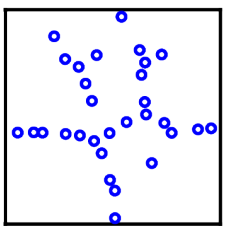

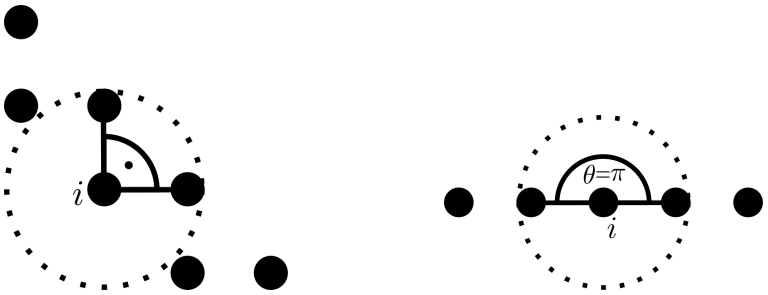

(a) $A = 1$ (b) $A = 0$

Figure 5.8.: (a): A configuration with solely perpendicular connecting vectors, resulting in $A = 1$. (b) A configuration with solely parallel connecting vectors, resulting in $A = 0$.

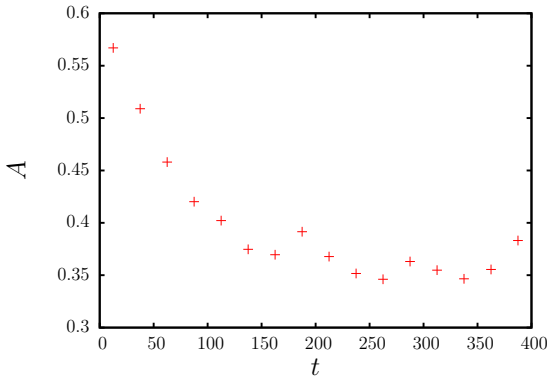

Figure 5.9.: Alignment factor of the system shown in Fig. 5.6. [Neighbourhood radius $r_n = 4\sigma$, averaged over $N = 30$ particles and 25 timesteps]

5.2.2. Radial distribution function

We use the radial distribution function (rdf) $g(r)$ to identify typical length-scales in a pattern. To compute $g(r)$

$$g(r) = \left\langle \sum_i \delta(r_i - r) \right\rangle \tag{5.2.2}$$

we first let the system reach a steady state and then count the number of particles per ring of radius r and width dr around a particle, so $g(r)$ is connected to the probability of finding a particle within distance [r,r+dr]. The number of particles is normalized by the area of the ring, excluding the parts which exceed the systems boundaries, as well as the number of particles and the the particle density. Normally the rdf converges to $g(r \gg 1) = 1$ for large distances since in an unordered system the probability of finding a particle in a certain distance approaches one. However, in our case the system is finite, and therefore the rdf decays to zero at maximum length existing in the system.

Figure 5.10(a) shows the rdf for the system in Fig. 5.6. We have marked the main peaks of $g(r)$ corresponding to the main length-scales. The corresponding distances between particles for each peak are shown in Fig. 5.10(b). Peak 1 and 2 correspond to the distance between a particle and its next and second next neighbour, respectively. Peak 3 and 4 are two characteristic lengths of the square structure in the centre of the box.

5.2.3. Van Hove function

We used the van Hove function, a time-dependent pair correlation function, for gaining insight into the nature of the patterns. It is defined as the probability of finding a particle j at distance r of particle i at time t. The van Hove function can be divided into the self and the distinct part, G_s and G_d,

$$\begin{aligned} G(r,t) &= G_s(r,t) + G_d(r,t) \\ &= \frac{1}{N}\left\langle \sum_{i=1}^{N} \delta(\mathbf{r} + \mathbf{r}_i(0) - \mathbf{r}_i(t)) \right\rangle + \frac{1}{N}\left\langle \sum_{i \neq j}^{N} \delta(\mathbf{r} + \mathbf{r}_i(0) - \mathbf{r}_j(t)) \right\rangle , \end{aligned} \tag{5.2.3}$$

where the self part gives the probability of a particle i travelling the distance $\mathbf{r}$ within time t and the distinct part describes the behaviour of all other particles. Using the

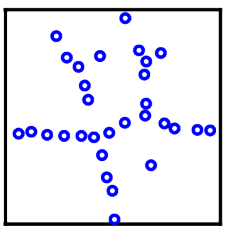

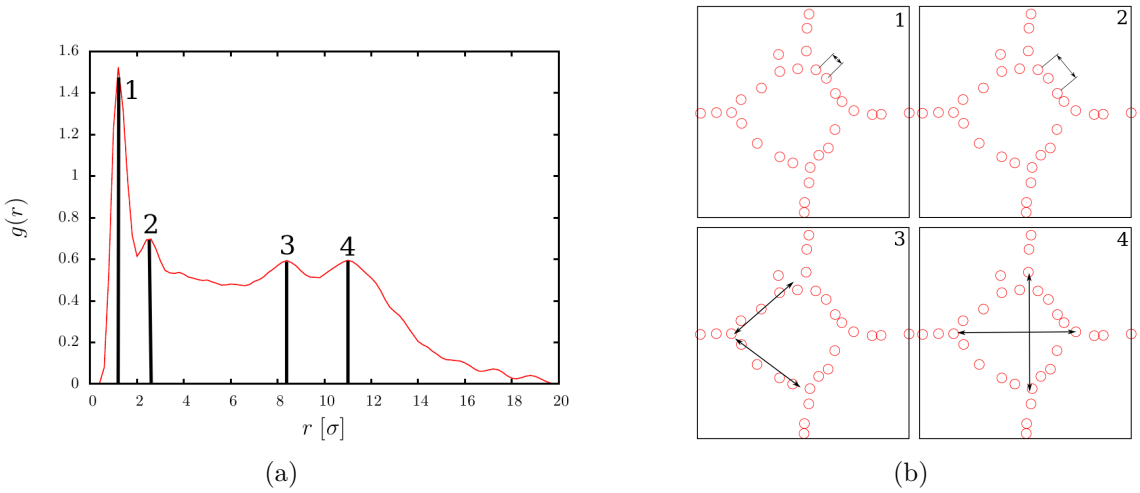

(a) (b)

Figure 5.10.: (a): Rdf of the system shown in Fig. 5.6 [$N = 30$, $L_x = L_y = 20\sigma$], averaged 26 independent simulations, each averaging over $n = 1000$ timesteps after a transient of $n_{\text{transient}} = 500$ timesteps. The four marked peaks correspond to examples of length-scales shown in (b).

van Hove function we can distinguish between static and stationary patterns in our system. Figure 5.11(a) shows the van Hove function of the system displayed in Fig. 5.12 for considered time intervals $\Delta t \in \{0, 100, 200\}$ in red, green and blue, respectively. The three time-intervals show how large the probability of finding a particle at distance r is at a certain time, corresponding to $\Delta t = 0$, or after a time interval $\Delta t = 100$, $\Delta t = 200$. The red curve takes similar shape as the rdf shown in Fig. 5.10, including the nearest neighbor peaks at $r = 2$ and $r = 3$ as well as the two peaks at $r = 8$ and $r = 11$. Also for $r \to 0$ we see $G(r)$ increasing dramatically. For larger time intervals all peaks dissolve and the curve smooths out. This indicates particles moving around instead of staying fixed relative to other particles. Figure 5.11(b) shows $G(r)$ for $\Delta t = 200$, the blue curve in Fig. 5.11 and its contributions of the self and distinct part, $G_s(r)$ and $G_d(r)$. The self part, which for $\Delta t = 0$ is a sharp peak at $r = 0$ dissolves and took in the displayed time the shape of a Gaussian. For a brownian particle in an open system the self part of a van Hove function is equivalent to the probability density distribution of its position. For time zero the distinct part of the van Hove function is equivalent to the radial distribution function. With increasing t the rdf starts to dissolve and smear out as particles move away from their initial relative positions. A crystal structure for instance is time-independent and would result in the same probability distribution of

the van Hove function for all t. However, if observe the initial distribution dissolve it does not necessarily mean that the structure of the particles is changing but rather the relative position of the single particles to each other. In this case stationary structure can be conserved.

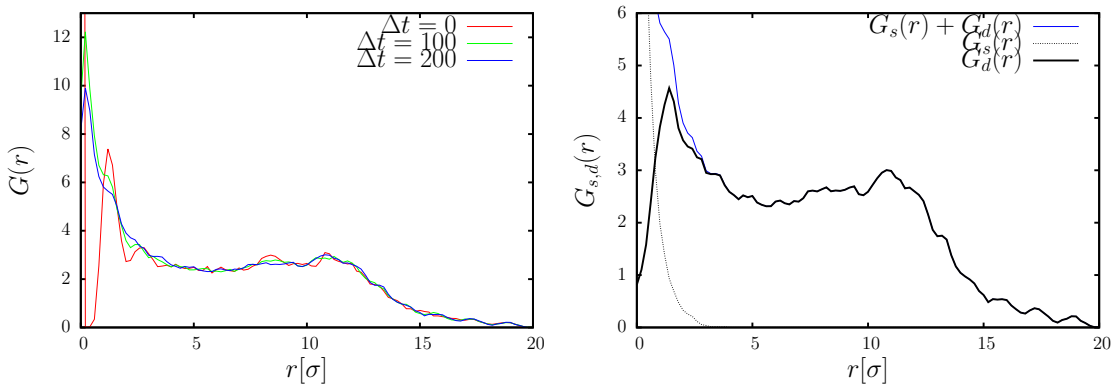

Figure 5.11.: (a): Van Hove function for the system shown in Fig. 5.12 for three time-intervals. (b): Van Hove function and its self and distinct part for $\Delta t = 200$.

5.3. Pattern formation

In this section we will first show some observed patterns, using both position- and momentum-space. We then examine their formation and characteristics and discuss by what mechanism they arise. Finally we briefly explore how patterns change with varying parameters.

Figure 5.12(a) and (b) shows snapshots of two simulations of $N = 100$ particles in a $L_x = L_y = 40\sigma$ square box using position- and momentum-space respectively. In Fig. 5.12(a) most particles form lines which meander through the system whereas few are close to walls. The particles close to the wall correspond to what we already observed for a single particle in a box in Sec. 4.1 where particles which were close to a wall initially would be attracted to it.

The pattern shown in Fig. 5.12(b) consists of lines forming polygonal areas. Some arms of the polygon are touching the wall, as in the bottom right of the box. Figure 5.12(c) shows a set of sampling paths for a particle in the centre of the box and $T_r = 0.015$, as used in the simulations in Fig. 5.12(a) and (b).

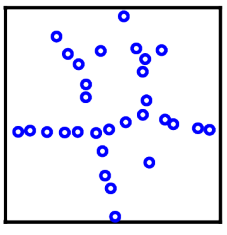

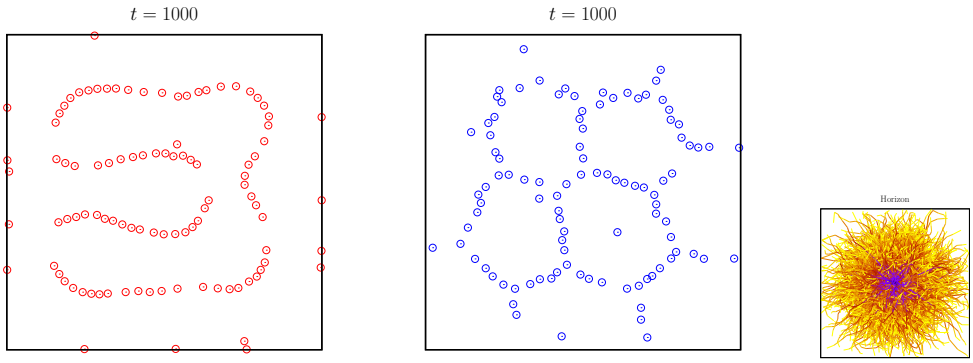

(a) using $F_{\mathcal{P}}$ (b) using $F_{\mathcal{M}}$ (c) Horizon for $T_r = 0.015$

Figure 5.12.: Pattern found in the system at time $t = 1500$ using (a) position- and (b) momentum-space of sampling trajectories for calculating the entropic force. [(a): $\frac{T_c}{T_r} = 0.5$, (b): $\frac{T_c}{T_r} = 4$, $L_x = L_y = 40\sigma$, $T_r = 0.015$, random initial position without particles overlapping]

Figure 5.13(a) and (b) show the corresponding alignment factors over time of the systems in Fig. 5.12. In Fig. 5.13(a) A decreases from initially $A = 0.5$ to $A = 0.12$ at time $t = 700$ where it reaches a plateau. At time $t = 1300$ A quickly increases to $A = 0.2$ and then slowly decreases again. The initial positions of the particles are chosen randomly and therefore $A(t = 0) = 0.5$. As the particles form structures, A approaches lower values since particles align. The increase at $t = 1300$ will be examined in Fig. 5.14. In Fig. 5.13(b) A decreases from $A(t = 0) = 0.5$ to $A = 0.35$ around $t = 200$ where it fluctuates around that value.

Figure 5.14(a)-(d) show the temporal evolution of the system in Fig. 5.12(a) at four times, and we compare it with the changes in the alignment factor (Fig. 5.14(e)). Figure 5.14(a) shows the system at time $t = 100$ when some particles already formed lines. In Fig. 5.14(b) at $t = 500$ most particles make up lines, some stick to the walls. In Fig. 5.14(c) the alignment factor reached the plateau with lowest A, as particles form lines meandering through the system. Figure 5.14(d) shows the system after the steep increase in A at $t = 1400$. Particles at position $(0.3, 0.4)$ are now scattered and unordered. From the decrease in A in Fig. 5.13(a) after $t = 1300$ we can see that the particles start realigning. However, throughout the entire simulation the same particles stay close to the walls. Note: The particle form lines and have very short distances to their nearest neighbours. Despite a rather soft repulsive force between two particles (force increases linearly with overlap of particles), particles

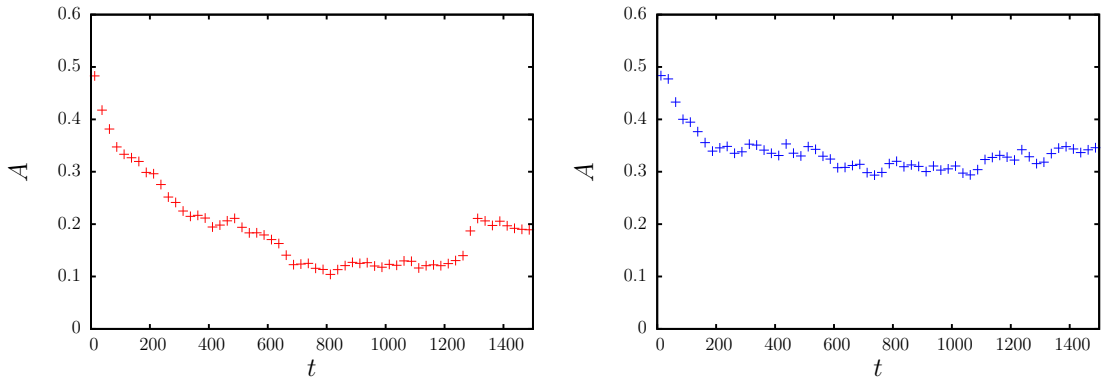

(a) corresponding to system in Fig. 5.12(a)

(b) corresponding to system in Fig. 5.12(b)

Figure 5.13.: Alignment factor A of (a),(b) the system shown in Fig. 5.12(a),(b). Radius of neighbourhood of a particle $r_n = 5\sigma$.

are occasionally pushed away from each other strongly. If by chance particles in a line are pushed towards each other, they briefly have larger overlap resulting in the particles gaining large momentum and locally destroying order. Such event occured around $t = 1300$. This effect only occurs when using $F_{\mathcal{P}}$. Further decreasing the repulsion between two overlapping particles would lead to particles passing through each other.

Figure 5.15(a)-(d) show the temporal evolution of the system in Fig. 5.12(b) (thus the dynamics is solved using $F_{\mathcal{M}}$) at four times and the comparison with its alignment factor, shown in Fig. 5.15(e). In Fig. 5.15(a) at time $t = 100$ the particles start forming lines. Figure 5.15(b) shows the system at $t = 500$ after the alignment factor already reached a plateau. The particles form up a polygonal structure, which is qualitatively maintained throughout the rest of the simulation, two times shown in Fig. 5.15(c) and (d). The particles locally lose order and realign afterwards, as visible in Fig. 5.15(c) in the top left corner where particles lost their linear structure and regained it at $t = 1400$ in Fig. 5.15(d).

Since the structure locally breaks up occasionally and yet reassemble to the same general structure we can conclude that a patterns will be the same for all times and initial conditions for a fixed set of parameters. The data shown in this section are typical.

In general, since every particle is entropically repelled by restricted areas, it prefers empty areas. Hence it makes sense for a large number of particles in a confined environment to form patterns in order to create those empty areas. Also due to

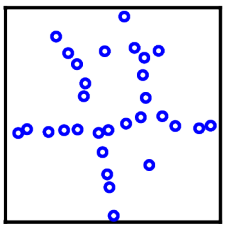

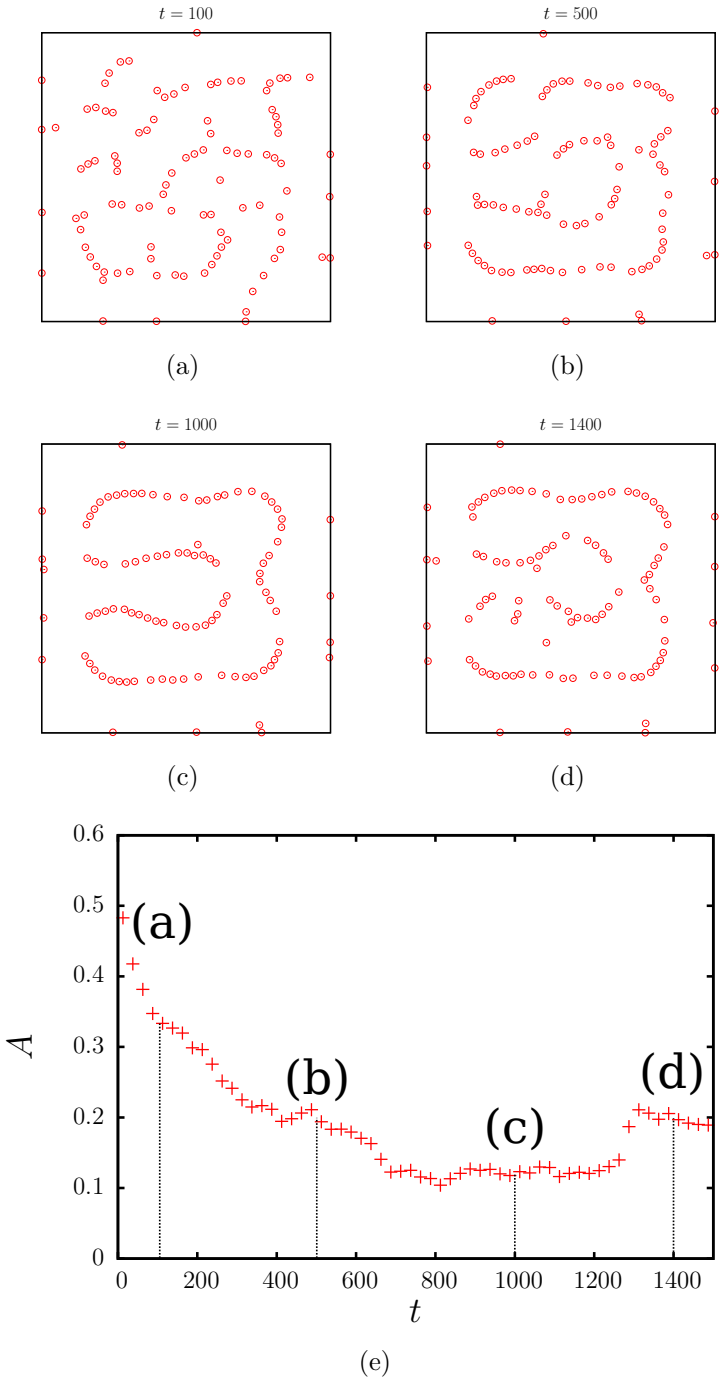

Figure 5.14.: (a)-(d): Four snapshots of the system shown in Fig. 5.12(a) at different points in their temporal evolution. (e): The alignment factor of the system with the four shown times marked.

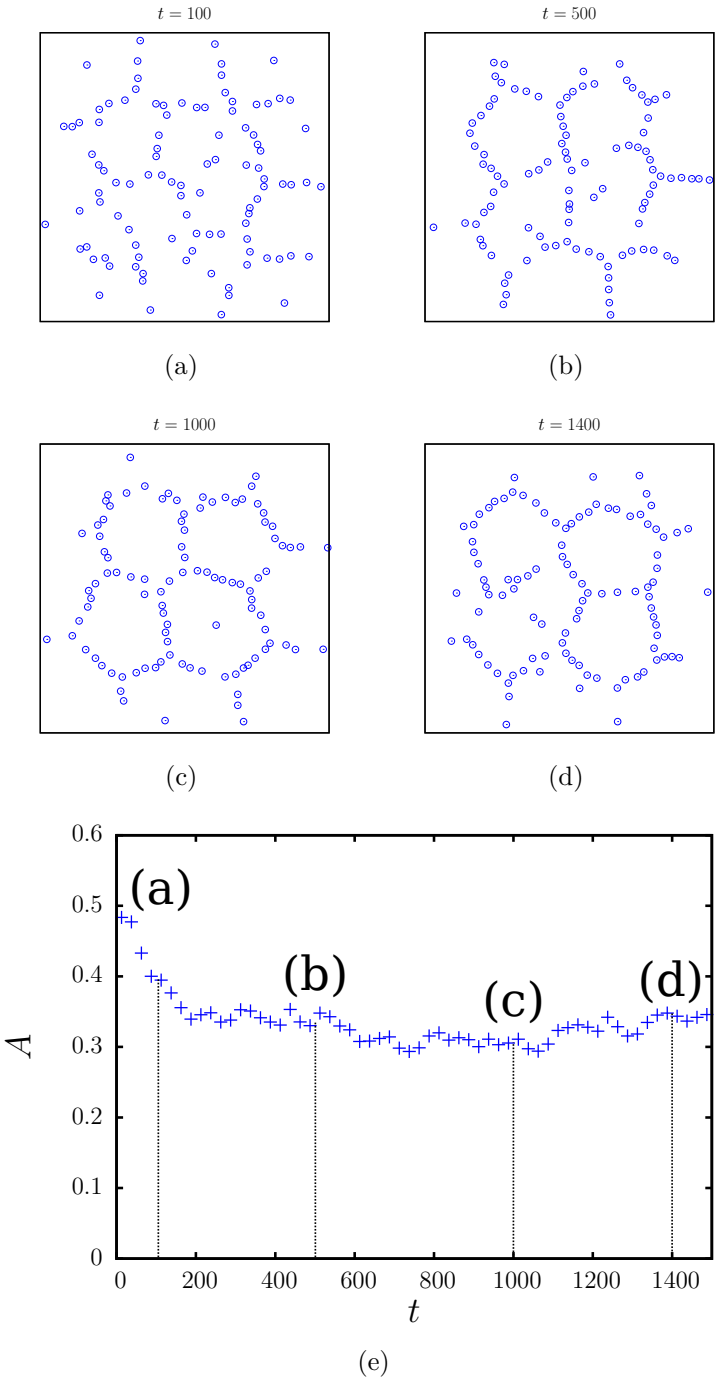

Figure 5.15.: (a)-(d): Four snapshots of the system shown in Fig. 5.12(b) at different points in their temporal evolution. (e): The alignment factor of the system with the four shown times marked.

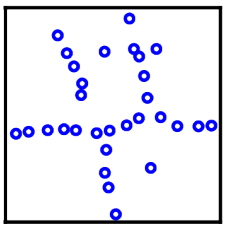

repulsion from walls particles seek a certain distance from them – excluding the minority of particles which stay close to walls and therefore effectively drop out of the dynamics of the simulation. It seems plausible for particles to form lines parallel to the walls, as walls generally exert greater repulsion than particles as they restrict a larger area. In order to get a deeper understanding of how or why particles form such patterns, we will examine the qualitative force being exerted from particles onto each other.

5.3.1. Force between two particles

First we examine the force exerted by a single particle of diameter σ onto another due to entropic forces. To that end we place two particles next to each other and calculate the entropic force for different distances. The setup is shown in Fig. 5.16(a). In Fig. 5.16(b) the entropic force for position and momentum-space in both directions parallel and perpendicular to the line joining the two centres is given. The horizontal axis denotes the distance of the particle centres from each other. In this simulation we used $T_r = 0.015$.

The perpendicular part fluctuates around zero. The parallel part for position-space in red for large distances is also zero but increases for decreasing distance. It has a peak around $d = 5\sigma$ and then decreases. For distances at almost at $d = 1\sigma$ when the particle would touch the force even becomes negative, meaning the particles would attract each other. The behaviour for momentum-space is similar. It increases steadily until around $d = 2\sigma$ there is a small kink. At $d = 1.25\sigma$ it reaches a peak and briefly decreases for even smaller distance, however it is repulsive for all distances. In (c) the same data is shown, magnified at the origin.

Concerning the perpendicular part the setup is symmetric and therefore a total force around zero makes sense. That the parallel part decreases for large distances is also plausible. For the red curve, position-space, the shape is similar to the particle-wall interaction, given in Fig. 3.6. The blue curve, momentum-space however shows different behaviour. Particles still exert a relatively strong repulsion onto each other for small distances.

5.3.2. Force between three particles

Since we face highly nonliner interactions, the interaction between two particles does not necessarily give adequate insight into the behaviour of more than two particles.

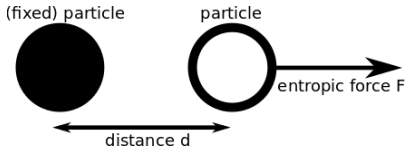

(a)

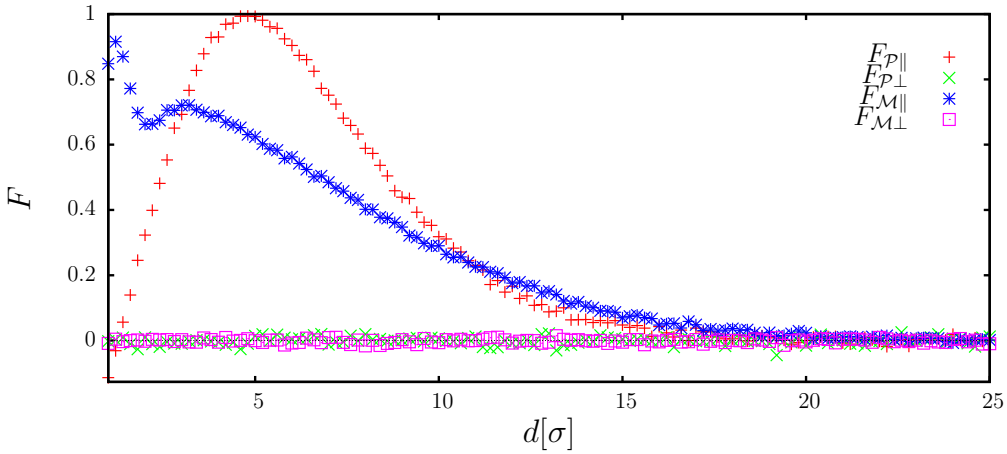

(b)

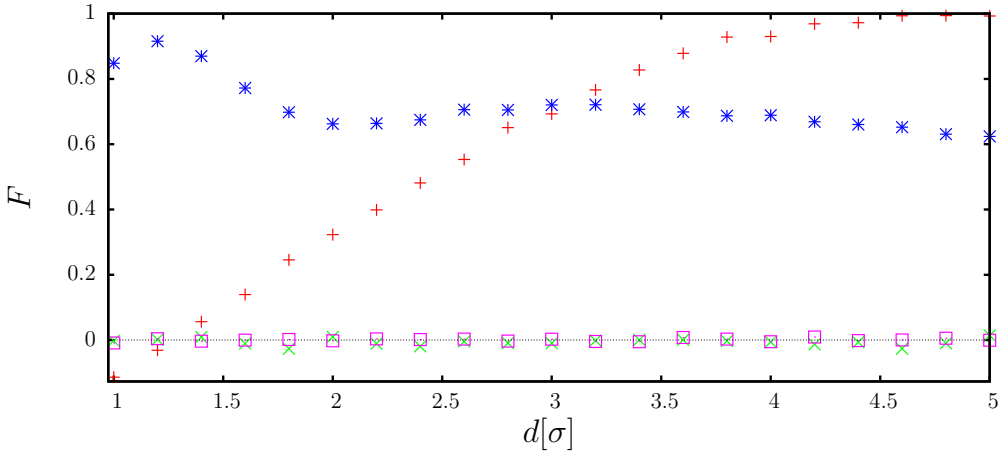

(c) magnification of (b) close to the origin

Figure 5.16.: Entropic force calculated using position and momentum-space respectively depending on distance to a fixed particle. [$T_r = 0.015$, every point averaged over $5 \cdot 10^6$ sampling trajectories, force was normalized to have its maximum value at 1]

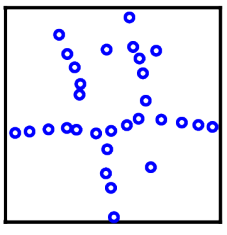

One configuration which could be observed frequently during the simulations was particles forming stable lines. Therefore we also examine the force of a particle between two fixed particles being moved from the centre outside. Figure 5.17(a) shows the entropic force normalized with maximum at $F = 1$ for variable d and d_p, where d_p is the distance between the centres of the two particles held fixed, and d is the distance between the test particle and the line joining the other two. In this simulation we used $T_r = 0.02$, however the qualitative shape of the force is of interest.

In 5.17(b) and (c) the force for different distances of the fixed particles to each other d_p the variable particle to the interseting line between the fixed particles d is shown. Fig. 5.17(d) and (e) contain the same data as (b) and (c) respectively for small distances d. The colour bar indicates the orientation of the force, red meaning repulsive and green attractive. While d goes from $d = 0$ to larger values, we have a minimum of $d_p = 2$. This is due to the definition of d_p as the distance of the centres of the fixed particles. For $d_p < 2$ the variable particle would overlap with the other particles. For both position and momentum-space the force is approximately zero for large distances d. With decreasing d the force increases in a manner similar to the two particle force in Fig. 5.16. Even the kink for momentum-space in Fig. 5.16 at $d = 3\sigma$ exists in Fig. 5.17(c) for $d_p = 2$ around $d = 1$. The force reaches a maximum at $d = 5\sigma$ for position- and $d = 3\sigma$ for momentum-space. Further decrease of d goes with decreasing force which reaches $F = 0$ for $d = 0$. Especially interesting is the area visible in Fig. 5.16(d) for $d \in [0, 1]$ and $d_p \in [2, 3]$, using $F_{\mathcal{P}}$, where the force is negative, that is, the test particle is attracted towards the mid point between the two fixed particles.

5.3.3. Pattern formation, using $F_{\mathcal{P}}$

For particles driven by an entropic force which was calculated using the position of their sampling paths, we found an attractive force between the particles. Two particles close to each other will feel comparibly small repulsion, or for even smaller distances than $d = \sigma$ an attractive force (see Fig. 5.18(a)). Once two particles come close enough they therefore tend to stay close. Thus a larger number of particles will form lines. Also and as a result from this attractive force, as discussed in Sec. 5.3.2, two particles exert a force on a third particle in between them, so that they align (see Fig. 5.18(b)).

In Sec. 4.1 we examined the behaviour of a single particle in a box, where the

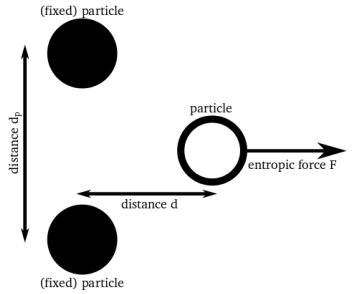

(a)

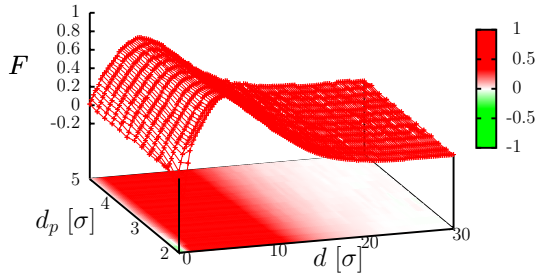

(b) Position-space

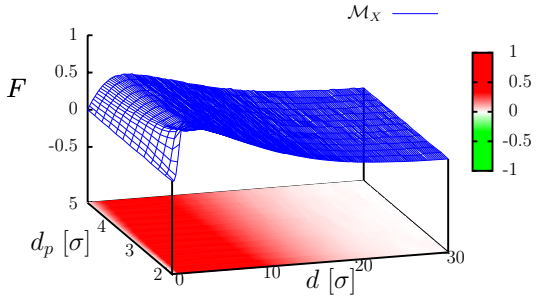

(c) Momentum-space

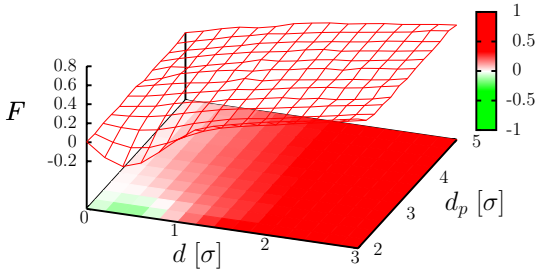

(d) Magnification of (b) for small d (position-space)

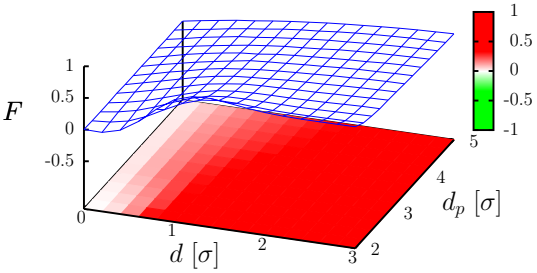

(e) Magnification of (c) for small d (momentum-space)

Figure 5.17.: Entropic force calculated using position-space and momentum-space of sampling trajectories, respectively, depending on distance to centre between two fixed particles and distance of those particles to each other (illustrated in (a)). [Averaged over $5 \cdot 10^6$ sampling trajectories, $T_c = 0.05$, $T_r = 0.02$]

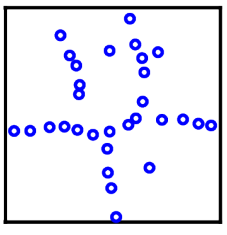

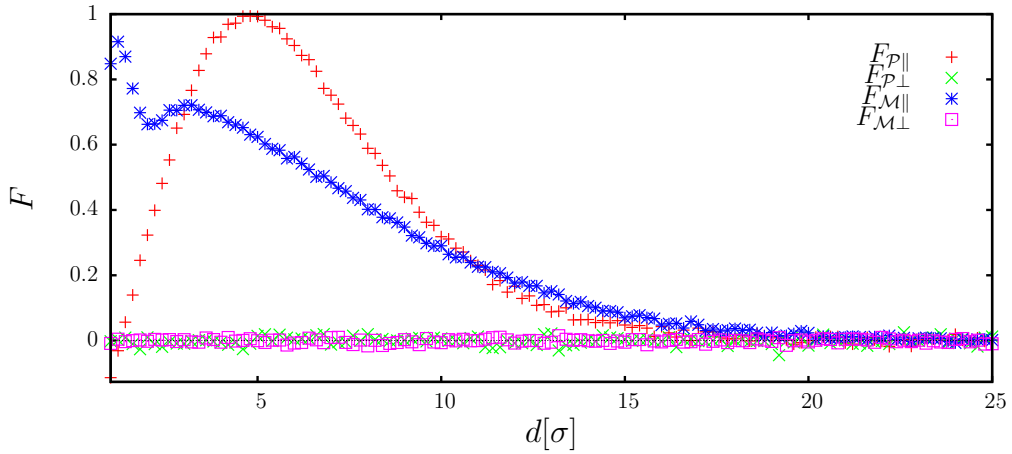

(a) Attractive region around $d = \sigma$

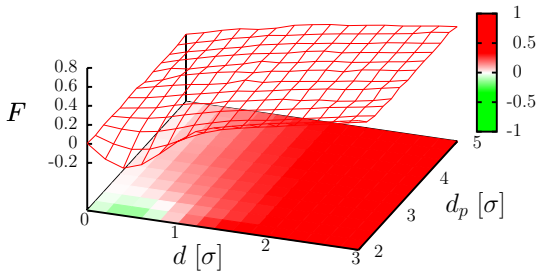

(b) Attractive region at $d = 0.5\sigma$ and $d_p = 2\sigma$

Figure 5.18.: Attractive region in the interaction of (a) two and (b) three particles, as introduced and discussed in Sec. 5.3.1 and 5.3.2.

phase diagram in Fig. 4.1 shows the performance in reaching the centre. We chose the parameters $T_c/T_r = 0.5$ and $T_r = 0.015$ for all simulations using $F_{\mathcal{P}}$. We discussed the choice of T_r in the beginning of Sec. 5. We use $T_c/T_r = 0.5$ in order to obtain relatively slow movement of particles, small fluctuations, hence allowing the formation of temporarily stable patterns. For a single particle with this set of parameters in Fig. 4.1 we are in the region where particles would stick to the wall if they are close enough to it. If we increase T_c/T_r such that fluctuations are large enough to prevent a particle from staying too close to a wall, that is, sticking to a wall, particles move too fast in order to form patterns – collisions of fast particles with emerging lines destroy any stable structure. Also, the phase diagram in Fig. 4.1 is valid for a single particles. Multiple particles in a system effectively decrease the accessible area of a single particle and therefore increase the tendency to stick to walls.

We now qualtitatively examine the formation of patterns using $F_{\mathcal{P}}$. We keep all parameters fixed and vary the particle density in the system. Figure 5.19 shows patterns for a system with a sampled area to box size ratio of $\mathcal{S} = 1$ which means the area explored by the sampling paths is roughly of size of the system. This is shown in Fig. 5.19(a). Figure 5.19(b)-(f) show patterns in the system which are representative, since the patterns qualitatively do not change with time. This was indicated in the beginning of Sec. 5.3 where we observed local decay of structures and the formation of similar structure thereafter. Also for different sets of initial conditions we observed the formation of the same patterns. Figure 5.19(b) shows a system with $N = 10$ particles of which two stay at the left wall while all others are positioned in the centre, equidistant to each other. In Fig. 5.19(c) with $N = 50$ particles form line segments. In Fig. 5.19(d) with $N = 90$ those segments already connect to each other and form larger structures. For $N = 140$ in Fig. 5.19(e) the formation of cells can be observed in the bottom left where lines connect with each other via small particles bridges. Figure 5.19(f) with with much larger density $N = 240$ cells are the dominating type of structure.

For $N = 10$ in Fig. 5.19(b) enough space is available such that particles keep relatively large distance to other particles and the walls (excluding particles sticking to the wall). For increasing particle density the formation of patterns becomes entropically more favorable for every single particle. Although every particle is only maximizing its own entropy, they form structures from which every particle benefits entropically. Initially the structures are positioned in the centre with distance from

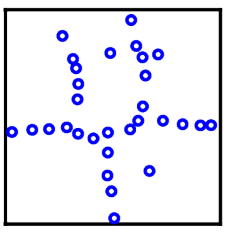

walls, for $N = 140$ they already connect with particles at the wall.

So using $F_{\mathcal{P}}$, upon increasing density particles start forming line segments which then form larger structures, lines through the system, and at last a cellular structure.

5.3.4. Pattern formation, using $F_{\mathcal{M}}$

Using momentum-space no attractive particle-particle interaction was observed (see Fig. 5.18(a)). Yet we observed the emergence of patterns, as seen in Fig. 5.12(b). Unlike for position-space where the force decreases to zero as particles come closer, using $F_{\mathcal{M}}$ they entropically exert a strong repulsion onto each other. So if a particle (using $F_{\mathcal{M}}$) in an otherwise perfect line moves out of symmetry, its two neighbouring particles will push it further away. Hence, lines must be highly unstable by themselves, some other force or effect keeps them in a semi stable structure. 'Semi' stable, since we observed in Fig. 5.15 that the structure can temporarily dissolve locally. Particles forming clean lines suddenly lose order, move around within the system for a short time before reassembling.

This additional force stabilizing patterns originates from walls or a number of particles blocking an area and thus having an equivalent effect as walls.

Figure 5.20 shows patterns observed in systems with $\mathcal{S} = 1$ using $F_{\mathcal{M}}$ for calculating the entropic force. Figure 5.20(b) shows $N = 20$ particles in the centre of a box forming a square cloud with the particles equidistant to each other and keeping a minimum distance to the walls. For $N = 30$ in Fig. 5.20(c) particles form lines parallel to the walls. The density is so high that particles in a cloud like in Fig. 5.20(b) repell each other, as well as being repelled by the walls and thus form lines or rather a circular structure. In Fig. 5.20(d) a circle formed in the bottom left part of the box, the other particles form lines which shape three cells adjacent to the circle. In Fig. 5.20(e) and (f) particles form cells with lines connecting the cells to the walls, and with increasing density the diameter of the cells decreases. For low particle density we did not observe particles positioned close to walls, only when the density is large enough such that particles touch the walls as part of a pattern.

As expected, no free lines, that is, lines without its ends attached to another structure or wall could be observed. A single line of particles is unstable and cannot exist over time.

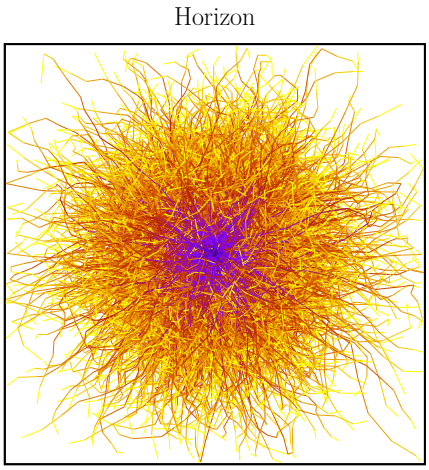

(a) $T_r = 0.015$, $\mathcal{S} = 1$

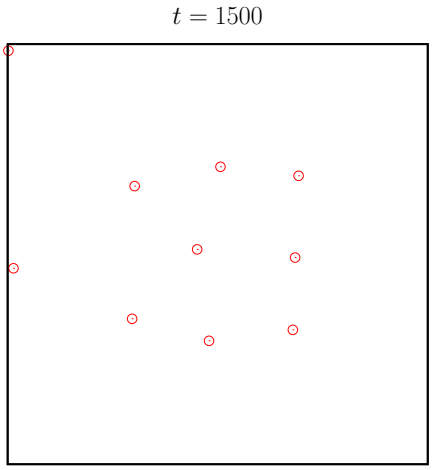

(b) N = 10

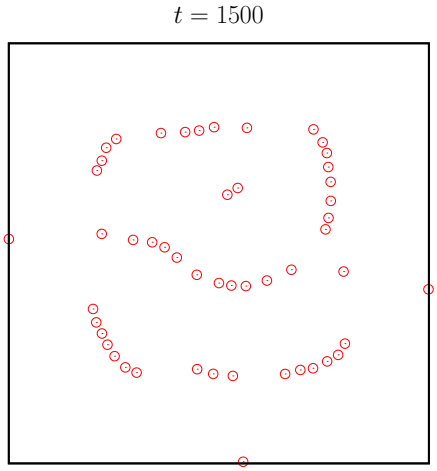

(c) N = 50

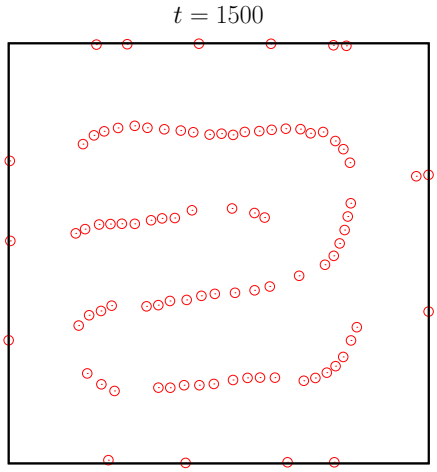

(d) N = 90

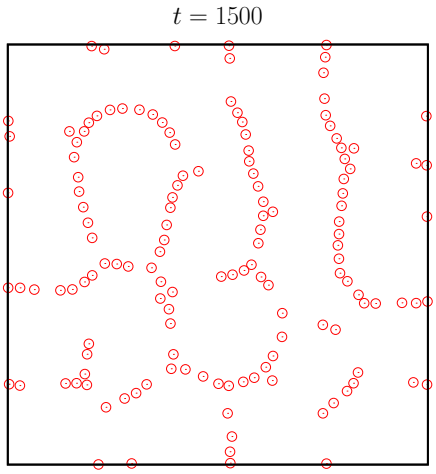

(e) N = 140

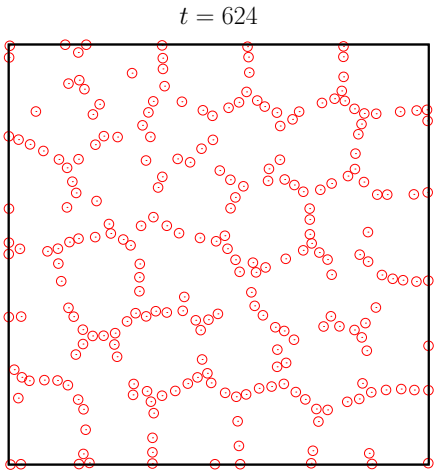

(f) N = 240

Figure 5.19.: Patterns in a square box with $\mathcal{S} = 1$ using $F_{\mathcal{P}}$. $[\frac{T_c}{T_r} = 0.5,\ T_r = 0.015]$

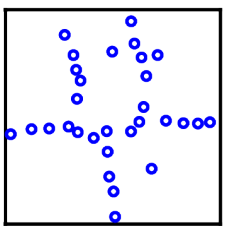

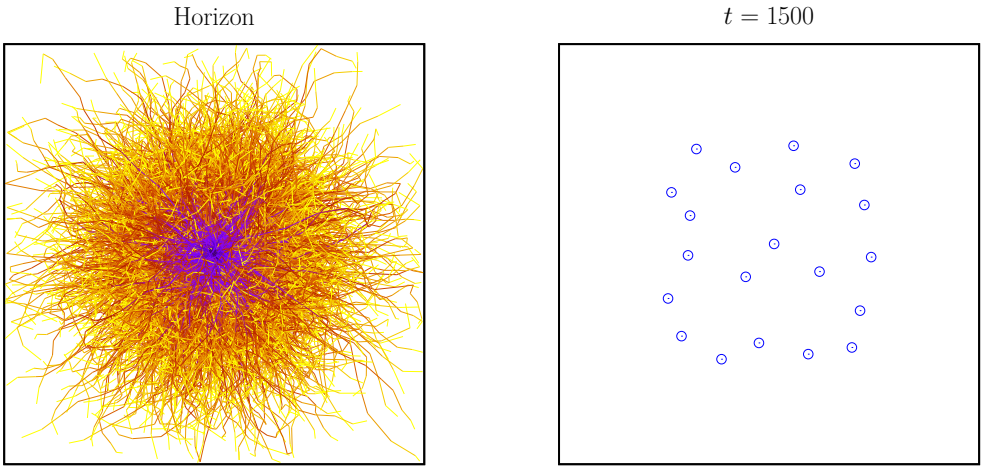

(a) $T_r = 0.015$, $\mathcal{S} = 1$ (b) N = 20

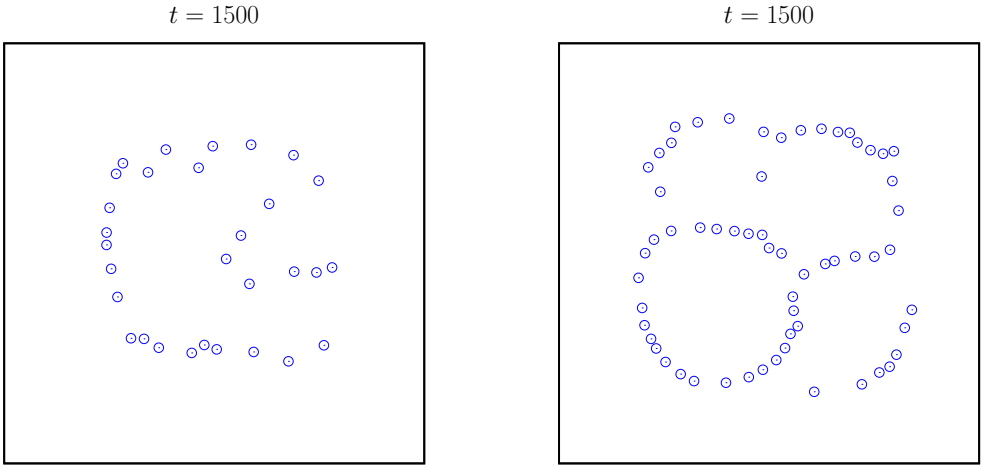

(c) N = 30 (d) N = 60

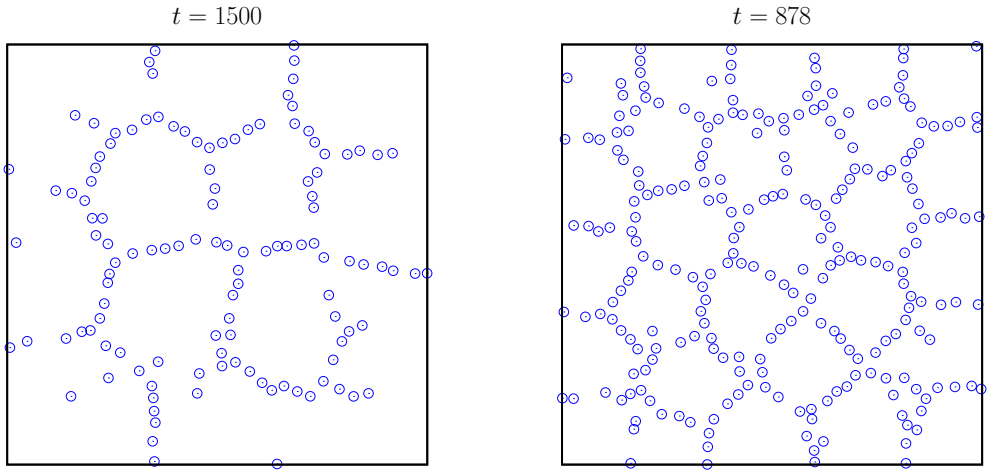

(e) N = 120 (f) N = 240

Figure 5.20.: Patterns in a square box with $\mathcal{S} = 1$ using $F_{\mathcal{M}}$. $[\frac{T_c}{T_r} = 4, T_r = 0.015]$

5.3.5. Comparing patterns

The difference in how patterns emerge between using position- and momentum-space is illustrated in Fig. 5.21. For $\mathcal{S} = 1.5$ an increasing number of particles in a box is shown. Using position-space, in Fig. 5.21(a) we observe single scattered particles attaching to each other, with increasing N forming short line segments in Fig. 5.21(b) and connecting to longer lines in Fig. 5.21(c). Using $F_{\mathcal{M}}$, in Fig. 5.21(d) particles are uniformly distributed within the centre of the box. For larger N in Fig. 5.21(e) particles form circles and in Fig. 5.21(f) form cells.

If the density is high enough, for both methods cellular structures can be observed. Using position-space this happens when for increasing density lines of particles make an increasing number of connections between each other, resulting in uniform cells. Using momentum-space, cells can be viewed as densely packed circles.

5.3.6. Analysing patterns, using $F_{\mathcal{P}}$

To better understand how patterns depend on N we extract their characteristic length-scales. For that, we calculated the radial distribution function (rdf) of each simulation and noted the positions of peaks. Figure 5.22(a) shows the rdf of a system with $N = 90$ and $\mathcal{S} = 1$, as shown in Fig. 5.19(d). We can identify the peak around $r = 1\sigma$ as the distance between two neighbouring particles and the next peak around $r = 2\sigma$ as the next-neighbour distance. The peaks at $r \in \{8, 16, 25, 33\}$ represent the distances between the lines in the system. The position of those peaks are shown in Fig. 5.22, plotted versus N, where we can identify five lines. Two lines are around $r = 2\sigma$. One is at $r = 8\sigma$ for $N = 10$, then increases to $r = 12\sigma$ at $N = 60$ and for large N smoothly decreases to $r = 8\sigma$. Another line can be identified with $r = 17\sigma$ for $N \geq 90$ which decreases to $r = 15\sigma$ for $N \geq 200$. A fifth line appears for $N \geq 30$ at $r = 21\sigma$, rises to $r = 25\sigma$ for $N = 80$ and keeps that value until $N = 180$.

The two lines at $r = 2\sigma$ correspond to the distance between two neighbouring particles in a chain and the second next particle, respectively. As soon as those peaks appear, we can assume particles start forming lines. For $N = 50$, $N = 80$, and $N = 100$ even the peak for the third next particle is visible around $r = 4\sigma$. The line around $r = 8\sigma$ indicates the distance between lines or line segments, or for $N \geq 140$ also the diameter of cells. For $N < 40$ it also includes the distance between single particles, as for instance in Fig. 5.19(b). The decrease in r for increasing N for $N > 100$ of the peaks associated with this line can be understood by comparing

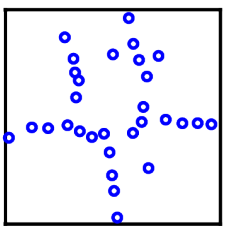

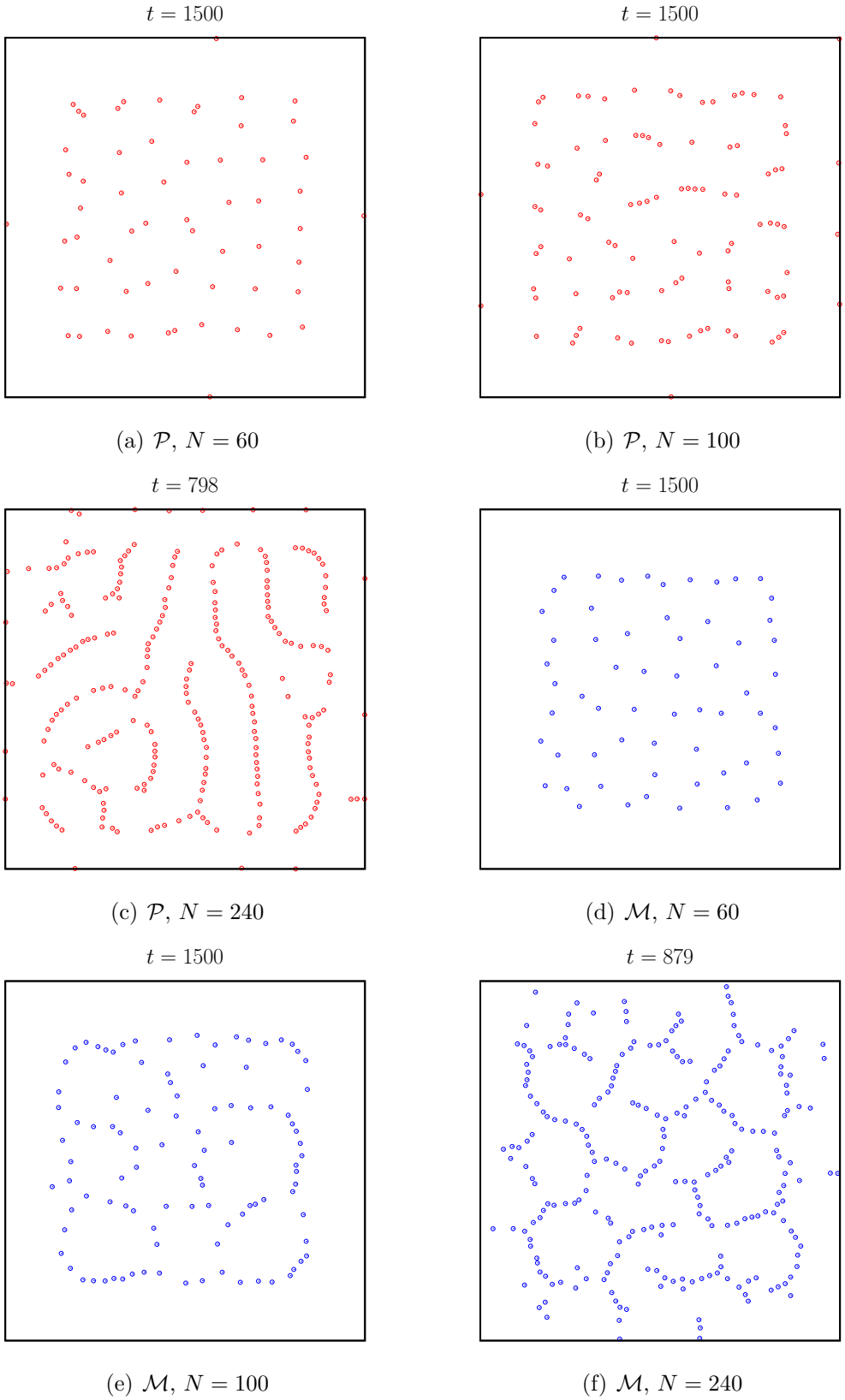

(a) $\mathcal{P}$, $N = 60$ (b) $\mathcal{P}$, $N = 100$

(c) $\mathcal{P}$, $N = 240$ (d) $\mathcal{M}$, $N = 60$

(e) $\mathcal{M}$, $N = 100$ (f) $\mathcal{M}$, $N = 240$

Figure 5.21.: Comparing patterns from simulations using position- and momentum-space with $\mathcal{S} = 1.5$.

Fig. 5.19(e) and (f). As the particles density increases, the size of structures or cells decreases due to limited space.

The line around $r = 16\sigma$ corresponds to the second next line segment or cell for $N \geq 90$. For $N < 90$ no peaks existed at that distance.

The fifth line, around $r = 21\sigma$ for $N \geq 30$ and $r = 26\sigma$ for $N \geq 80$, corresponds to the maximum characteristic length of the structure in the centre of the box. This includes the peak at $r = 17\sigma$ for $N = 10$ which corresponds to the maximum distance between two particles in the centre of the box (see Fig. 5.19(b)). With increasing N more particles take space in the centre and thus the size of structures (or for $N = 10$ the size of the cloud) increases. Comparing Fig. 5.19(c) with (d) shows this. For $N = 90$ in Fig. 5.19 particles take more space and the size of the structure increases from $r = 22\sigma$ for $N = 50$ to $r = 26\sigma$ for $N = 90$. Also this line is the first multiple of the first line for $N < 90$ and the second multiple for $N \geq 90$.

In Fig. 5.22(a), the peak at $r = 33\sigma$ is not in the diagram in Fig. 5.22(b). This peak corresponds to the distance between an outer line and the particles at the opposite wall. Those distances $r > 30\sigma$ do not reveal any additional information about patterns within the system wherefore we do not take them into account. This includes the single point in Fig. 5.22(b) at $r = 30\sigma$ for $N = 20$.

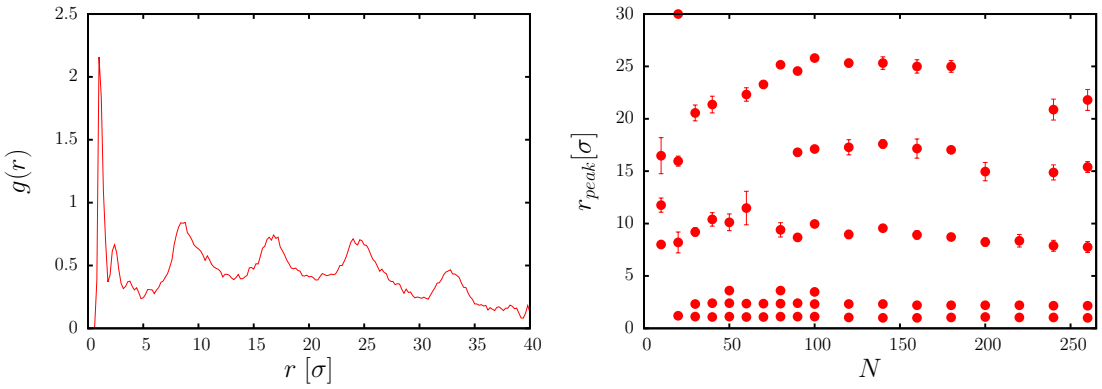

(a) (b)

Figure 5.22.: (a): Rdf of system with $\mathcal{S} = 1$,$N = 90$ as shown in Fig. 5.19(d). (b): Peaks in rdf for different N.

We now compare the diagram in Fig. 5.22(b) with the corresponding diagrams for $\mathcal{S} = 0.5$ and $\mathcal{S} = 1.5$, so for systems with the box size smaller and larger than the area covered by the sampling paths, respectively.

Figure 5.23(a) and (b) show the positions of the peaks for $\mathcal{S} = 0.5$ and $\mathcal{S} = 1.5$

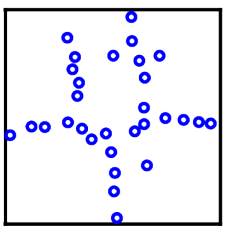

respectively. The general shape of the diagram is the same as for $\mathcal{S} = 1$. We can identify two lines around $r = 2\sigma$ for the first and second neighbour of particles in chains, as well as the peaks around $r = 7\sigma$ corresponding to the distance between line segments or the diameter of cells. For $\mathcal{S} = 0.5$ for $N \in [10, 30]$ and $N \in [80, 100]$ the first multiple of those peaks are visible. For $\mathcal{S} = 1.5$ however we can identify more multiples, indicated by the approximately equidistant positions of the peaks for every N in Fig. 5.23(b).

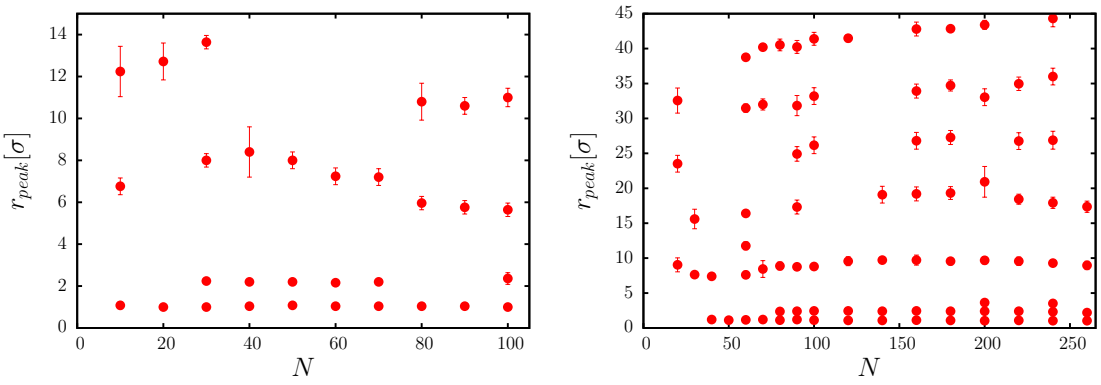

(a) $\mathcal{S} = 0.5$ (b) $\mathcal{S} = 1.5$

Figure 5.23.: Position of peaks for variable N in a system with (a): $\mathcal{S} = 0.5$, (b): $\mathcal{S} = 1.5$

5.3.7. Analysing patterns, using $F_{\mathcal{M}}$

Figure 5.24 shows the position of peaks in the radial distribution functions of simulations for $\mathcal{S} = 1$ using momentum-space of the sampling trajectories for calculating the entropic force, from the same system shown in Fig. 5.20. Similar to the previously discussed results in Fig. 5.22(b) we observe two lines around $r = 2\sigma$ resulting from the next and second next neighbouring particles, as well lines around $r = 10\sigma$ and $r = 20\sigma$, and for $N \geq 160$ a line around $r = 25\sigma$. At $r = 10\sigma$ we observe the line corresponding to distance of lines to each other or cell diameter, increasing with particle density until $N = 60$ and $r = 13\sigma$ then steadily decreasing to $r = 7\sigma$. For increasing N, this is due to the formation of lines and structures from equidistant particles and then increasing density leading to smaller cells. The other two lines are multiples of this. The line at $r = 20\sigma$ splits into two lines for $N \geq 140$, when cells decreased in size leading to a larger number of cells and therefore more multiples of

their diameter, that is, multiples of the characteristic length of the system's pattern.

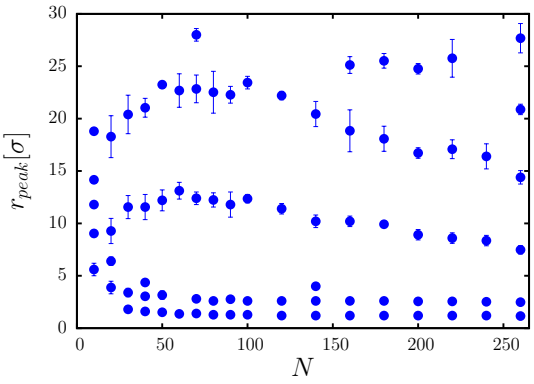

Figure 5.24.: Peaks in rdf for variable N with $\mathcal{S} = 1$ using $F_{\mathcal{M}}$.

For systems with $\mathcal{S} = 0.5$ and $\mathcal{S} = 1.5$ those plots a shown in Fig. 5.25. Like for position-space in the previous section in Fig. 5.23, we observe the same general behaviour as for $\mathcal{S} = 1$ in Fig. 5.24. Two lines around $r = 2\sigma$ corresponding to next neighbours as well as a line around $r = 9\sigma$ as characteristic length in the system and its multiples. Beside that, in Fig. 5.25(b) lines seem to split for increasing N given that the systems geometry allows structures for further increase of density (which is not the case for $\mathcal{S} = 0.5$). At $N = 50$ we can interpret a line with $r = 6\sigma$ splitting into the line at $r = 12\sigma$ and the two next neighbour lines. Also we can assume a split at $N = 220$ for $r = 25\sigma$ into $r = 22\sigma$ and $r = 32\sigma$.

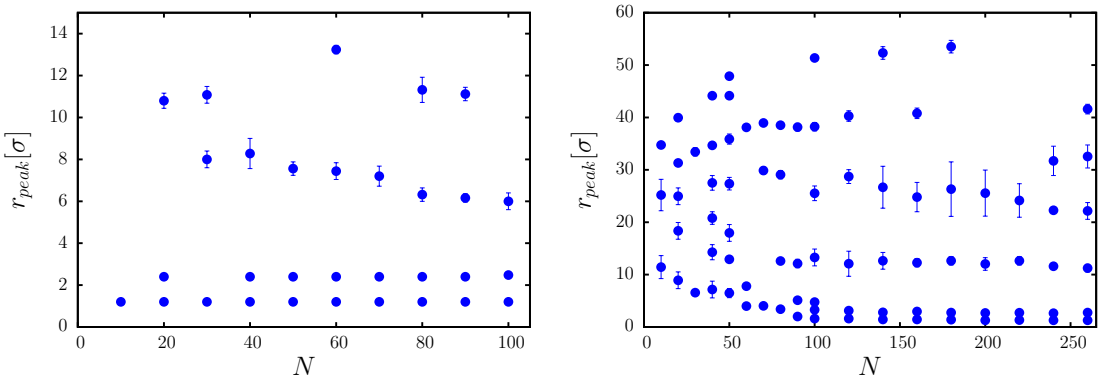

Figure 5.25.: Position of peaks for variable N in a system with (a): $\mathcal{S} = 0.5$, (b): $\mathcal{S} = 1.5$

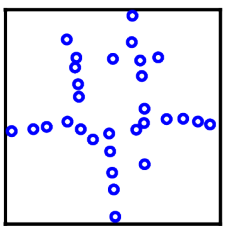

5.3.8. Influence of walls

In Fig. 5.21(c) and (f) particles in the centre of the box have a horizon too small in order to detect walls and the patterns are coherent with what we observe for $\mathcal{S} < 1.5$. In order to learn about the influence of the system's geometry on the formation of structures, we show in Fig. 5.26 a system with circular boundaries. We chose the radius of the circle such that $\mathcal{S} = 1$. Figure 5.26(a) shows a set of sampling trajectories for a particles in the centre of the circle. In Fig. 5.26(b) using $F_{\mathcal{P}}$, $N = 90$ particles form two concentric circles, also a number of particles is at the boundary. For $N = 160$ in Fig. 5.26(c) we see the formation of cells. Figures 5.26(d)-(f) show for momentum-space the transition from particles forming circles for $N = 40$ to cells for $N = 160$. Particles, like for a square system, tend to align with the walls and therefore form circles until for higher density a cellular structure arises.

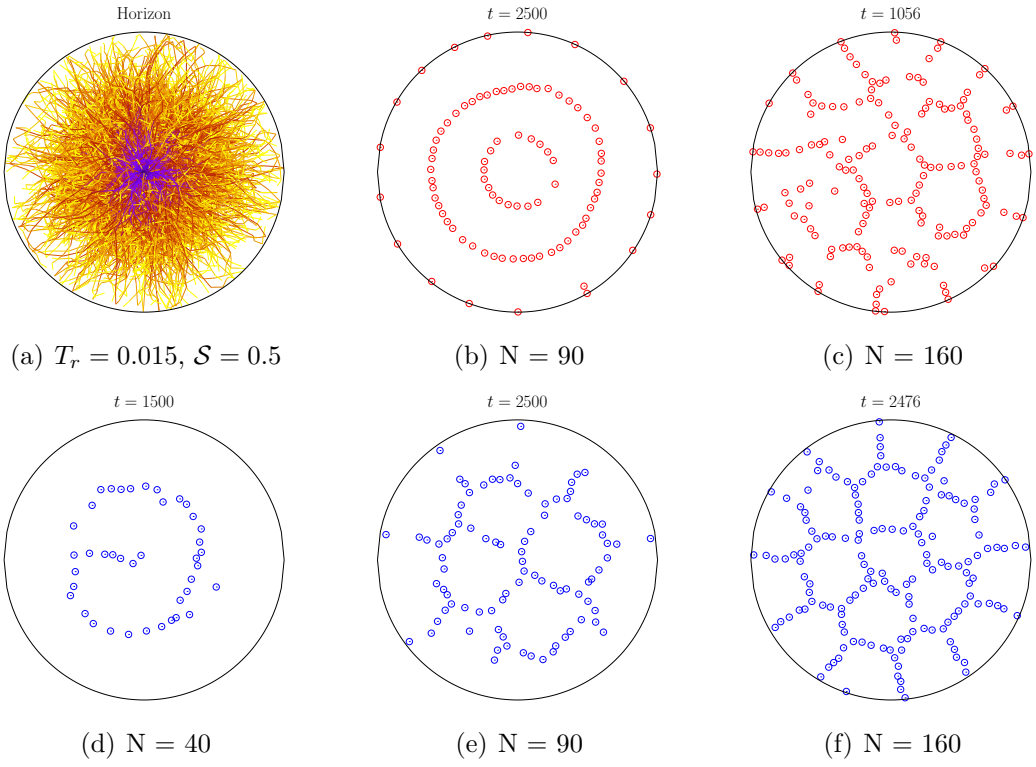

(a) $T_r = 0.015$, $\mathcal{S} = 0.5$ (b) N = 90 (c) N = 160

(d) N = 40 (e) N = 90 (f) N = 160

Figure 5.26.: Circular boundary conditions with $\mathcal{S} = 1$.

In order to truly understand the impact of the walls on the patterns we remove the walls and study the system with periodic boundary conditions where particles

solely act relative to each other's position. Figure 5.27 shows a system equivalent to a $\mathcal{S} = 0.5$ square box with periodic boundary condition. Figure 5.27(a) shows particles driven by the entropic force calculated using $F_{\mathcal{P}}$, Fig. 5.27(b) using $F_{\mathcal{M}}$. For both methods patterns emerge, plainly through interaction with each other.

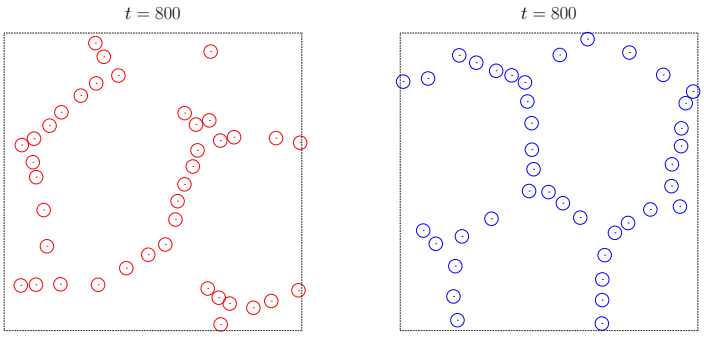

(a) $\mathcal{P}$, periodic boundary condition

(b) $\mathcal{M}$, periodic boundary condition

Figure 5.27.: A $\mathcal{S} = 0.5$ square box with periodic boundary conditions.

5.3.9. Conclusion

For the type A interaction we found that particles move to the centre of the box where they continually collide, which is expected and no pattern emerges. For type B interaction we observed the formation of various patterns. For position- and momentum-space we were able to identify two different sources of patterns. Using position-space particles find the direct neighbourhood of other partlicles entropically favorable and therefore have the tendency to form chains. For increasing particle density those chains grow in length and, as accessible space diminishes, the chains grow into larger structures. The final structure we identified as cellular.

We found the same final structure also when using $F_{\mathcal{M}}$, however the formation of structures works differently with that method. As observed in Fig. 5.16, using $F_{\mathcal{M}}$ particles repell each other for all distances, unlike particles using $F_{\mathcal{P}}$. Therefore the formation of chains is not possible, or rather a linear structure is not stable. Instead, as soon as particle density exceeded a certain value particles spontaneously form circles, or for that matter, closed structures. With increasing density they connect with walls and ultimately form similar cellular structures as for position-space. Using radial distribution functions we analysed the characteristic lengths for

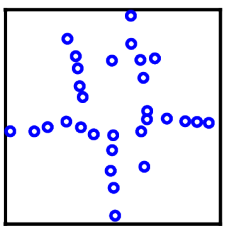

different sets of parameters and were able to confirm this emerging of a common final structure.

In the following section we examine the dynamics of a number of particles in a bottleneck system for both type A and B particle interaction.

5.4. Many-particles in a bottleneck system

In this section we examine the dynamics of 25 particles in a bottleneck system in analogy to an evacuation scenario. The system has the same geometry as used for simulations shown in Sec. 4.4. We use a sampling horizon corresponding to $T_r = 0.015$ for which a single particle moves towards the centre of the small box first before leaving it (see Fig. 4.9). Note that the larger box is chosen to be of infinite size. The length of the bottleneck is set to $l_{BN} = 0.2$. For these simulations we will exclusively use momentum-space for the calculation of the entropic force since particles then have a lower tendency of sticking to walls. For the small box the ratio between area covered by sampling paths and box size corresponds to $\mathcal{S} = 3$.

5.4.1. "Blind agents" (Type A)

Particles with type A interaction can be brought into correspondence with a class of agents in an evacuation scenario which ignore the existence of other agents during their decision making process – viewing the calculation of the entropic force as an intelligent process of taking a decision. In that sense we refer to them as "blind" agents, well aware of the system's geometry but blind to other particles.

Figure 5.28 shows 25 "blind" particles in a bottleneck system. Fig. 5.28(a) - (f) show the evolution of the system, where (f) is giving a larger view on the system in order to learn about how the escaped particles arrange. Fig. 5.28(g) shows the time evolution of the number of escaped particles. The particles gather in the centre in Fig. 5.28(b), bump into each other, practically push each other away while trying to get to the centre, and start streaming out doing so. Once outside, they gain a certain distance to the exit and then, slowly moving randomly, stay in a group with little interaction. As soon as they reached that state, they do not feel each other. During sampling they do not see each other anyway, and in real space they barely move and therefore have almost no interaction. Since particles do not interact with each other they can freely move as long as they do not touch and push each other around.

The two particles leaving last, shown in Fig. 5.28(e) and (f), simply take longer in finding the larger box i.e. finding the larger box entropically more favorable. As visible in Fig. 5.28(g) they leave around $\Delta t = 23$ later than the previous particle.

5.4.2. "Seeing agents" (Type B)

For type B interaction, particles can be viewed as agents looking for an empty area or pathway out of the small box. As introduced in section 5.2, when sampling, other particles are viewed as solid obstacles. Figure 5.28(a) shows the initial position of $N = 25$ particles inside the small box. At $t = 50\ \delta t$ in Fig. 5.29(b) some particles already escaped through the bottleneck while all remaining arrange themselves inside the small box, forming lines or queues, as shown in Fig. 5.29(c). The particle about to escape in Fig. 5.29(c), is the same as the one on the right in Fig. 5.29(d). A particle in the bottleneck blocks all sampling trajectories of other particles, thus letting it seem as if the channel was a dead end. As a consequence, any particle will wait until the previous one reached the large box before entering. Figure 5.29(f) shows the system at time $t = 1720\ \delta t$ when most particles already escaped and gained some distance to the exit. As soon as enough free space is available, they distance themselves from each other and the small box, giving other particles space to escape. Figure 5.29(g) shows the number of escaped particles versus time. Until $t = 600\ \delta t$, particles leave the small box in regular time-intervals, later the intervals increase on average. This increase can be explained through the decreasing particle density inside the small box. Fewer particles take up less space, giving remaining particle more space to explore while sampling, thus reducing the tendency of escaping. This can be viewed as a decreasing pressure inside the small box.

5.4.3. Comparison

Figure 5.30 shows the number of particles remaining in the small box versus time for $N = 25$ and both type A and B, averaged over 51 simulations. For type A, the green curve, particles in general are faster in escaping than for type B, magenta curve. This is due to effect for type B of particles blocking sampling trajectories while escaping, thus causing other particles to wait.

We ran the simulations again for $N = 50$ and compared the escape times. Figure 5.31(a) shows the number of remaining particles versus time for both simulations with $N = 25$ and $N = 50$. The results for $N = 25$ are shifted such that their initial

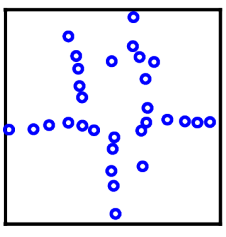

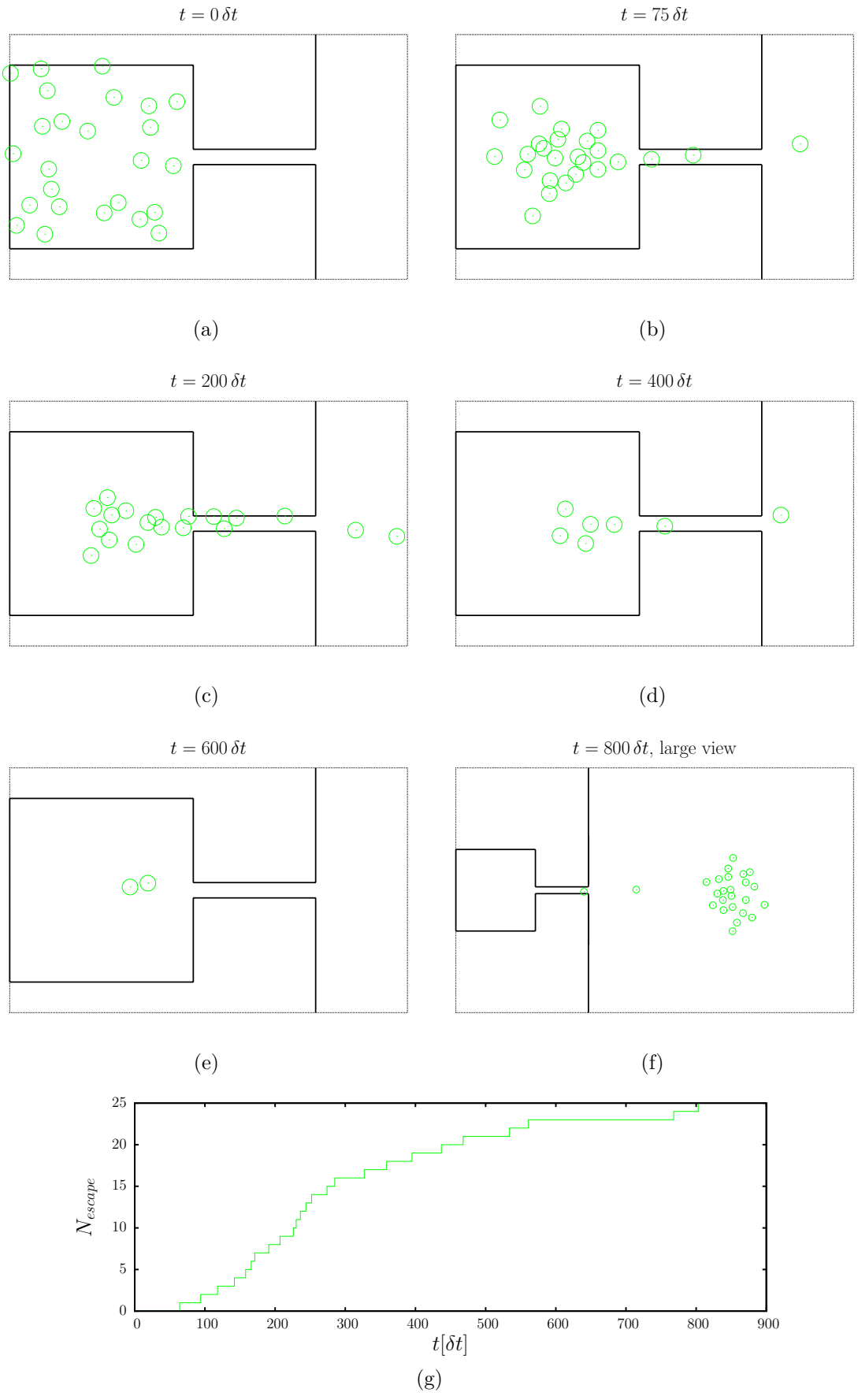

Figure 5.28.: Snapshots of 25 particles in a bottleneck potential with an infinitely large big box for $T_r = 0.015$. Type A interaction. [$l_{BN} = \sigma$, using $F_{\mathcal{M}}$, $\frac{T_c}{T_r} = 4$]

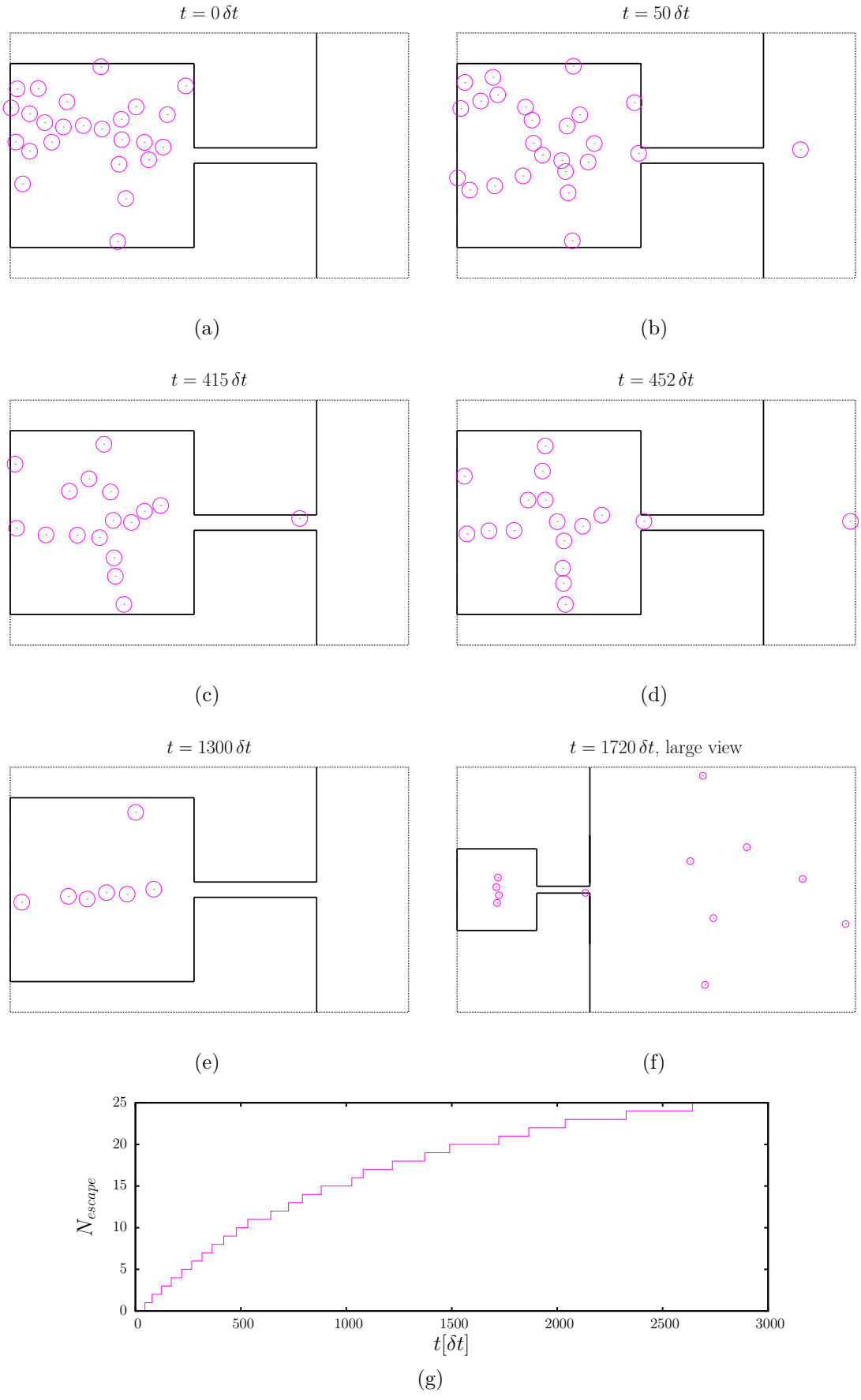

Figure 5.29.: Snapshots of 25 particles in a bottleneck potential with an infinitely large big box for $T_r = 0.015$. Type B interaction. [$l_{BN} = 0.2$, using $F_{\mathcal{M}}$, $\frac{T_c}{T_r} = 4$]

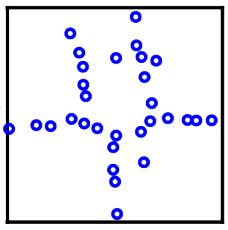

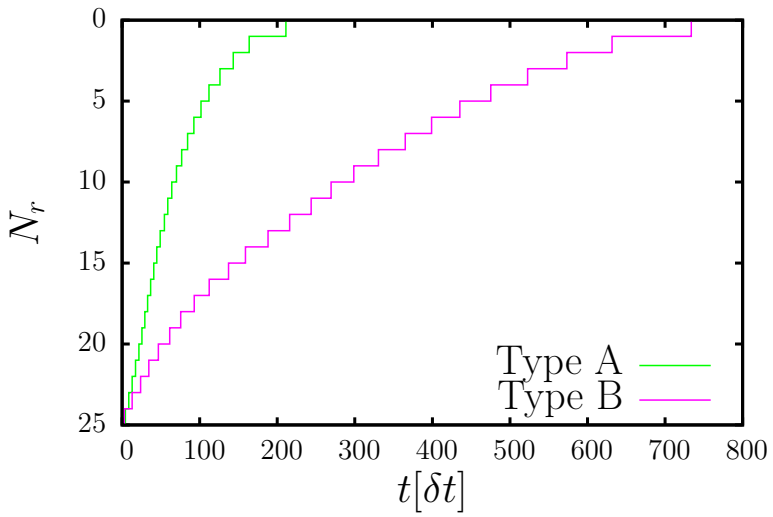

Figure 5.30.: Average time evolution of particles escaping a bottleneck system. Calculations are averaged over 51 simulations, each of $N = 25$ particles, using $F_{\mathcal{M}}$, $\frac{T_c}{T_r} = 1$.

time matches the time when in the other simulation $N_r = 25$ particles remain. We see that the times for both simulations match. We can thereby assume that the performance of the particles is independent from the past evolution of the system. For larger numbers of particles remaining the slope of the both curves for type A and B seems linear before changing around $N_r = 10$ and $N_r = 25$, respectively.

Figure 5.31(b) shows the length of the time intervals between two particles escaping. For type A the time intervals are constant at $\delta t^* = 4$ for $N_r > 13$. At $N_r = 13$ we observe a transition to a linear increase of δt^* and yet another transition at $N_r = 5$ to an even stronger increase. For type B δt^* slightly increases from $\delta t^* = 10$ to $\delta t^* = 12$ until $N_r = 23$, where a transition to a stronger increase in δt^* occurs.

For numbers of remaining particles larger than a critical number $N_r > N_c$ we can expect almost constant time interval lengths between two particles escaping. For the shown simulations we have $N_c = 13$ and $N_c = 23$ for type A and B, respectively.

5.4.4. Conclusion

We examined the dynamics of a number of entropically driven particles in a bottleneck system for both type A and B interaction. We viewed the simulations as an evacuation scenario where we could identify two different strategies. For type A, particles move directly to the exit and escape, frequently colliding with other

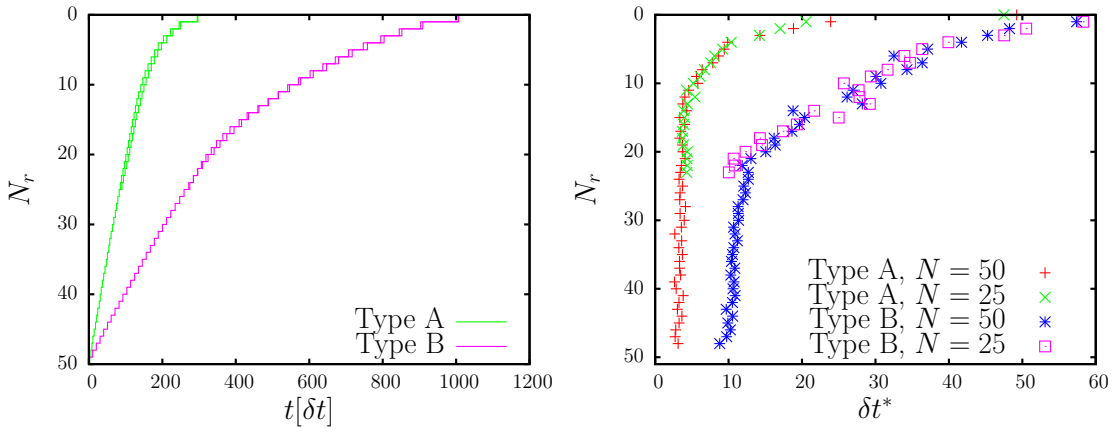

Figure 5.31.: (a): Number of remaining particles versus time with results from both simulations with $N = 25$ and $N = 50$. The results for $N = 25$ are shifted such that their initial time matches the time when in the other simulation $N_r = 25$ particles remain. (b): Number of remaining particle versus time intervals between two particles escaping. [Averaged over 51 simulations, using $F_{\mathcal{M}}$, $\frac{T_c}{T_r} = 1$]

particles. For type B, particles leave through the bottleneck one by one, forming lines while waiting for other particles to exit.

Further analysis of the simulations for both $N = 25$ and $N = 50$ particles showed a change in length of the time intervals between two particles escaping. There seems to be a transition at a certain particle density in the small box where the length of those intervals strongly increases (see Fig. 5.31). This suggests that the behaviour of the system is practically independent of its preceding evolution.

Our model includes single entities individually assessing the current situation and adapting to changing environments and thus associates with agent-based models. The observed behaviour for type A and B interaction can be interpreted as herding and queuing, as also found in various agent-based evacuation models [10, 11].

This behaviour is remarkable given the complete absence of specific rules governing the particles. They solely maximize their entropy, or for that matter the free area around themselves. All emerging behaviour originates from this single basic principle.

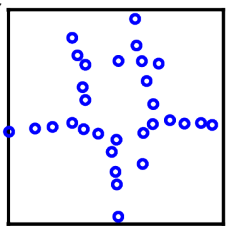

6. Discussion and outlook

Following [3], we defined the causal entropy on the set of possible future paths of finite temporal length through phase space of the system

$$S_c(\mathbf{X}, \tau) = -k_\mathrm{B} \int \Pr(\mathcal{X}_\tau|\mathbf{x}(0)) \ln \left[\Pr(\mathcal{X}_\tau|\mathbf{x}(0))\right] \mathcal{D}\mathcal{X}_\tau \ . \tag{3.1.2}$$

We maximized this causal entropy by applying the causal entropic force

$$\mathbf{F}_c(\mathbf{X}_0, \tau) = T_c \boldsymbol{\nabla}_\mathbf{X} S_c(\mathbf{X}, \tau)|_{\mathbf{X}_0} \tag{1.0.1}$$

on the system. In Sec. 1 we briefly introduced the idea of the causal entropy and causal entropic force whereas in Sec. 3.1 and 3.2 we derived and discretized an expression for the causal entropic force which we used in numerical simulations.

For both discrete and continuous representation of space and time we examined the behaviour of a single particle driven by the causal entropic force. We found that the particle moves towards the centre of a box where it has maxium causal entropy, or maximum accessible free area around it. For increasing horizon the particle started to find the walls of a system entropically favorable. For the discrete case we were able to analytically reproduce and verify parts of the numerical results using a random-walk based approach.

Also for both discrete and continuous space and time we examined success times of a single particle in a bottleneck system. We consistently found particles not succeeding within simulation time for small horizon and decreasing success times for increasing horizon, as discussed in Sec. 4.5 and shown in Fig. 6.1. In Sec. 3.2.1 we drew a connection between the dynamics of polymers and a particle driven by causal entropic force. This allowed us to compare experimental data of DNA molecules in a setup with two areas of different (configurational) entropy with our numerical results of an equivalent setup in Sec. 4.6. We were able to reproduce the

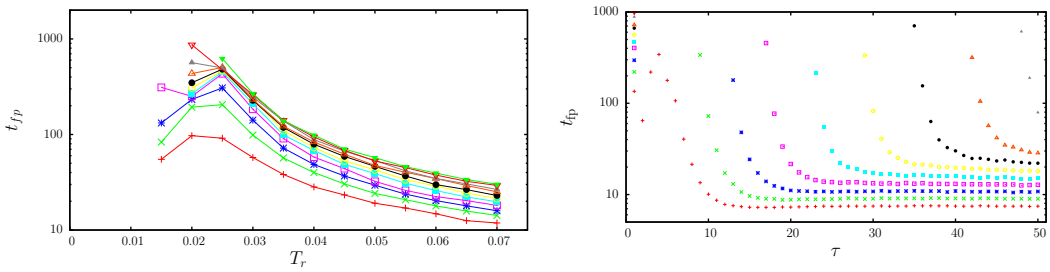

(a) Continuous (see Fig. 4.14)

(b) Discrete (see Fig. 2.16)

Figure 6.1.: Average success times of a particle in a bottleneck system for different horizons and lengths of the bottleneck. Results of the continuous and the discrete simulations for comparison.

qualitative behaviour of DNA molecules in the given setup, giving us confidence in the validity of the polymer-analogy.

By introducing a number of independent entropically driven particles in a bottleneck system, we found parallels of our model to an agent-based evacuation model [21]. Depending on the definition of causal entropy we observed herding behaviour, where particles form a crowd at the exit as well as queuing behaviour (see Fig. 6.2). Both are found in the literature for this type of evacuation model [10, 11].

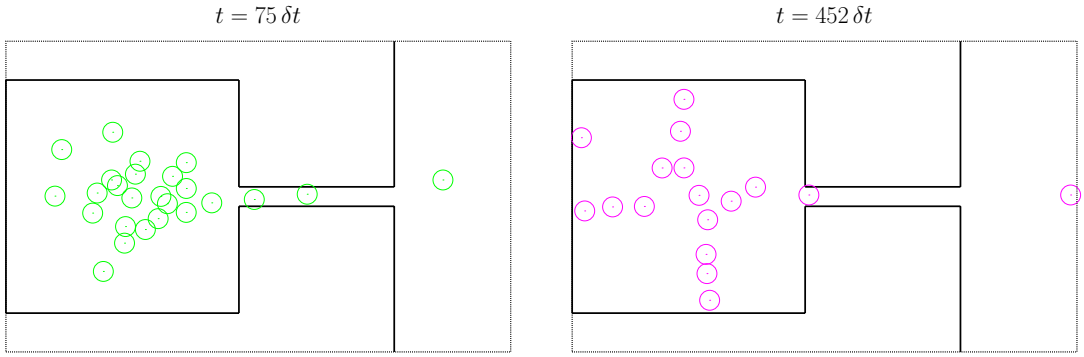

(a) Herding

(b) Queuing

Figure 6.2.: Snapshots of particles in a bottleneck potential (see Fig. 5.28 and 5.29).

Furthermore, we observed the formation of patterns for a number of particles in a box. We seperately examined the cases where particle use position- or momentum-space of sampling paths (discussed in Sec. 3.2.2) and identified two different origins

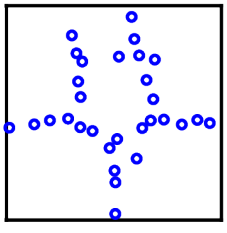

of pattern formation. For position-space particles form lines which grow in length for increasing particle density. Conversely, for momentum-space sampling particles cannot form stable lines but instead spontaneously form circles for sufficiently large particle density (see Fig. 6.3). We used radial distribution functions and

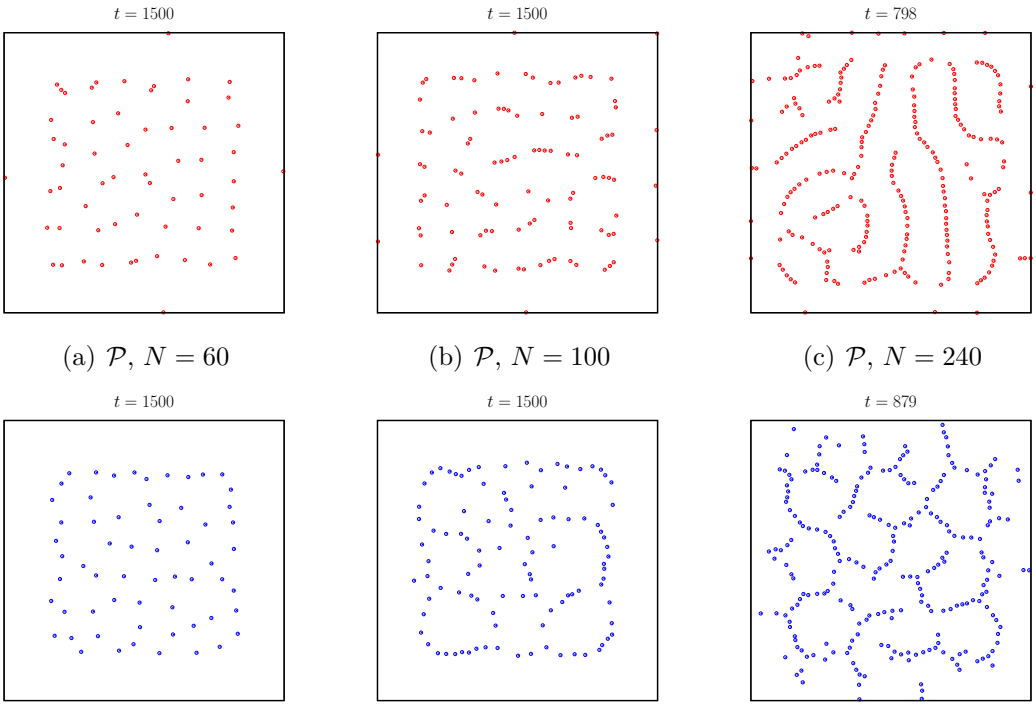

(a) $\mathcal{P}$, $N = 60$ (b) $\mathcal{P}$, $N = 100$ (c) $\mathcal{P}$, $N = 240$

(d) $\mathcal{M}$, $N = 60$ (e) $\mathcal{M}$, $N = 100$ (f) $\mathcal{M}$, $N = 240$

Figure 6.3.: Comparing patterns from simulations using position- and momentum-space of sampling trajectories for calculating the entropic force. (see Fig. 5.21)

collected the positions of peaks, depicting characteristic length-scales in the corresponding system. Comparing structures for increasing particle density in position- and momentum-space, we found different characteristic lengths up to a certain particle density (see Fig. 6.4). As soon a the density is large enough, in both cases we observed the formation of cells as final structure before higher density and fluctuations would not allow any pattern formation (see Fig. 6.5).

Future work will include the investigation of group behaviour and swarming as result of entropy maximization and without the need of any arbitrary rule or behavioural condition. We consider two models:

- Individual entities being able to share information and thus entropically ben-

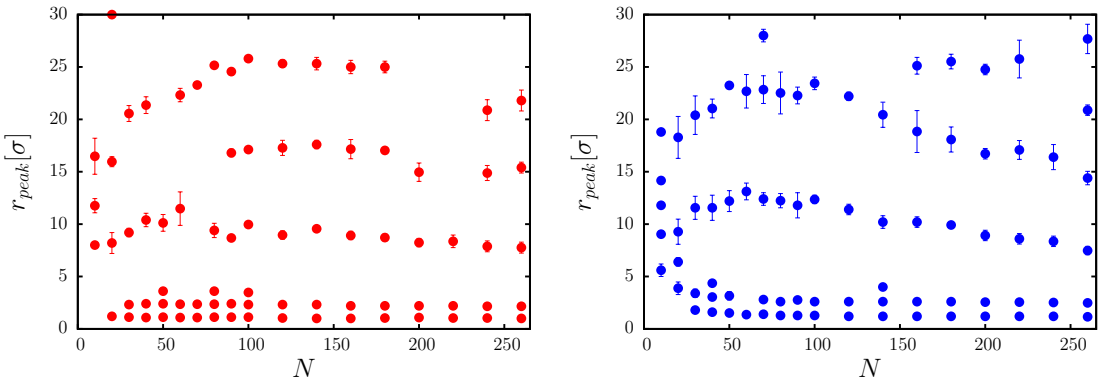

(a) Using position-space

(b) Using momentum-space

Figure 6.4.: Peaks in rdf for variable N depicting characteristic length-scales in the corresponding system (see Fig. 5.22 and 5.24).

efiting from the proximity of other entities, and

- a shared entropy, corresponding to a collective consciousness or hive mind, where every entity instantaneously reacts to changing environment of every other entity.

Further optimization of the code would allow extending the simulation to a three-dimensional model and exploring more complex behaviour and structures. This bears great potential especially concerning group behaviour.

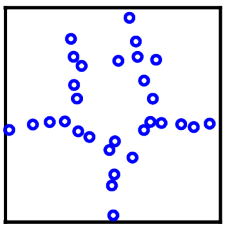

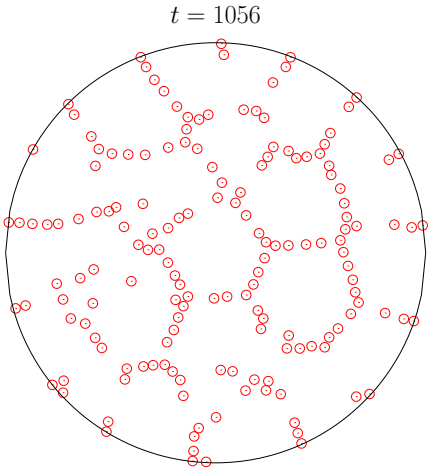

(a) N = 160

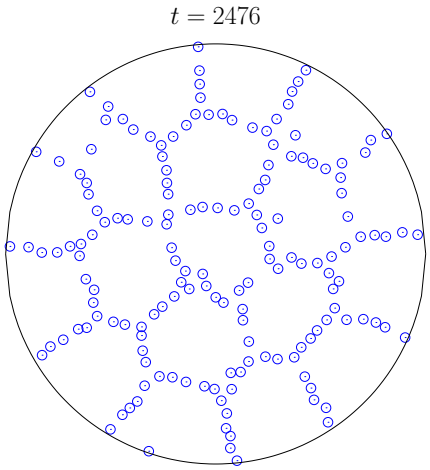

(b) N = 160

Figure 6.5.: Formation of cells connected to the walls of the system as final type of observed structure for increasing particle density (see Fig. 5.26).

Appendices

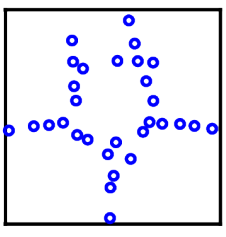

A.

A.1. Finding steady state density distribution from transition matrix

For a 3x3 lattice of shape

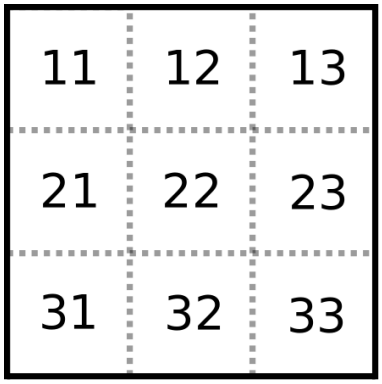

Figure A.1.: Indices of nine fields on a 3×3 lattice.

the corresponding vector describing the state of the system concerning the probabilities to find a particle in field i is

$$\mathbf{v}^T = \left[p_{11}, p_{12}, p_{13}, p_{21}, p_{22}, p_{23}, p_{31}, p_{32}, p_{33}\right] \tag{A.1.1}$$

$$\sum_i p_i = 1 \,, \tag{A.1.2}$$

while the transition probabilities t_i^j to move from field i to j for this system look as

follows:

$$\mathbf{A} = \begin{bmatrix} t_{11}^{11} & t_{12}^{11} & t_{13}^{11} & t_{21}^{11} & t_{22}^{11} & t_{23}^{11} & t_{31}^{11} & t_{32}^{11} & t_{33}^{11} \\ t_{11}^{12} & t_{12}^{12} & t_{13}^{12} & t_{21}^{12} & t_{22}^{12} & t_{23}^{12} & t_{31}^{12} & t_{32}^{12} & t_{33}^{12} \\ t_{11}^{13} & t_{12}^{13} & t_{13}^{13} & t_{21}^{13} & t_{22}^{13} & t_{23}^{13} & t_{31}^{13} & t_{32}^{13} & t_{33}^{13} \\ t_{11}^{21} & t_{12}^{21} & t_{13}^{21} & t_{21}^{21} & t_{22}^{21} & t_{23}^{21} & t_{31}^{21} & t_{32}^{21} & t_{33}^{21} \\ t_{11}^{22} & t_{12}^{22} & t_{13}^{22} & t_{21}^{22} & t_{22}^{22} & t_{23}^{22} & t_{31}^{22} & t_{32}^{22} & t_{33}^{22} \\ t_{11}^{23} & t_{12}^{23} & t_{13}^{23} & t_{21}^{23} & t_{22}^{23} & t_{23}^{23} & t_{31}^{23} & t_{32}^{23} & t_{33}^{23} \\ t_{11}^{31} & t_{12}^{31} & t_{13}^{31} & t_{21}^{31} & t_{22}^{31} & t_{23}^{31} & t_{31}^{31} & t_{32}^{31} & t_{33}^{31} \\ t_{11}^{32} & t_{12}^{32} & t_{13}^{32} & t_{21}^{32} & t_{22}^{32} & t_{23}^{32} & t_{31}^{32} & t_{32}^{32} & t_{33}^{32} \\ t_{11}^{33} & t_{12}^{33} & t_{13}^{33} & t_{21}^{33} & t_{22}^{33} & t_{23}^{33} & t_{31}^{33} & t_{32}^{33} & t_{33}^{33} \end{bmatrix} = \begin{bmatrix} 0 & \frac{1}{3} & 0 & \frac{1}{3} & 0 & 0 & 0 & 0 & 0 \\ \frac{1}{2} & 0 & \frac{1}{2} & 0 & \frac{1}{4} & 0 & 0 & 0 & 0 \\ 0 & \frac{1}{3} & 0 & 0 & 0 & \frac{1}{3} & 0 & 0 & 0 \\ \frac{1}{2} & 0 & 0 & 0 & \frac{1}{4} & 0 & \frac{1}{2} & 0 & 0 \\ 0 & \frac{1}{3} & 0 & \frac{1}{3} & 0 & \frac{1}{3} & 0 & \frac{1}{3} & 0 \\ 0 & 0 & \frac{1}{2} & 0 & \frac{1}{4} & 0 & 0 & 0 & \frac{1}{2} \\ 0 & 0 & 0 & \frac{1}{3} & 0 & 0 & 0 & \frac{1}{3} & 0 \\ 0 & 0 & 0 & 0 & \frac{1}{4} & 0 & \frac{1}{2} & 0 & \frac{1}{2} \\ 0 & 0 & 0 & 0 & 0 & \frac{1}{3} & 0 & \frac{1}{3} & 0 \end{bmatrix} . \tag{A.1.3}$$

Assume we have an initial distribution of

$$\mathbf{v}_0 = \begin{bmatrix} 1, 0, 0, 0, 0, 0, 0, 0, 0 \end{bmatrix} \tag{A.1.4}$$

meaning the particle initially is at field 11, i.e. the chance to find the particle at 11 at time $t = 0$ is $p_{11}(0) = 1$. The probability distribution for $t = 1$ then can be found by multiplying the transition matrix $\mathbf{A}$ on the vector

$$\mathbf{v}_1 = \mathbf{A} \cdot \mathbf{v}_0 \tag{A.1.5}$$

where the distribution then is

$$\mathbf{v}_0^T = \begin{bmatrix} 0, \frac{1}{2}, 0, \frac{1}{2}, 0, 0, 0, 0, 0 \end{bmatrix} , \tag{A.1.6}$$

meaning with probability 0.5 the particle is at field 12 or 21, respectively.

By letting the system evolve infinitely long, the system will converge to a steady state, if such a state exists, which yields

$$\mathbf{v}_{ss} = \mathbf{A}\mathbf{v}_{ss} , \tag{A.1.7}$$

meaning it will not be changed by multiplication of the matrix on it, neither its distribution, nor its length (again: eigenvalue $\lambda = 1$, conservation of length). However, by finding the eigenvector to the eigenvalue 1 of the matrix, the steady state can be determined simply through normalization of the eigenvector. For this transitionma-

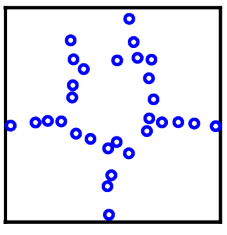

trix **A** the steady state is

$$\mathbf{v}_{\lambda=1}^{T} = \left[\frac{1}{12}, \frac{1}{8}, \frac{1}{12}, \frac{1}{8}, \frac{1}{6}, \frac{1}{8}, \frac{1}{12}, \frac{1}{8}, \frac{1}{12}\right] . \tag{A.1.8}$$

The resulting probability distribution is shown in Fig. A.2:

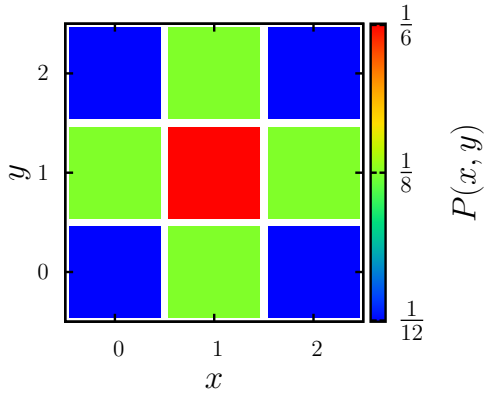

Figure A.2.: Probability distribution of a particle's position on the lattice. We find three different probabilities for a corner field $p_c = \frac{1}{12}$, a wall field $p_w = \frac{1}{8}$ and the middle field $p_m = \frac{1}{6}$.

A.2. Finding temporal evolution of density distribution

In order to determine the first passage time for a particle performing a random walk in a bottleneck system as illustrated in Fig. A.3 moving to the first field in the big box we use a transition matrix for that system to examine the evolution of the initial state of the particle starting in the bottom left corner of the small box.

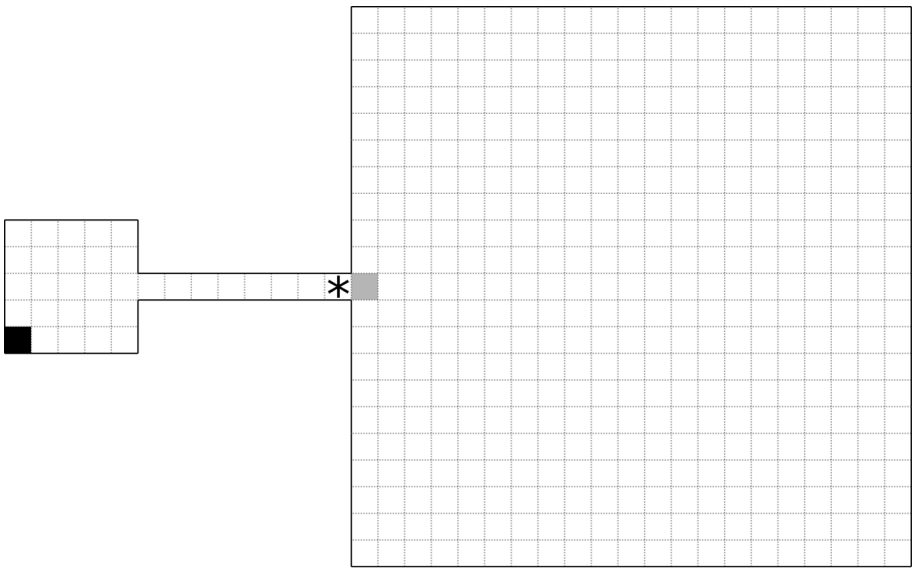

Figure A.3.: Schematic of a lattice bottleneck system. The length of the bottleneck varies in the simulations. In black the initial position of the particle for each simulation, in grey the field for which the fpt (first passage time) is being calculated or measured, the asterisk denotes the field adjacent to the fpt field.

The circle marks the field adjacent to the first passage field. We can break the system down to only the small box and the bottleneck as shown in A.4 and use a 33x33 transition matrix. For calculating the first passage time we 'drain' the system from the probability to move from the last field (marked with a circle) to the first passage field, which in this system is

$$t_{fpt} = \sum_{t=0}^{\infty} p_*(t) \cdot \frac{1}{2} \cdot (t+1) \; . \tag{A.2.1}$$

This probability is being subtracted from the last field

$$p'_*(t) = p_*(t) - p_*(t) \cdot \frac{1}{2} \tag{A.2.2}$$

in order to eliminate the case of the particle moving back into the system. Once it reaches the fpt field, its propagation is stopped. That way the first passage time can be calculated sufficiently.

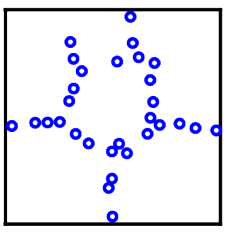

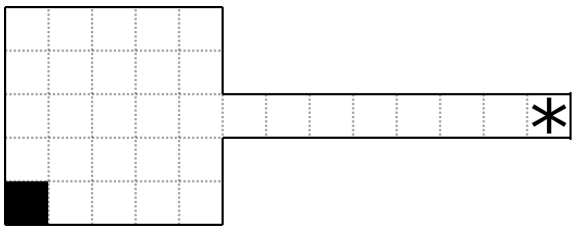

Figure A.4.: Schematic of the system considered while noting the transition matrix. The field marked with the asterisk is being drained from the probability to move to the fpt field every timestep in order to calculate the first passage time of a particle, which once hit the fpt field will not come back into the system.

B. Patterns

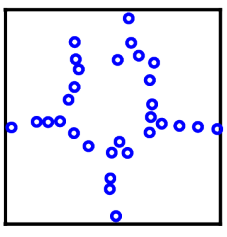

B.1. Box, $\mathcal{S} = 0.5$, $F_{\mathcal{P}}$

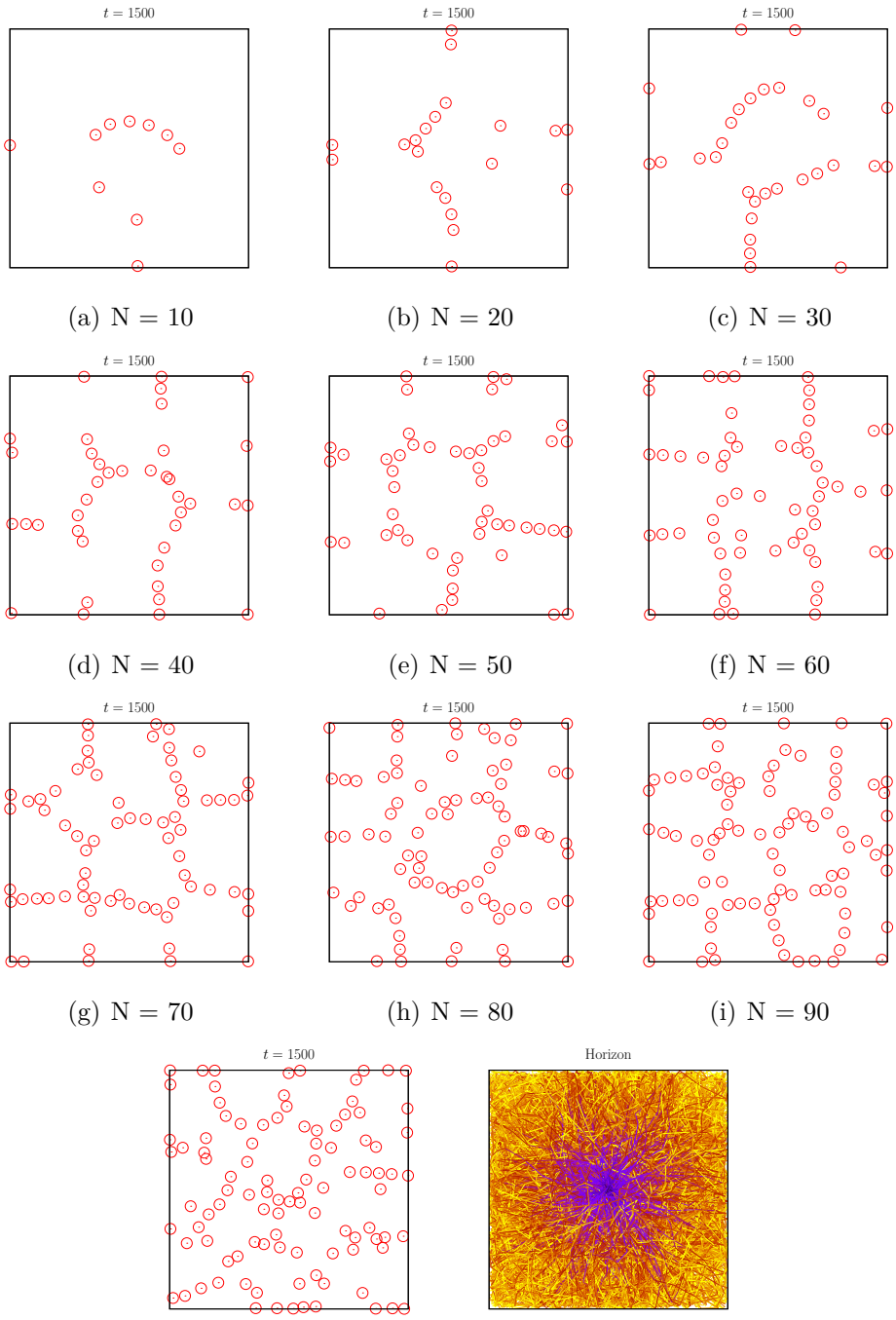

(a) N = 10 (b) N = 20 (c) N = 30

(d) N = 40 (e) N = 50 (f) N = 60

(g) N = 70 (h) N = 80 (i) N = 90

(j) N = 100 (k) $T_r = 0.015$, box size $L = 0.5$

Figure B.1.: $\mathcal{S} = 0.5$, $F_{\mathcal{P}}$, $\frac{T_c}{T_r} = 0.5$, $T_r = 0.015$

B.2. Box, $\mathcal{S} = 0.5$, $F_{\mathcal{M}}$

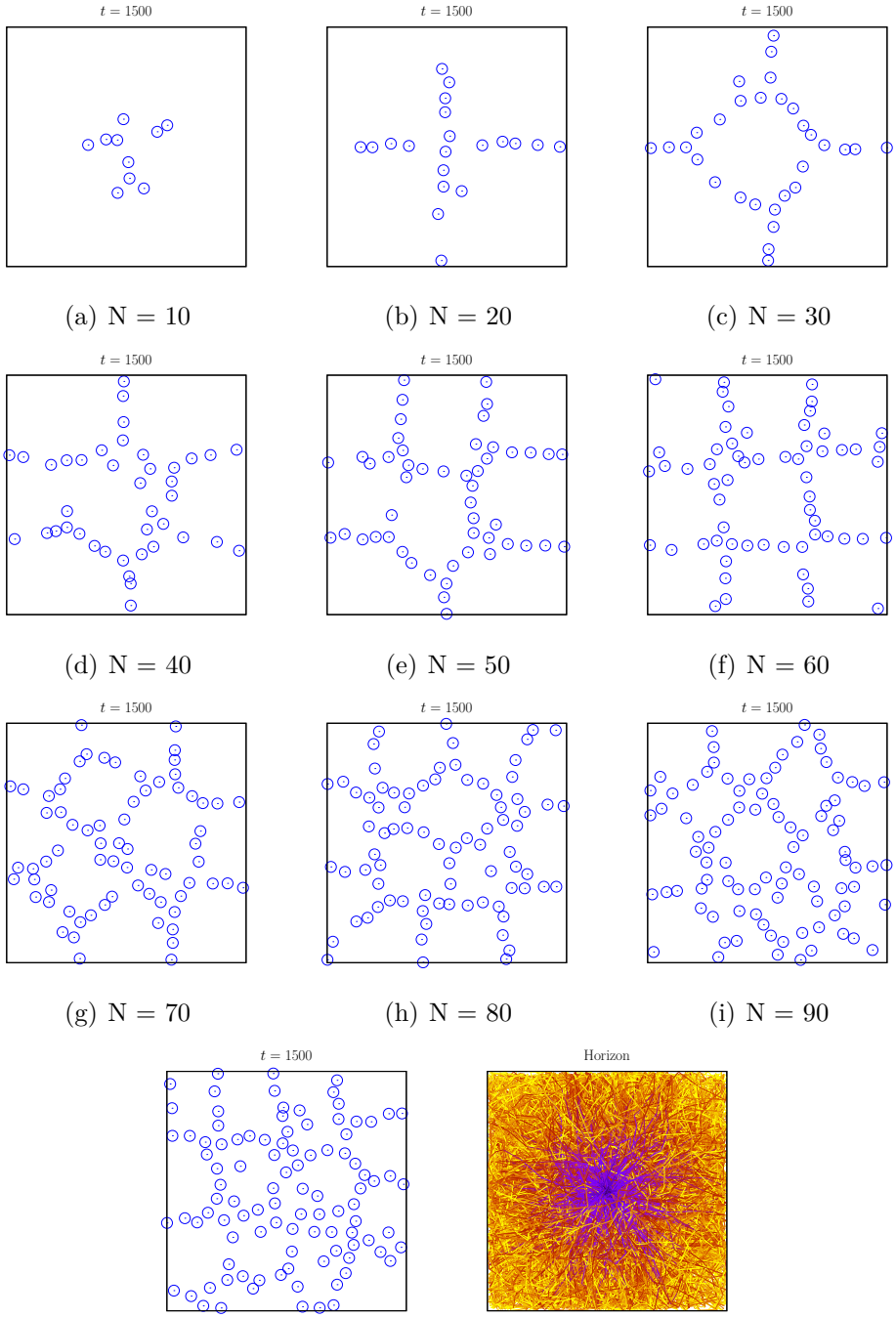

(a) N = 10 (b) N = 20 (c) N = 30

(d) N = 40 (e) N = 50 (f) N = 60

(g) N = 70 (h) N = 80 (i) N = 90

(j) N = 100 (k) $T_r = 0.015$, box size $L = 0.5$

Figure B.2.: $\mathcal{S} = 0.5$, $F_{\mathcal{M}}$, $\frac{T_c}{T_r} = 4$, $T_r = 0.015$

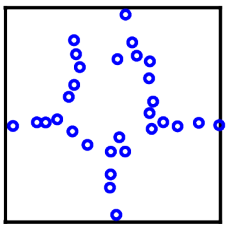

B.3. Box, $\mathcal{S} = 1.0$, $F_{\mathcal{P}}$

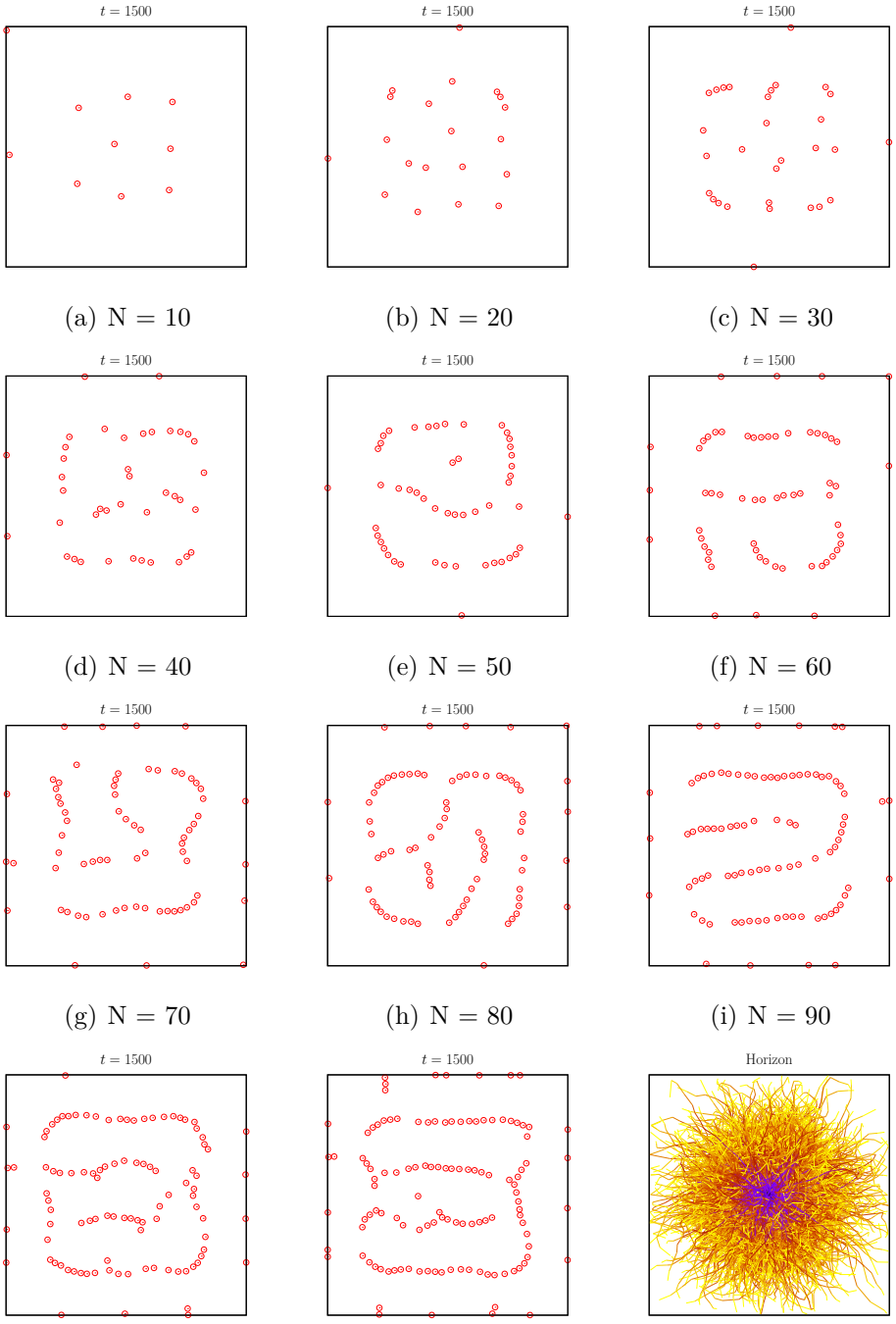

(a) N = 10 (b) N = 20 (c) N = 30

(d) N = 40 (e) N = 50 (f) N = 60

(g) N = 70 (h) N = 80 (i) N = 90

(j) N = 100 (k) N = 120 (l) $T_r = 0.015$, box size $L = 1.0$

Figure B.3.: $\mathcal{S} = 1.0$, $F_{\mathcal{P}}$, $\frac{T_c}{T_r} = 0.5$, $T_r = 0.015$

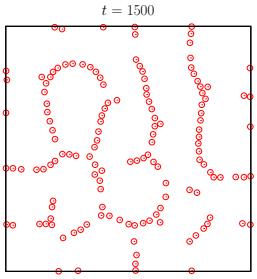

(a) N = 140

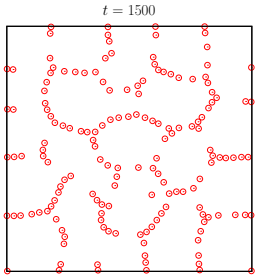

(b) N = 160

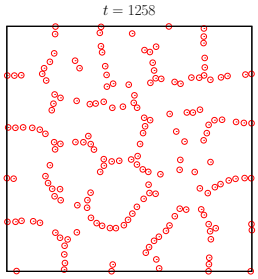

(c) N = 180

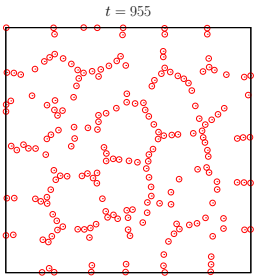

(d) N = 200

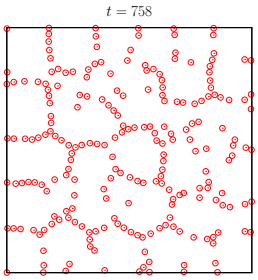

(e) N = 220

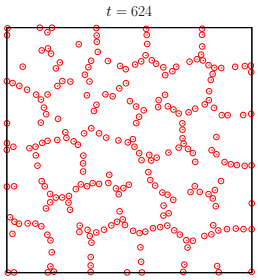

(f) N = 240

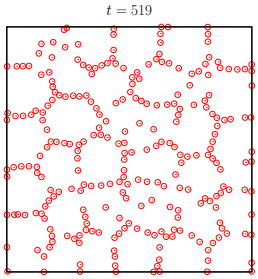

(g) N = 260

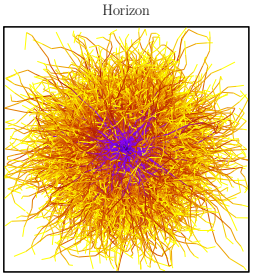

(h) $T_r = 0.015$, box size $L = 1.0$

Figure B.4.: $\mathcal{S} = 1.0$, $F_{\mathcal{P}}$, $\frac{T_c}{T_r} = 0.5$, $T_r = 0.015$

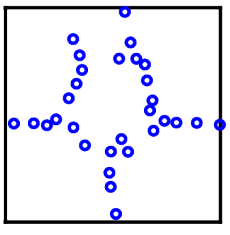

B.4. Box, $\mathcal{S} = 1.0$, $F_{\mathcal{M}}$

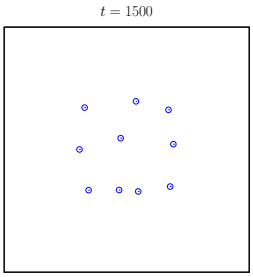

(a) N = 10

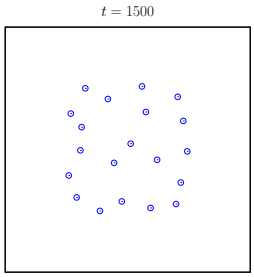

(b) N = 20

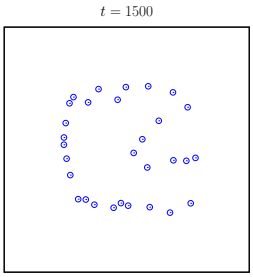

(c) N = 30

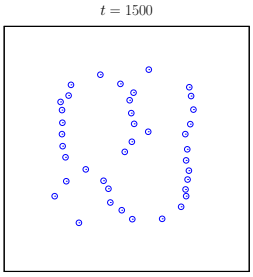

(d) N = 40

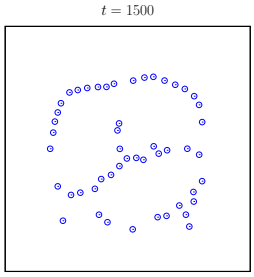

(e) N = 50

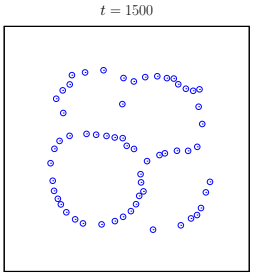

(f) N = 60

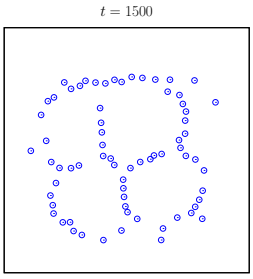

(g) N = 70

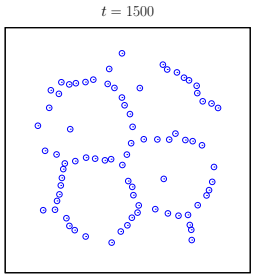

(h) N = 80

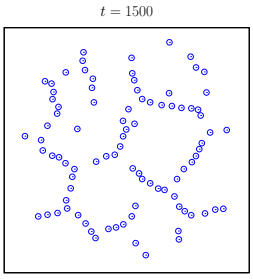

(i) N = 90

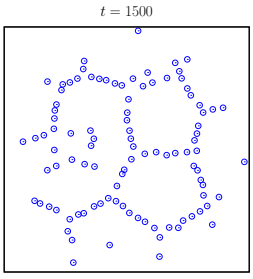

(j) N = 100

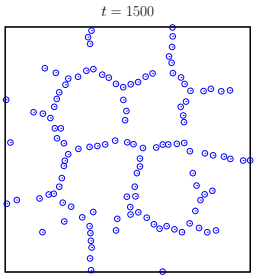

(k) N = 120

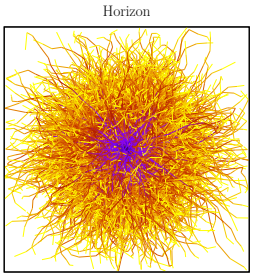

(l) $T_r = 0.015$, box size $L = 1.0$

Figure B.5.: $\mathcal{S} = 1.0$, $F_{\mathcal{M}}$, $\frac{T_c}{T_r} = 4$, $T_r = 0.015$

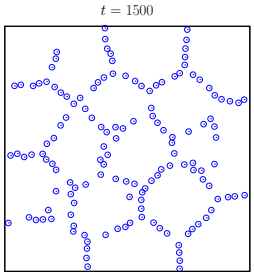

(a) N = 140

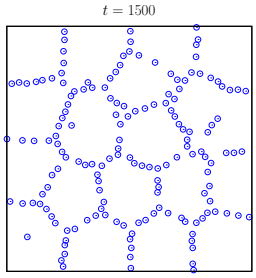

(b) N = 160

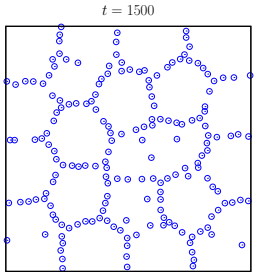

(c) N = 180

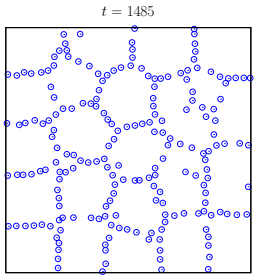

(d) N = 200

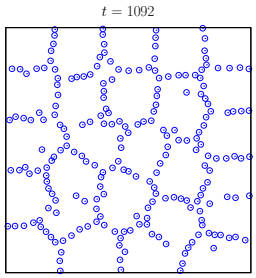

(e) N = 220

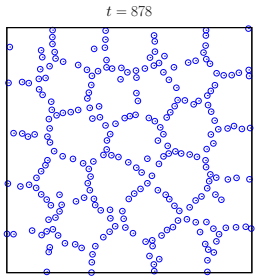

(f) N = 240

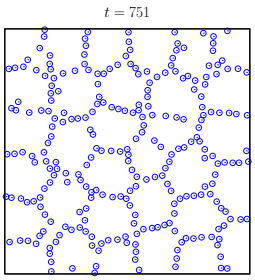

(g) N = 260

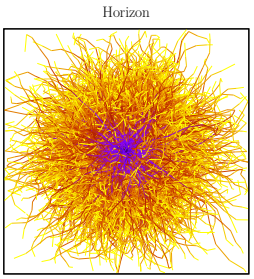

(h) $T_r = 0.015$, box size $L = 1.0$

Figure B.6.: $\mathcal{S} = 1.0$, $F_{\mathcal{M}}$, $\frac{T_c}{T_r} = 4$, $T_r = 0.015$

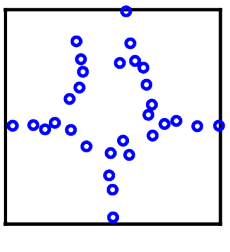

B.5. Box, $\mathcal{S} = 1.5$, $F_{\mathcal{P}}$

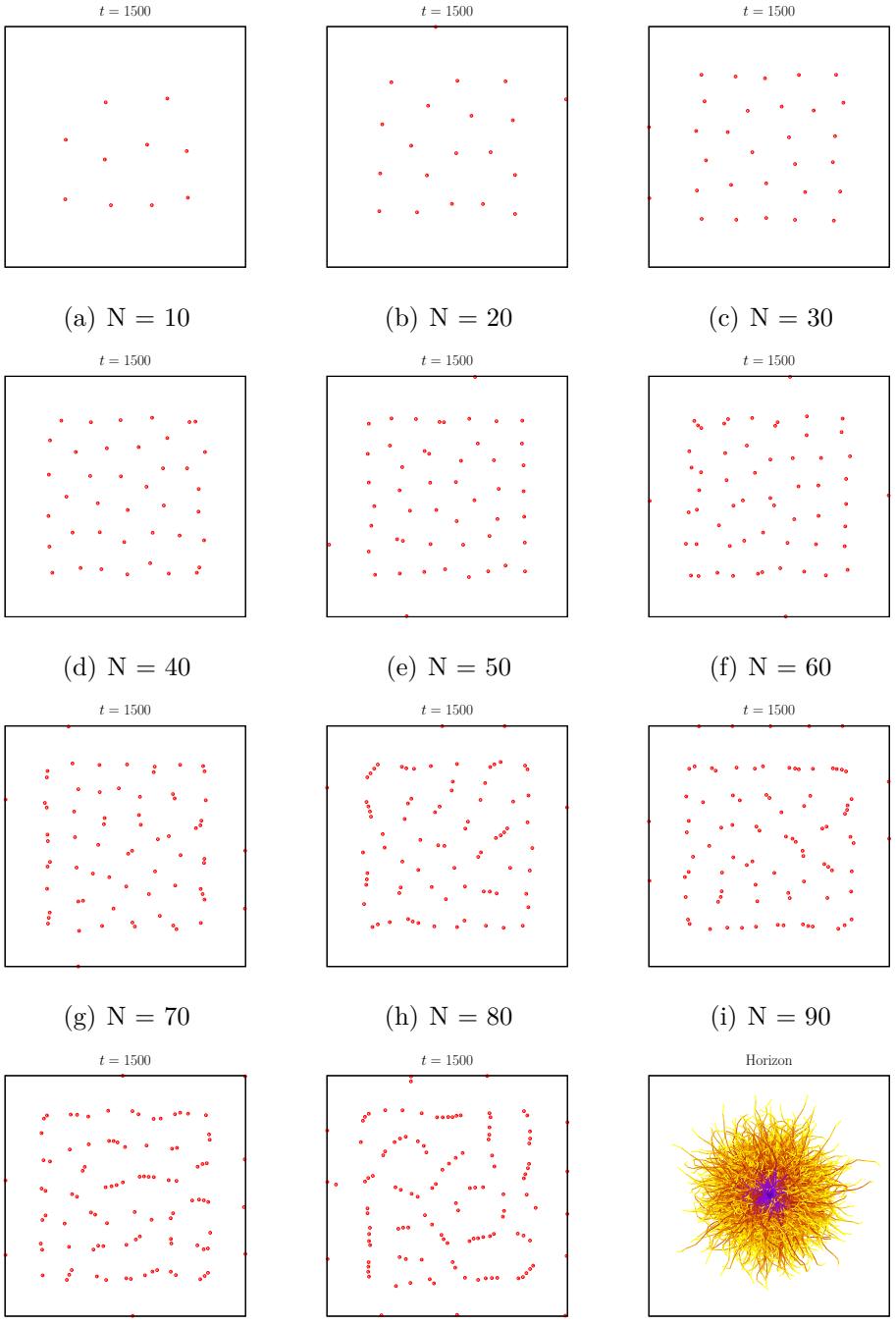

(a) N = 10 (b) N = 20 (c) N = 30

(d) N = 40 (e) N = 50 (f) N = 60

(g) N = 70 (h) N = 80 (i) N = 90

(j) N = 100 (k) N = 120 (l) $T_r = 0.015$, box size $L = 1.5$

Figure B.7.: $\mathcal{S} = 1.5$, $F_{\mathcal{P}}$, $\frac{T_c}{T_r} = 4$, $T_r = 0.015$

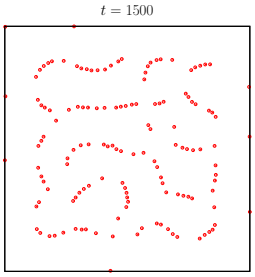

(a) N = 140

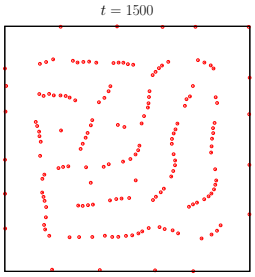

(b) N = 160

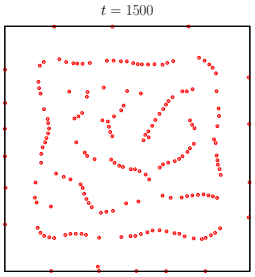

(c) N = 180

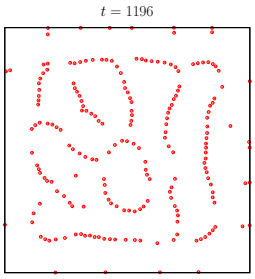

(d) N = 200

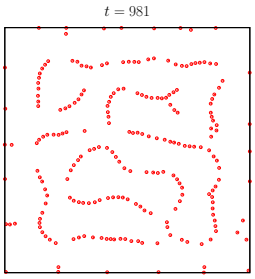

(e) N = 220

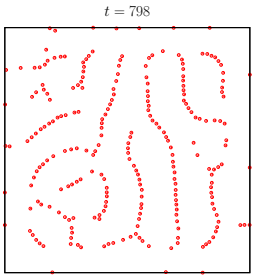

(f) N = 240

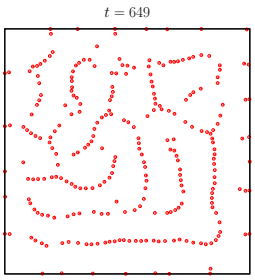

(g) N = 260

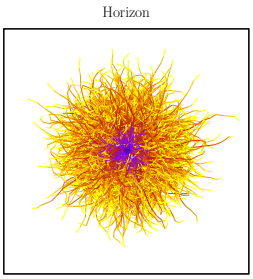

(h) $T_r = 0.015$, box size $L = 1.5$

Figure B.8.: $\mathcal{S} = 1.5$, $F_{\mathcal{P}}$, $\frac{T_c}{T_r} = 4$, $T_r = 0.015$

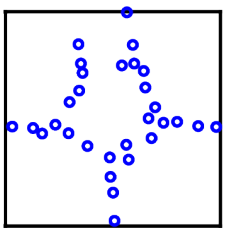

B.6. Box, $\mathcal{S} = 1.5$, $F_{\mathcal{M}}$

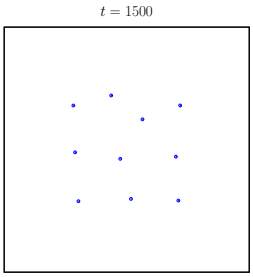

(a) N = 10

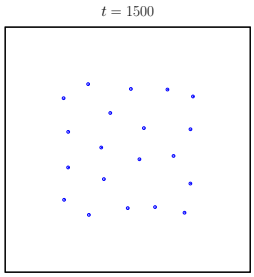

(b) N = 20

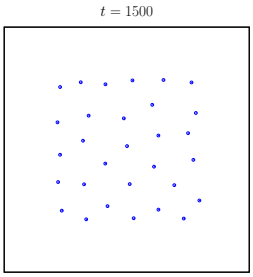

(c) N = 30

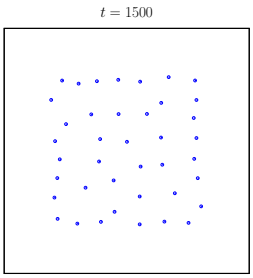

(d) N = 40

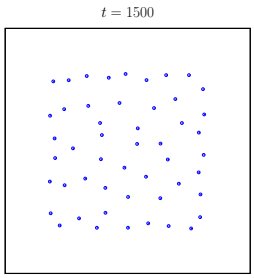

(e) N = 50

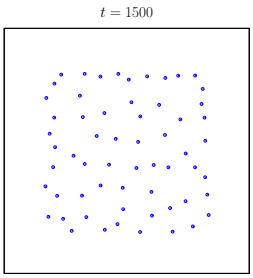

(f) N = 60

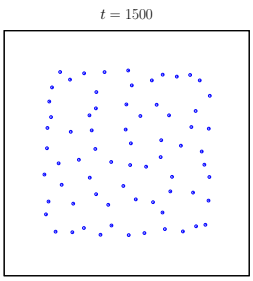

(g) N = 70

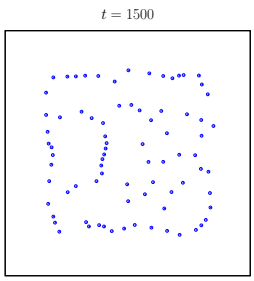

(h) N = 80

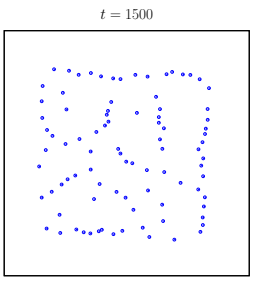

(i) N = 90

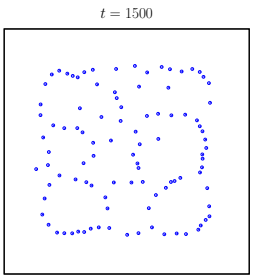

(j) N = 100

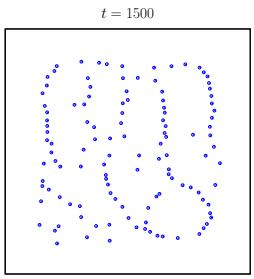

(k) N = 120

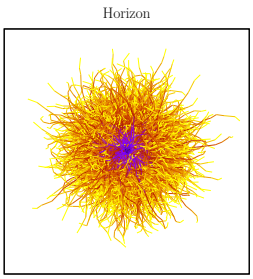

(l) $T_r = 0.015$, box size $L = 1.5$

Figure B.9.: $\mathcal{S} = 1.5$, $F_{\mathcal{M}}$, $\frac{T_c}{T_r} = 4$, $T_r = 0.015$

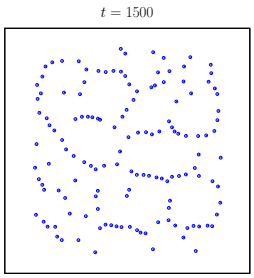

(a) N = 140

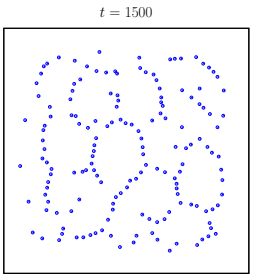

(b) N = 160

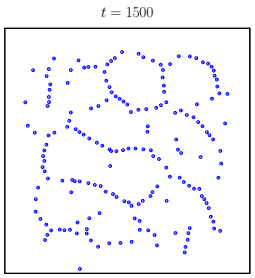

(c) N = 180

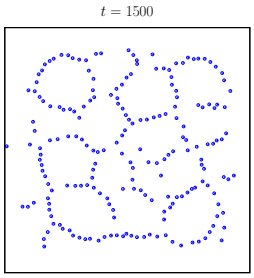

(d) N = 200

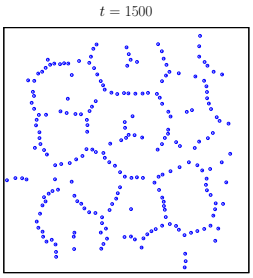

(e) N = 220

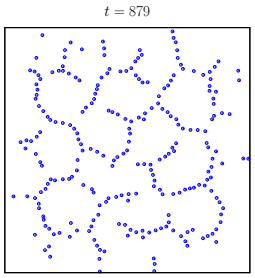

(f) N = 240

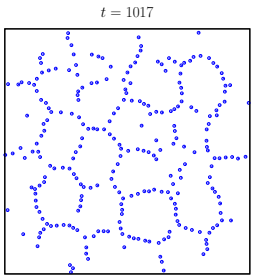

(g) N = 260

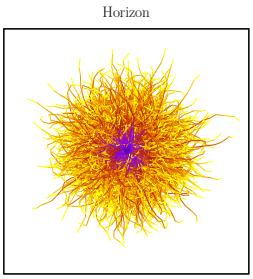

(h) $T_r = 0.015$, box size $L = 1.5$

Figure B.10.: $\mathcal{S} = 1.5$, $F_{\mathcal{M}}$, $\frac{T_c}{T_r} = 4$, $T_r = 0.015$

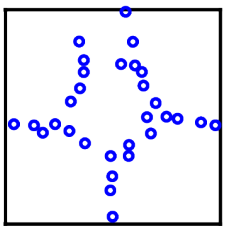

B.7. Circular, $\mathcal{S} = 0.5$, $F_{\mathcal{P}}$

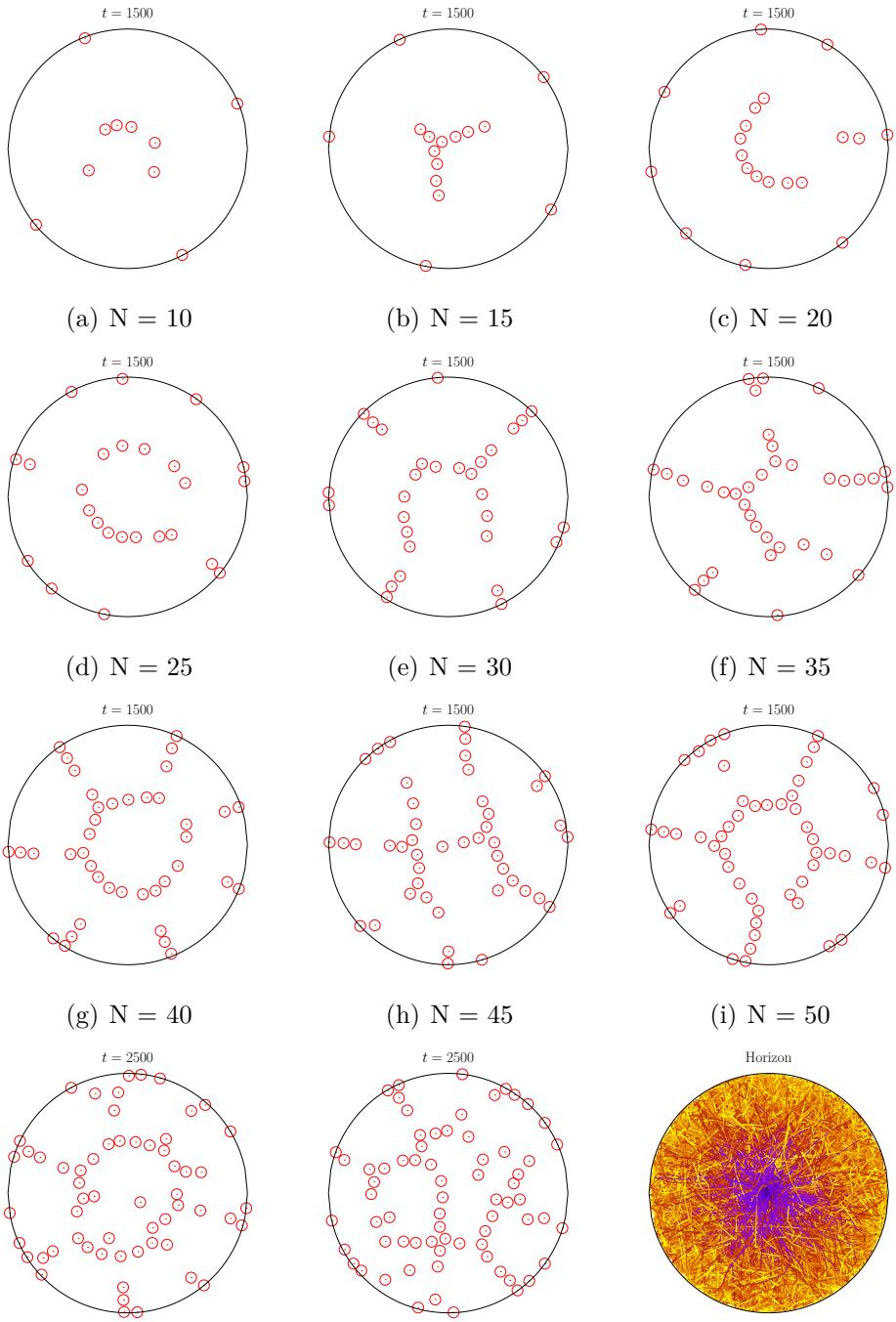

(a) N = 10 (b) N = 15 (c) N = 20

(d) N = 25 (e) N = 30 (f) N = 35

(g) N = 40 (h) N = 45 (i) N = 50

(j) N = 60 (k) N = 70 (l) $T_r = 0.015$, radius $r = 0.25$

Figure B.11.: $\mathcal{S} = 0.5$, $F_{\mathcal{P}}$, $\frac{T_c}{T_r} = 0.5$, $T_r = 0.015$

B.8. Circular, $\mathcal{S} = 0.5$, $F_{\mathcal{M}}$

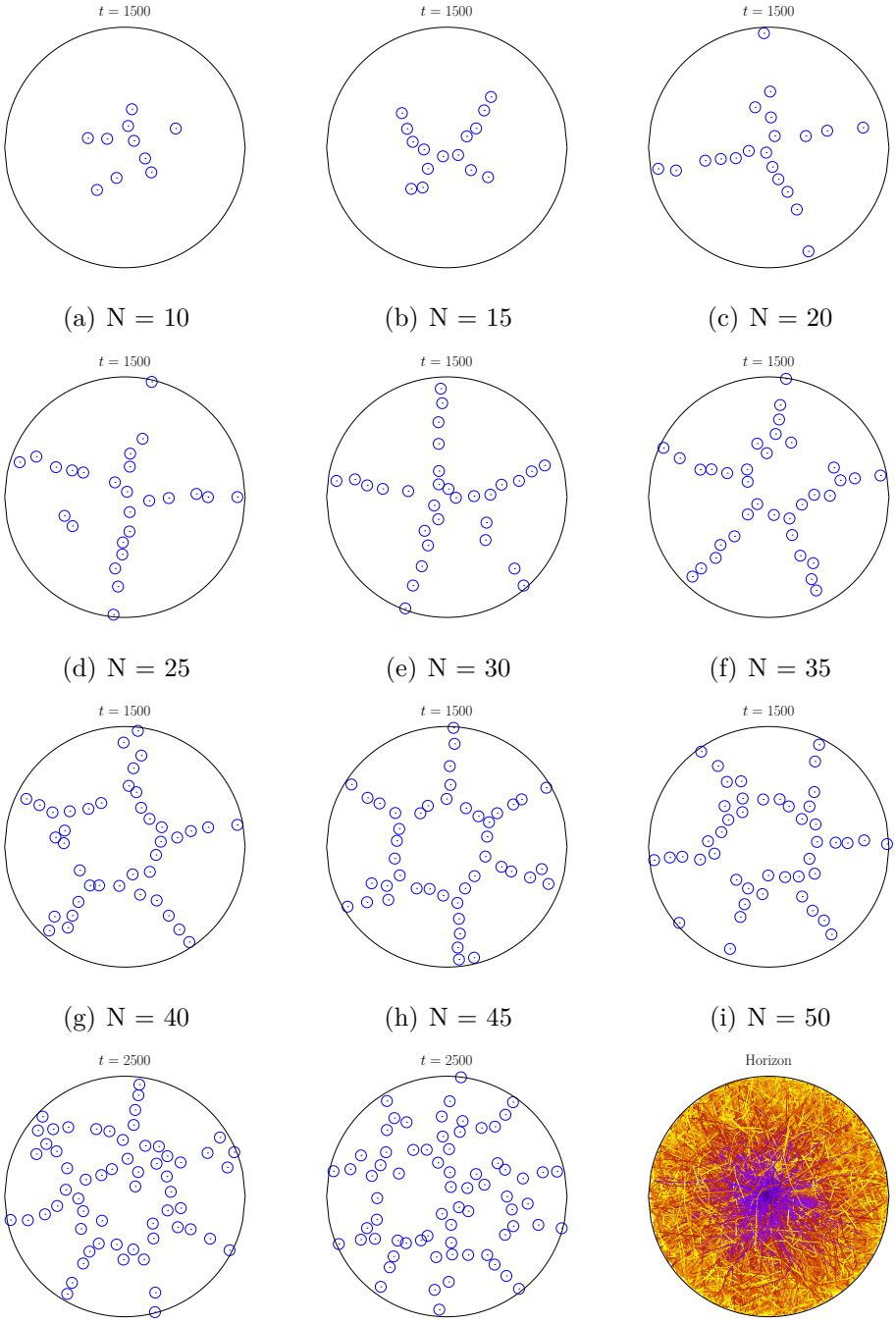

(a) N = 10 (b) N = 15 (c) N = 20

(d) N = 25 (e) N = 30 (f) N = 35

(g) N = 40 (h) N = 45 (i) N = 50

(j) N = 60 (k) N = 70 (l) $T_r = 0.015$, radius $r = 0.25$

Figure B.12.: $\mathcal{S} = 0.5$, $F_{\mathcal{M}}$, $\frac{T_c}{T_r} = 4$, $T_r = 0.015$

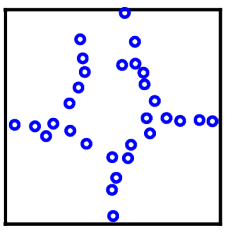

B.9. Circular, $\mathcal{S} = 1.0$, $F_{\mathcal{P}}$

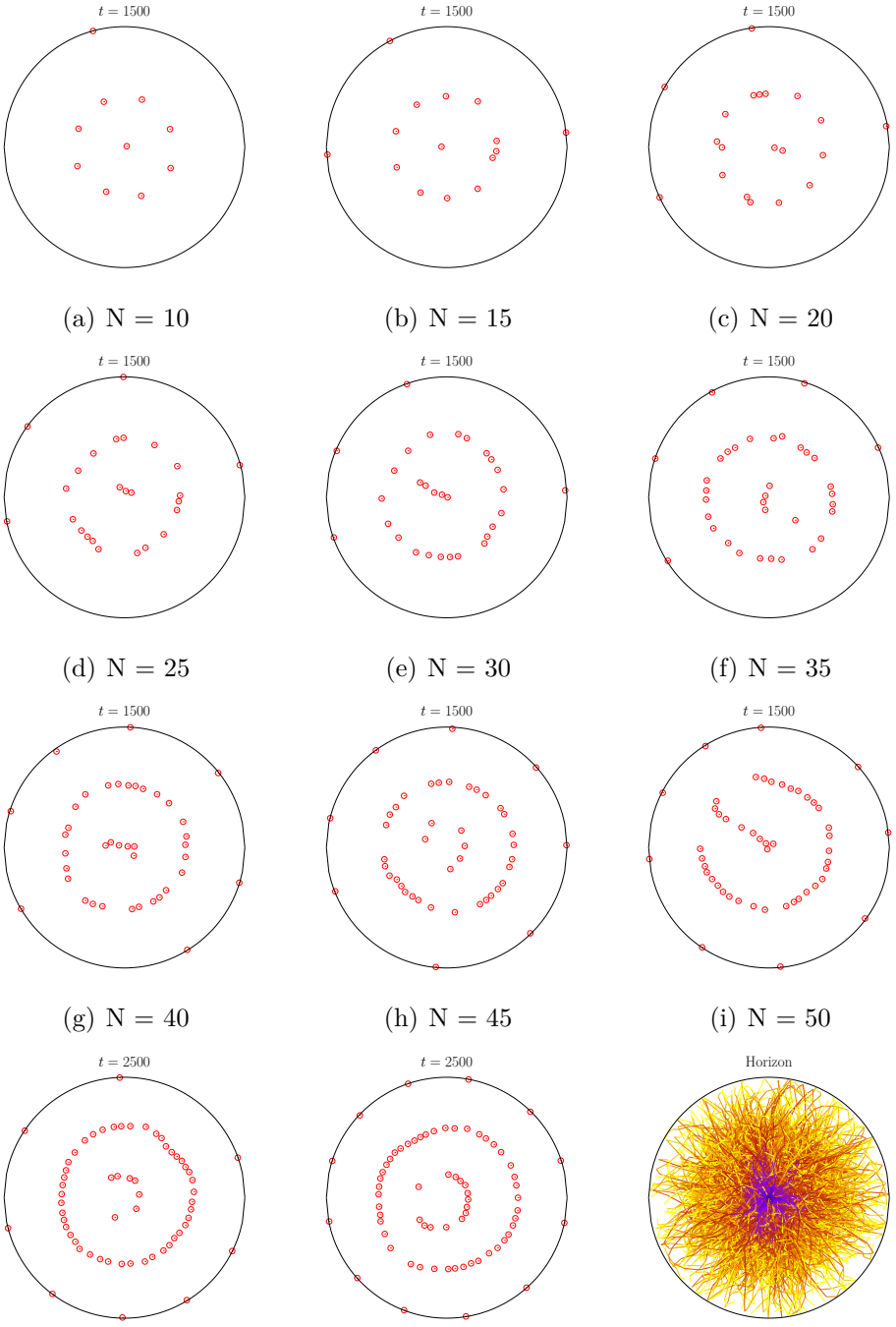

(a) N = 10 (b) N = 15 (c) N = 20

(d) N = 25 (e) N = 30 (f) N = 35

(g) N = 40 (h) N = 45 (i) N = 50

(j) N = 60 (k) N = 70 (l) $T_r = 0.015$, radius $r = 0.5$

Figure B.13.: $\mathcal{S} = 1.0$, $F_{\mathcal{P}}$, $\frac{T_c}{T_r} = 0.5$, $T_r = 0.015$

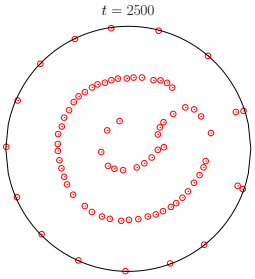

(a) N = 80

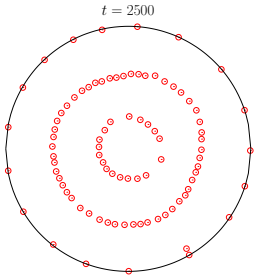

(b) N = 90

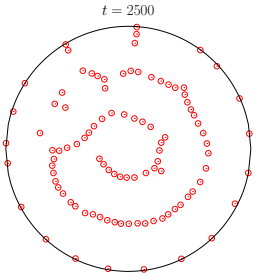

(c) N = 100

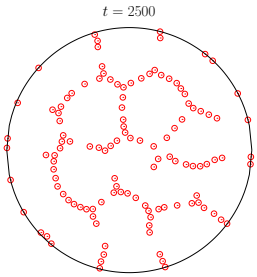

(d) N = 120

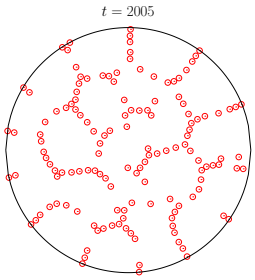

(e) N = 140

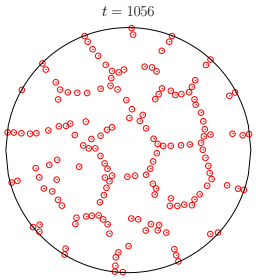

(f) N = 160

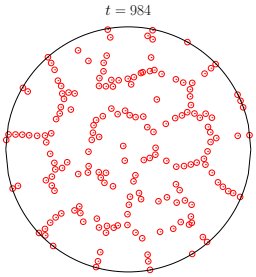

(g) N = 180

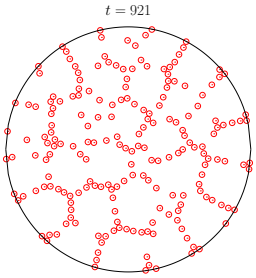

(h) N = 200

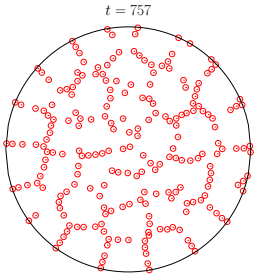

(i) N = 220

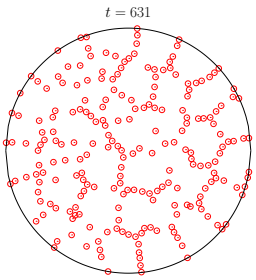

(j) N = 240

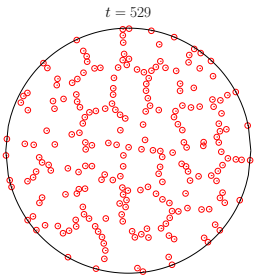

(k) N = 260

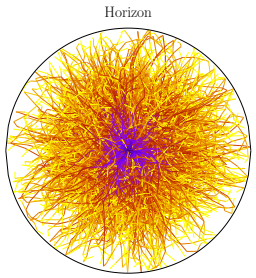

(l) $T_r = 0.015$, radius $r = 0.5$

Figure B.14.: $\mathcal{S} = 1.0$, $F_{\mathcal{P}}$, $\frac{T_c}{T_r} = 0.5$, $T_r = 0.015$

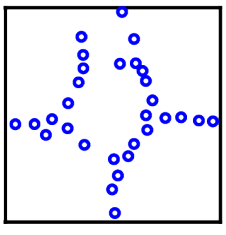

B.10. Circular, $\mathcal{S} = 1.0$, $F_{\mathcal{M}}$

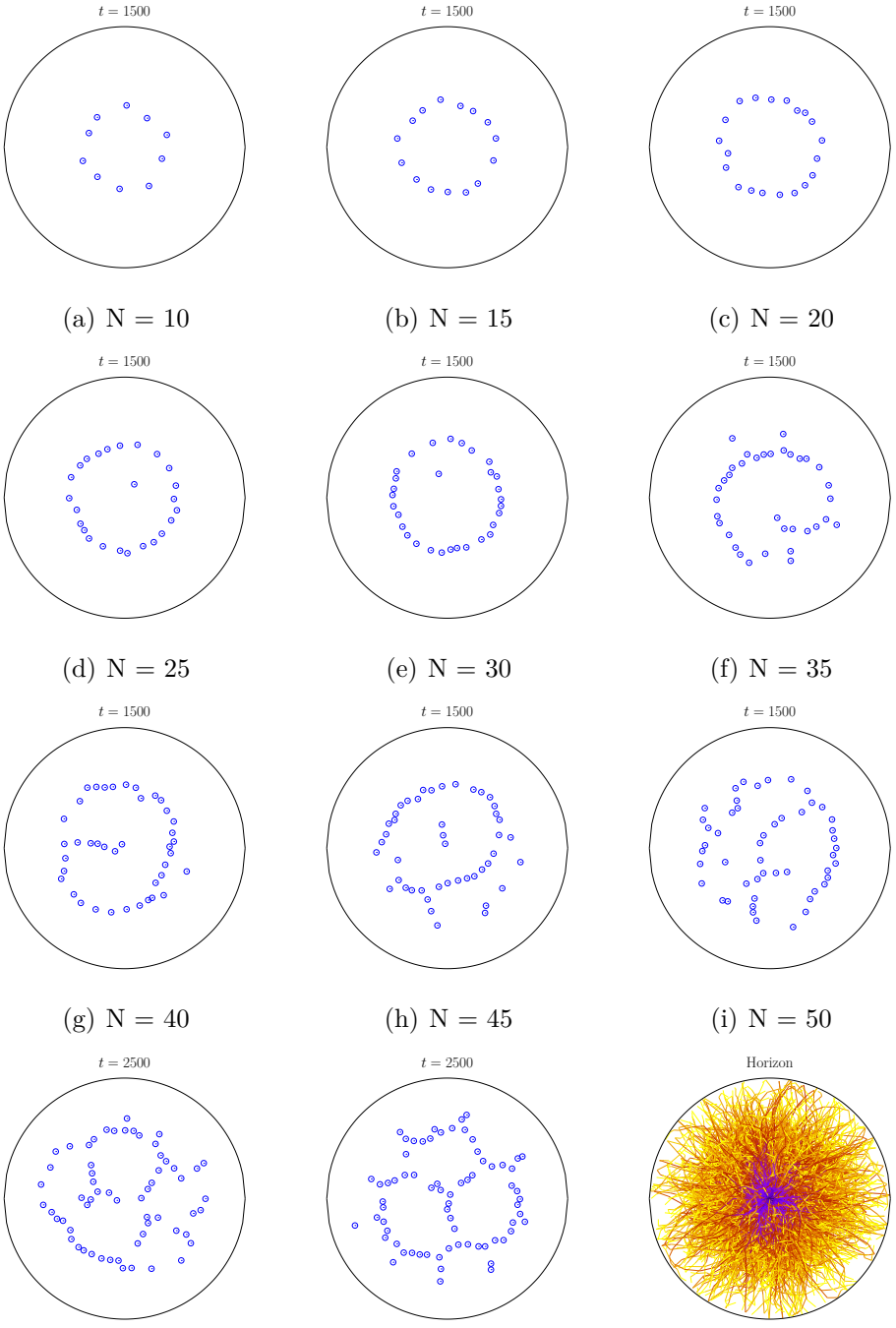

(a) N = 10 (b) N = 15 (c) N = 20

(d) N = 25 (e) N = 30 (f) N = 35

(g) N = 40 (h) N = 45 (i) N = 50

(j) N = 60 (k) N = 70 (l) $T_r = 0.015$, radius $r = 0.5$

Figure B.15.: $\mathcal{S} = 1.0$, $F_{\mathcal{M}}$, $\frac{T_c}{T_r} = 4$, $T_r = 0.015$

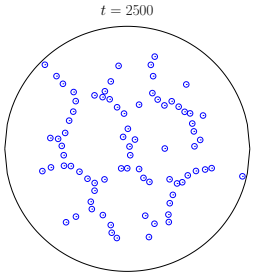

(a) N = 80

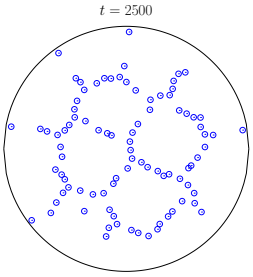

(b) N = 90

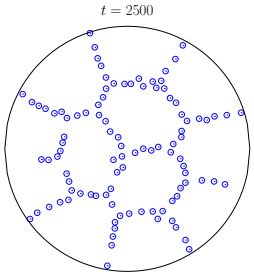

(c) N = 100

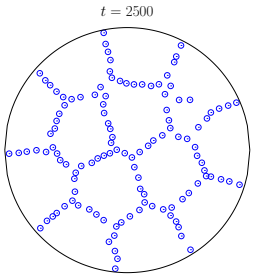

(d) N = 120

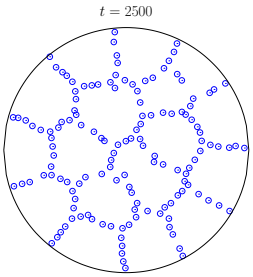

(e) N = 140

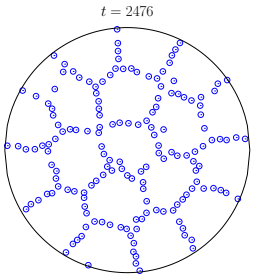

(f) N = 160

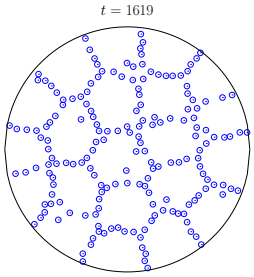

(g) N = 180

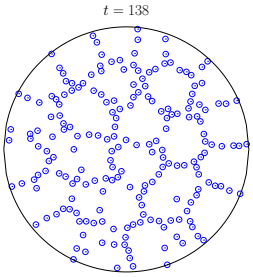

(h) N = 200

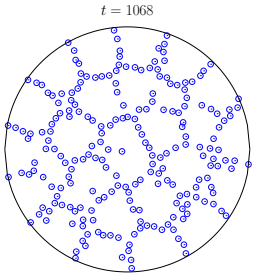

(i) N = 220

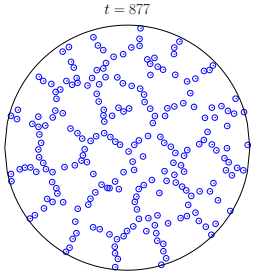

(j) N = 240

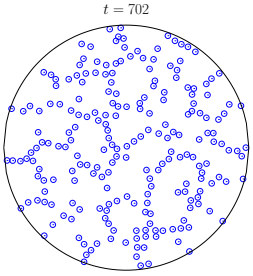

(k) N = 260

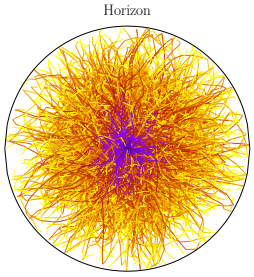

(l) $T_r = 0.015$, radius $r = 0.5$

Figure B.16.: $\mathcal{S} = 1.0$, $F_{\mathcal{M}}$, $\frac{T_c}{T_r} = 4$, $T_r = 0.015$

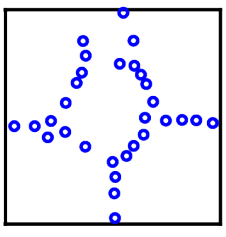

B.11. Circular, $\mathcal{S} = 1.5$, $F_{\mathcal{P}}$

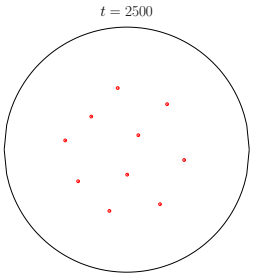

(a) N = 10

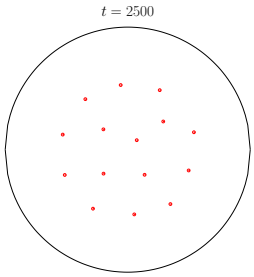

(b) N = 15

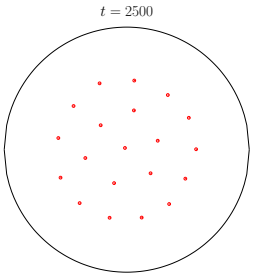

(c) N = 20

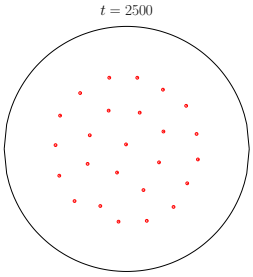

(d) N = 25

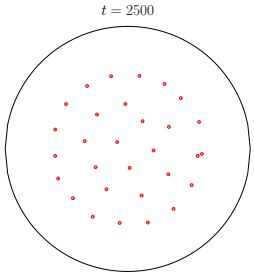

(e) N = 30

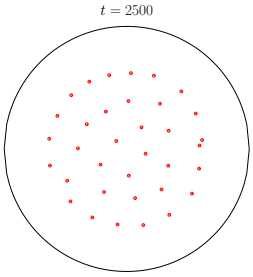

(f) N = 35

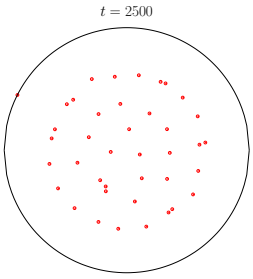

(g) N = 40

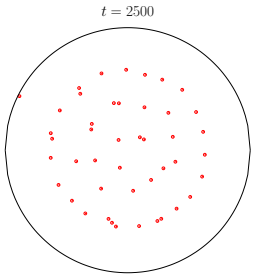

(h) N = 45

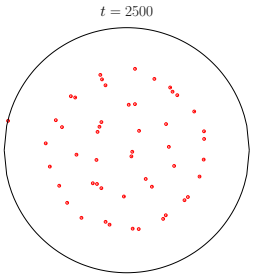

(i) N = 50

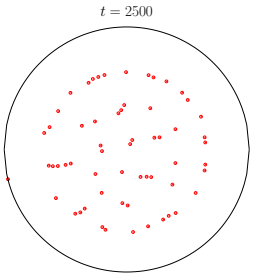

(j) N = 60

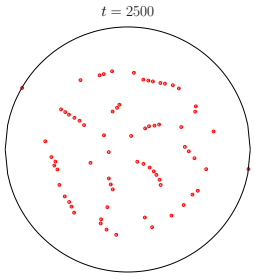

(k) N = 70

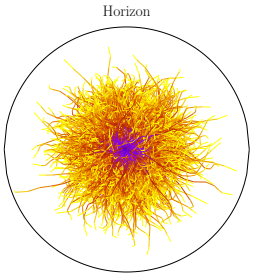

(l) $T_r = 0.015$, radius $r = 0.75$

Figure B.17.: $\mathcal{S} = 1.5$, $F_{\mathcal{P}}$, $\frac{T_c}{T_r} = 0.5$, $T_r = 0.015$

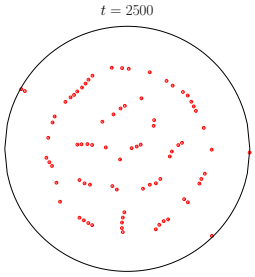

(a) N = 80

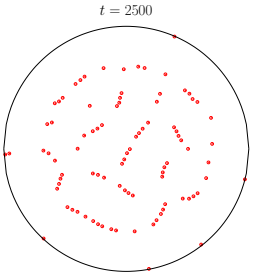

(b) N = 90

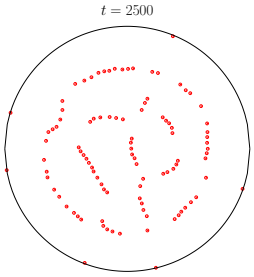

(c) N = 100

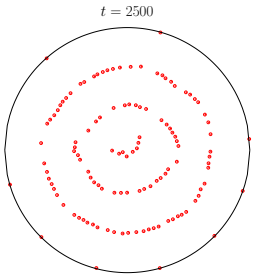

(d) N = 120

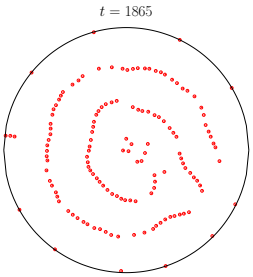

(e) N = 140

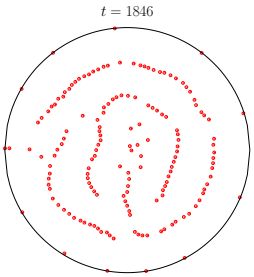

(f) N = 160

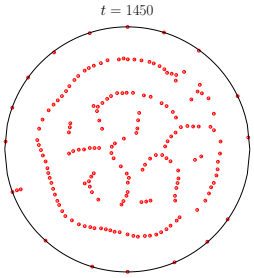

(g) N = 180

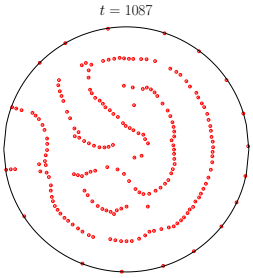

(h) N = 200

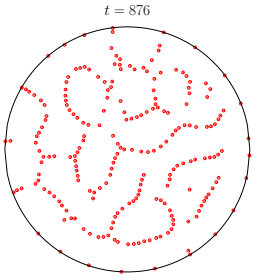

(i) N = 220

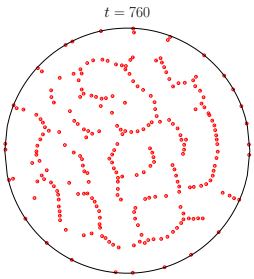

(j) N = 240

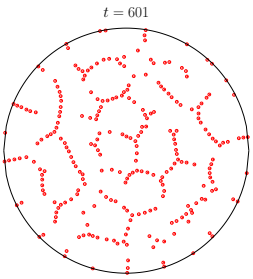

(k) N = 260

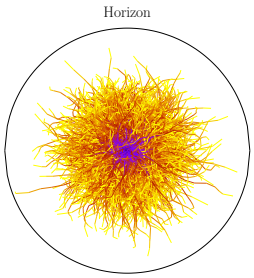

(l) $T_r = 0.015$, radius $r = 0.75$

Figure B.18.: $\mathcal{S} = 1.5$, $F_{\mathcal{P}}$, $\frac{T_c}{T_r} = 0.5$, $T_r = 0.015$

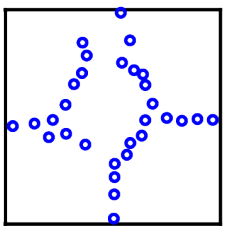

B.12. Circular, $\mathcal{S} = 1.5$, $F_{\mathcal{M}}$

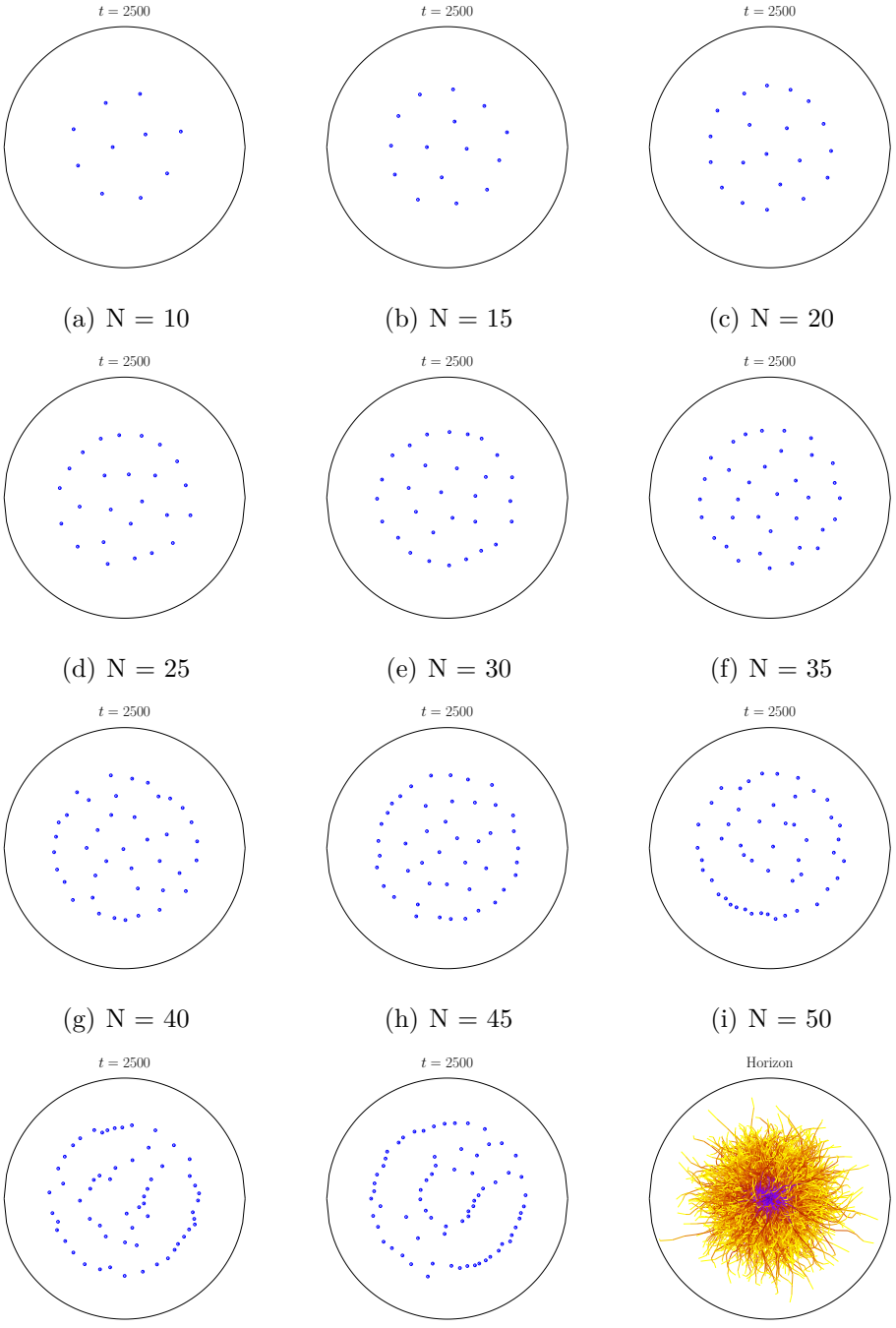

(a) N = 10 (b) N = 15 (c) N = 20

(d) N = 25 (e) N = 30 (f) N = 35

(g) N = 40 (h) N = 45 (i) N = 50

(j) N = 60 (k) N = 70 (l) $T_r = 0.015$, radius $r = 0.75$

Figure B.19.: $\mathcal{S} = 1.5$, $F_{\mathcal{M}}$, $\frac{T_c}{T_r} = 4$, $T_r = 0.015$

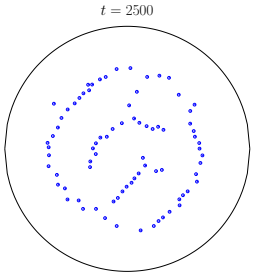

(a) N = 80

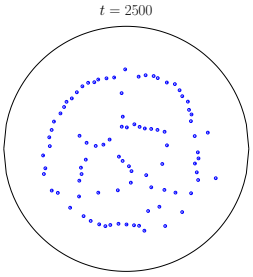

(b) N = 90

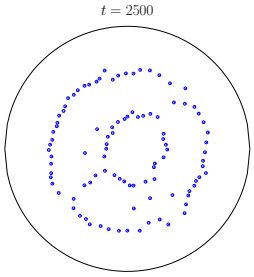

(c) N = 100

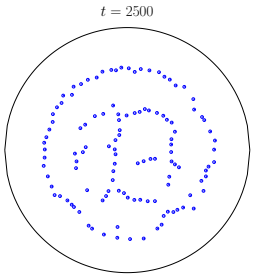

(d) N = 120

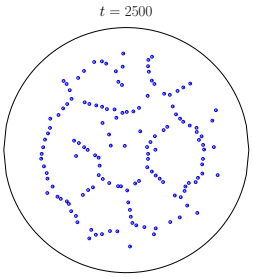

(e) N = 140

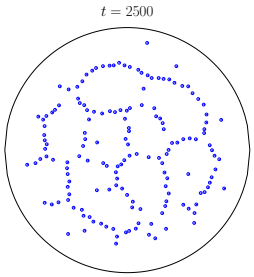

(f) N = 160

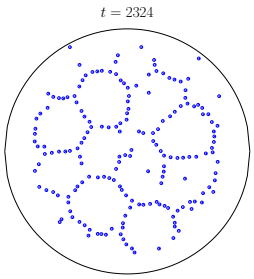

(g) N = 180

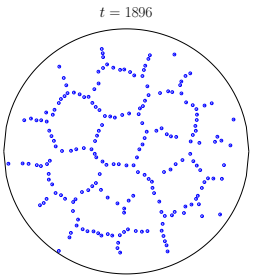

(h) N = 200

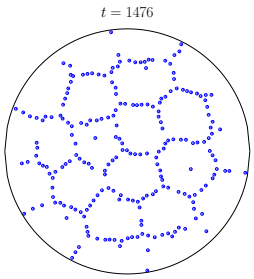

(i) N = 220

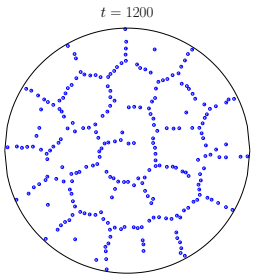

(j) N = 240

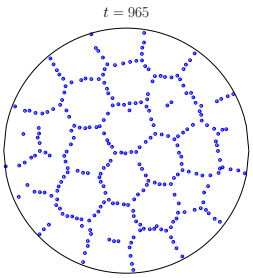

(k) N = 260

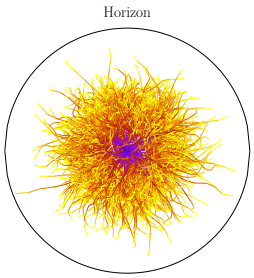

(l) $T_r = 0.015$, radius $r = 0.75$

Figure B.20.: $\mathcal{S} = 1.5$, $F_{\mathcal{M}}$, $\frac{T_c}{T_r} = 4$, $T_r = 0.015$

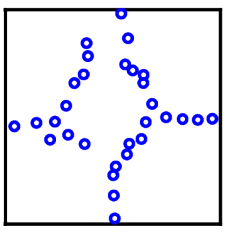

Bibliography

[1] Samuel F. Taylor, Naftali Tishby, and William Bialek. Information and fitness, 2007.

[2] B C Mazzag. Mathematical Models in Biology. PhD thesis, University of California, Davis, 2002.

[3] A. D. Wissner-Gross and C. E. Freer. Causal entropic forces. Physical Review Letters, 110:168702, Apr 2013.

[4] Sylvain Gelly, Levente Kocsis, Marc Schoenauer, Michèle Sebag, David Silver, Csaba Szepesvári, and Olivier Teytaud. The grand challenge of computer go: Monte carlo tree search and extensions. Commun. ACM, 55(3):106–113, March 2012.

[5] Alicia P Melis, Brian Hare, and Michael Tomasello. Engineering cooperation in chimpanzees: tolerance constraints on cooperation. Animal Behaviour, 72(2):275–286, 2006.

[6] Amanda M Seed, Nicola S Clayton, and Nathan J Emery. Cooperative problem solving in rooks (corvus frugilegus). Proceedings of the Royal Society of London B: Biological Sciences, 275(1641):1421–1429, 2008.

[7] Joshua M Plotnik, Richard Lair, Wirot Suphachoksahakun, and Frans BM de Waal. Elephants know when they need a helping trunk in a cooperative task. Proceedings of the National Academy of Sciences, 108(12):5116–5121, 2011.

[8] Richard P. Mann and Roman Garnett. The entropic basis of collective behaviour. Journal of The Royal Society Interface, 12(106), 2015.

[9] Axel Kleidon. Life, hierarchy, and the thermodynamic machinery of planet earth. Physics of Life Reviews, 7(4):424 – 460, 2010.

[10] Xiaoshan Pan, CharlesS. Han, Ken Dauber, and KinchoH. Law. A multi-agent based framework for the simulation of human and social behaviors during emergency evacuations. AI & Society, 22(2):113–132, 2007.

[11] Da Silva R Toyama MC, Bazzan ALC. An agent-based simulation of pedestrian dynamics: from lane formation to auditorium evacuation. Proceedings of the fifth international joint conference on autonomous agents and multiagentsystems, Hakodate, Japan, 8–12 May 2006, page 108–10, 2006.

[12] Nikos Zarboutis and Nicolas Marmaras. Searching efficient plans for emergency rescue through simulation: the case of a metro fire. Cognition, Technology & Work, 6(2):117–126, 2004.

[13] N. Pelechano, J. M. Allbeck, and N. I. Badler. Controlling individual agents in high-density crowd simulation. In Proceedings of the 2007 ACM SIGGRAPH/Eurographics Symposium on Computer Animation, SCA '07, pages 99–108, Aire-la-Ville, Switzerland, Switzerland, 2007. Eurographics Association.

[14] Cyrus Levinthal. Are there pathways for protein folding. Journal de Chimie Physique, 65(1):44–45, 1968.

[15] M. Karplus and D. L. Weaver. Protein-folding dynamics. Nature, 260:404–406, April 1976.

[16] Jeffery Skolnick and Andrzej Kolinski. Simulations of the folding of a globular protein. Science, 250(4984):1121–1125, 1990.

[17] S F Edwards and K F Freed. The entropy of a confined polymer. i. Journal of Physics A: General Physics, 2(2):145, 1969.

[18] Daniel Svenšek and Rudolf Podgornik. Confined nanorods: Jamming due to helical buckling. Physical Review E, 77:031808, Mar 2008.

[19] Parvin Bayati, Leila Ghassab, and Ali Najafi. Entropic forces exerted on a rough wall by a grafted semiflexible polymer. The European Physical Journal E, 37(10), 2014.

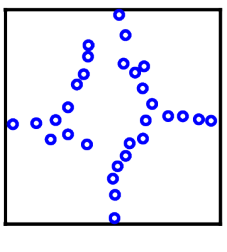

[20] S. W. P. Turner, M. Cabodi, and H. G. Craighead. Confinement-induced entropic recoil of single dna molecules in a nanofluidic structure. Physical Review Letters, 88:128103, Mar 2002.

[21] Jianyong Shi, Aizhu Ren, and Chi Chen. Agent-based evacuation model of large public buildings under fire conditions. Automation in Construction, 18(3):338 – 347, 2009.

Erklärung nach §18(8) der Prüfungsordnung für den Bachelor-Studiengang Physik und den Master-Studiengang Physik an der Universität Göttingen:

Hiermit erkläre ich, dass ich diese Abschlussarbeit selbständig verfasst habe, keine anderen als die angegebenen Quellen und Hilfsmittel benutzt habe und alle Stellen, die wörtlich oder sinngemäß aus veröffentlichten Schriften entnommen wurden, als solche kenntlich gemacht habe.
Darüberhinaus erkläre ich, dass diese Abschlussarbeit nicht, auch nicht auszugsweise, im Rahmen einer nichtbestandenen Prüfung an dieser oder einer anderen Hochschule eingereicht wurde.

Göttingen, den October 12, 2015

(Hannes Hornischer)